Non-Destructive Evaluation of Hydrogen Embrittlement in Cadmium-Plated High Strength Steel Using Ultrasonic Surface Waves and Eddy Currents

by

Hamidreza SHAHMIRI

MANUSCRIPT-BASED THESIS PRESENTED TO ÉCOLE DE TECHNOLOGIE SUPÉRIEURE IN PARTIAL FULFILLMENT FOR THE DEGREE OF DOCTOR OF PHILOSOPHY
Ph.D.

MONTREAL, JUNE 8, 2021

ÉCOLE DE TECHNOLOGIE SUPÉRIEURE
UNIVERSITÉ DU QUÉBEC

BOARD OF EXAMINERS

THIS THESIS HAS BEEN EVALUATED

BY THE FOLLOWING BOARD OF EXAMINERS

Mr. Martin Viens, Thesis Supervisor
Department of mechanical engineering, École de technologie supérieure

Mr. François Blanchard, President of the Board of Examiners
Department of electrical engineering, École de technologie supérieure

Mr. Pierre Bélanger, Member of the jury
Department of mechanical engineering, École de technologie supérieure

Mr. Vincent Demers, Member of the jury
Department of mechanical engineering, École de technologie supérieure

Mr. Thomas Krause, External Evaluator
Department of physics, Royal military college of Canada

THIS THESIS WAS PRENSENTED AND DEFENDED

IN THE PRESENCE OF A BOARD OF EXAMINERS

JULY 7, 2021

AT ÉCOLE DE TECHNOLOGIE SUPÉRIEURE

ACKNOWLEDGMENT

The present research was supported financially by *Fonds de recherche Nature et technologies* (FRQNT) and the Natural Sciences and Engineering Research Council (NSERC) via the Consortium for Research and Innovation in Aerospace in Québec (CRIAQ) under the project DPHM-601. Funding received from NSERC Collaborative Research and Training Experience (CREATE) program under the project *oN DuTy!* is also acknowledged. Special thanks to industrial partners to DPHM-601 for providing test samples and technical support.

I offer my sincere gratitude to my research director, Professor Martin Viens, for giving me the opportunity to pursue doctoral studies under his supervision, for providing me all the necessary means for my research, and for being a great mentor. I would like to extend my thanks to the president of the jury Professor François Blanchard and respected jury members Professor Pierre Bélanger, Professor Vincent Demers and Professor Thomas Krause for accepting to evaluate the present thesis and for their valuable comments and suggestions. I am especially grateful to Professor Pierre Bélanger for his constructive suggestions during my proposal defence, allowing me to use the laser setup developed by his lab team, and also for allowing me access to the licences of the software necessary for my work.

Many thanks to my former colleagues, Dr. Ehsan Mohseni and Dr. Hamid Habibzadeh Boukani, for assisting me in my studies and helping me settle down in Canada as a foreign student.

Finally, I would like to thank my wife Mahzad for being my companion during this journey. I am also forever indebted to my parents for their selfless love and support through every step of my life.

ÉVALUATION NON DESTRUCTIVE, À L'AIDE D'ONDES ACOUSTIQUES DE SURFACE ET DE COURANTS DE FOUCAULT, DE LA FRAGILISATION PAR L'HYDROGÈNE DANS DES ACIERS À HAUTE RÉSISTANCE PLAQUÉS AU CADMIUM

Hamidreza SHAHMIRI

RÉSUMÉ

La fragilisation par l'hydrogène (FH) est un grave phénomène de détérioration des matériaux qui peut provoquer une rupture soudaine de pièces métalliques soumises à des charges statiques ou cycliques, entraînant des interruptions de service et des pertes financières. La FH peut entraîner une fracture différée de composants dont la microstructure est vulnérable et qui contiennent des concentrations extrêmement faibles d'hydrogène diffusif. Les sources d'infiltration d'hydrogène dans le matériau peuvent être soit externes, comme une réaction de corrosion, soit internes, comme l'électroplacage. Les composants en acier 4340 à haute résistance, plaqués au Cd et utilisés pour la fabrication de trains d'atterrissage d'avion, sont particulièrement sujets à la FH. Ces pièces sont traitées thermiquement au cours d'un processus appelé étuvage pour encourager l'exfiltration de l'hydrogène induit par électroplacage. Cependant, il existe des préoccupations concernant l'efficacité de l'étuvage ainsi que l'effet des retards inévitables entre l'électroplacage et l'étuvage sur le risque de FH. Il est donc avantageux de développer une méthode de contrôle non destructif (CND) pour s'assurer que le niveau d'hydrogène dissous soit abaissé en dessous d'un certain seuil de concentration dans les pièces plaquées au Cd. En d'autres termes, une telle méthode de CND doit idéalement être en mesure d'évaluer quantitativement la susceptibilité des pièces en acier plaquées au Cd à la FH. Cependant, de nombreux défis entravent la réalisation de cet objectif. Premièrement, ces faibles concentrations d'hydrogène sont en dehors de la plage de sensibilité de nombreuses techniques de CND conventionnelles. De plus, la recherche sur le CND de la FH s'est jusqu'à présent concentrée sur des pièces soumises à une charge directe d'hydrogène; ce qui implique de fortes concentrations d'hydrogène et donc des résultats qui peuvent ne pas être applicables au cas de l'acier plaqué au Cd. En tant qu'étape initiale, mais nécessaire, dans la recherche pour résoudre le problème, la présente étude évalue la faisabilité de méthodes de CND qui ont été jugées potentiellement sensibles aux variations induites par l'hydrogène dans les propriétés des matériaux proches de la surface des échantillons d'acier plaqués au Cd. Le but était de faire la distinction entre des échantillons à faible et à forte susceptibilité à la FH. À cette fin, des mesures non destructives basées sur des ondes acoustiques de surface (OAS) ainsi qu'un contrôle par courants de Foucault (CCF) ont été effectués sur plusieurs échantillons fabriqués dans des conditions sans étuvage, d'étuvage différé et d'étuvage immédiat. Des tests destructifs ainsi que des techniques de microscopie ont été réalisés en parallèle pour caractériser les échantillons à tester. Des simulations informatiques des résultats de CND ont également été effectuées pour évaluer les changements induits par l'hydrogène dans les propriétés des matériaux étudiés.

Mots-clés : Contrôle non destructif (CND); Fragilisation par l'hydrogène (FH); Acier à haute résistance; Revêtement de cadmium; Ondes acoustiques de surface (OAS); Ultrasons; Contrôle par courants de Foucault (CCF)

NON-DESTRUCTIVE EVALUATION OF HYDROGEN EMBRITTLEMENT IN CADMIUM-PLATED HIGH STRENGTH STEEL USING ULTRASONIC SURFACE WAVES AND EDDY CURRENTS

Hamidreza SHAHMIRI

ABSTRACT

Hydrogen embrittlement (HE) is a serious material deterioration phenomenon that can cause sudden failure of metallic parts subjected to static or cyclic loads, leading to service interruptions and financial losses. HE can result in delayed fracture of components with vulnerable microstructure that contain exceedingly small concentrations of diffusive hydrogen. Sources of hydrogen ingress into material can be either external, such as a corrosion reaction, or internal, such as electroplating process. Cd-plated 4340 high strength steel components, used for manufacturing aircraft landing gears, are particularly prone to HE. Such parts are heat-treated during a process called baking to encourage the egress of electroplating-induced hydrogen. However, there are concerns about the efficiency of baking as well as the effect of inevitable delays between electroplating and baking on the risk of HE. It is therefore beneficial to develop a non-destructive evaluation (NDE) method to ensure that dissolved hydrogen level is dropped below a certain concentration threshold in Cd-plated parts. In other words, such NDE method shall ideally be able to quantitatively evaluate the susceptibility of Cd-plated steel parts to HE. However, there are numerous challenges which hinder achieving this goal. Firstly, such small hydrogen concentrations are below the sensitivity level of many conventional NDE techniques. Moreover, research on NDE of HE has so far has been focused on parts subjected to direct hydrogen charging that involve high hydrogen concentrations, the results of which may not be applicable to case of Cd-plated steel. As an initial but necessary step in research to address the problem, the present study assesses the feasibility of candidate NDE methods that were deemed sensitive to hydrogen-induced variations in near-surface material properties of Cd-plated steel samples. The aim was to distinguish between samples with low and high HE susceptibilities. For this purpose, non-destructive measurements based on surface acoustic waves (SAW) as well as eddy current testing (ECT) were performed on several samples manufactured in not-baked, late-baked and immediately-baked conditions. Destructive tests as well as microscopy techniques were performed in parallel to characterize test samples. Computer simulations of NDE results were also performed to evaluate the hydrogen-induced changes in relevant material properties.

Keywords: Non-Destructive Evaluation (NDE); Hydrogen Embrittlement (HE); High Strength Steel; Cadmium Coating; Surface Acoustic Waves (SAW); Ultrasound; Eddy Current Testing (ECT)

TABLE OF CONTENTS

Page

LIST OF TABLES

Page

LIST OF FIGURES

Page

LIST OF ABREVIATIONS

AC	Alternating Current
AIDE	Adsorption Induced Dislocation Emission
ASNT	American Society for Non-destructive Testing
Cd	Cadmium
CT	Computed Tomography; Compact Tension
DEFACTANT	Defect Acting Agent Mechanism
ECT, EC	Eddy Current Testing
EHE	Environmental Hydrogen Embrittlement
EMAT	Electromagnetic Acoustic Transducer
ERD	Energy Recoil Detection
ES	Embrittled Sample
FBW	First Backwall Echo
FCC	Face Centered Cubic
FFT	Fast Fourier Transform
HCP	Hexagonal Close Packed
HE	Hydrogen Embrittlement
HEDE	Hydrogen Enhanced Decohesion Theory
HELP	Hydrogen Enhanced Localized Plasticity
HESIVT	Hydrogen-Enhanced Strain-Induced Vacancy Theory
IDT	Interdigital Transducers
IG	Intergranular Fracture Mode

IHE	Internal Hydrogen Embrittlement
ISL	Incremental Step Loading
LDV	Laser Doppler vibrometer
MT	Magnetic-particle Testing
MVC	Microvoid coalescence
N	Number of samples; Number of turns of a coil
NDE	Non-Destructive Evaluation
NDT	Non-Destructive Testing
NES	Non-Embrittled Sample
NRA	Nuclear Reaction Analysis
NT	Neutron Tomography
PT	Penetrant Testing
QC	Quasi-Cleavage Fracture Mode
RT	Radiographic Testing
SAW	Surface Acoustic Waves
SD	Standard Deviation
SEM	Scanning Electron Microscope
SLT	Sustained-Load Tests
SNR	Signal-to-Noise Ratio
TDA	Thermal Desorption Analysis
UT	Ultrasonic Testing
UTS	Ultimate Tensile Strength

LIST OF SYMBOLS

A	Ampere
at. %	Atomic percent
dB	Decibel
HV	Vickers Hardness
Hz	Hertz
J	Joule
K	Kelvin
mol	Mole
Pa	Pascal
ppm	Parts per million
ppma	Parts per million atoms
ppmm	Parts per million by mass
rad	Radians
V	Volt
W	Watt
A	Main SAW signal amplitude
C	Hydrogen concentration
$C_{H,tot}$	Total hydrogen concentration
D	Diameter
E	Young's modulus
FBW	Amplitude of SAW first backwall echo

f	Linear temporal frequency (or simply frequency)
J_∞	Steady-state flow of hydrogen according to Fick's first law of diffusion
j_t	Total flux of permeating hydrogen
K	Stress intensity factor
K_{IC}	Critical stress intensity factor for mode I loading
K_{TH}	Stress intensity threshold for HE
k	Angular spatial frequency (wavenumber)
P	Pressure
p	Hydrogen gas pressure
R	Ideal gas constant
R_a	Linear roughness
S_a	Surface roughness
T	Temperature
t_{Cd}	Cd coating thickness
u	Displacement
V	Wave velocity; Voltage
V_l	Longitudinal wave velocity
V_r	SAW velocity
V_t	Shear wave velocity
$\bar{V}_H$	Molar volume of hydrogen
Z	Electrical impedance; Surface height difference
α	Attenuation coefficient
γ	Surface energy

Δt	Time delay between SAW signals
Δx	SAW propagation distance
θ	Solid solubility of hydrogen
θ_R	Rayleigh angle
λ	Wavelength
λ_r	Rayleigh wavelength
μ	Shear modulus
ν	Poisson's ratio
ρ	Density
σ	Stress; Electrical Conductivity
τ	Period of time
Φ	Hydrogen permeability coefficient
ω	Angular temporal frequency (or simply angular frequency)

INTRODUCTION

Hydrogen embrittlement (HE) is a complex and insidious material deterioration phenomenon observed in different metallic alloys subjected to hydrogen. It can adversely affect the mechanical performance of industrial parts and even cause premature failures leading to significant losses. For example, a comprehensive investigation on aviation incidents since the Second World War indicated that 6-7% of aircraft failures could be related to deleterious effects of HE (Findlay & Harrison, 2002). All material degradation processes involving hydrogen (in any form) that cause an apparent transition from ductile to brittle behaviour are referred to as HE (Barrera *et al*, 2018). Sources of hydrogen ingress into a material can either be external, such as a corrosion reaction during service, known as environmental hydrogen embrittlement (EHE), or they can be internal due to manufacturing processes such as steel making, electroplating and acid pickling, known as internal hydrogen embrittlement (IHE) (Sriraman *et al*, 2013). At high hydrogen pressures, hydrogen can penetrate into a material in molecular form. At moderate and low hydrogen pressures, however, it is the atomic hydrogen that diffuses into the metal lattice and remains there in either a mobile state (hydrogen in solid solution or weak trap sites) or an immobile state (strong trap sites) (Nagumo, 2016). HE processes can be roughly categorized into two groups based on the nature of the damage by hydrogen. The first are those that create recognizable defects (blisters, bubbles, floccules, gas porosity and disruption cracks) which usually develop at high hydrogen pressures, involve hydrogen penetration in molecular form, and are frequently referred to as hydrogen damage or hydrogen attack. The second type of HE happens when hydrogen atoms present in microstructure induce loss of ductility and a reduction in load-bearing capacity of material, and eventually cause delayed fracture under the effect of external or residual stress (Kovalev, 2002). This type of HE creates many concerns because it can be caused by exceedingly small amounts of dissolved hydrogen, in order of less than 1 ppm of mass fraction (Zamanzadeh, 1982; Wang *et al*, 2006). It is therefore considerably difficult to detect, and the adverse effects do not show until it is already too late. Although research regarding the effects of hydrogen on iron and steel was started in the second half of the nineteenth century (Johnson, 1875) and has continued with an accelerated pace ever since, the mechanisms behind delayed fracture by IHE

are still under dispute with widely different explanations proposed (Barrera *et al*, 2018). However, it is established that a combination of diffusive hydrogen, susceptible microstructure, and stress beyond a certain intensity threshold are the precursors for catastrophic failure by IHE (Sriraman *et al*, 2013). Brittle fracture theories explain HE based on the decrease in the cohesive strength of materials induced by hydrogen atoms. In addition, plasticity theories rely on hydrogen-induced plastic instability and reduction in load-bearing capacity by activation of dislocations and generation of lattice defects (e.g. voids). However, both brittle and plasticity-dominated theories emphasize the role of increased hydrogen contents in areas of high stress concentration (e.g. a crack tip) and effects of loading/straining on the development of HE (Nagumo, 2016).

High strength alloy steels, e.g. SAE 4340, offer advantageous mechanical properties such as good fatigue resistance and enhanced toughness after proper heat-treatment. They are used for manufacturing critical components, e.g. automotive crankshafts and aircraft landing gears, which must endure high cyclic loads (Puchi-Cabrera *et al*, 2007). These components are prone to wear and corrode because of harsh working conditions and electrochemical vulnerability, which dictates the need for application of protective coatings. In case of aircraft landing gears, electroplating with Cadmium (Cd) is still a common practice due to exceptional anti-corrosive properties of this metal despite the concerns regarding its toxicity (Wang & Chang, 2018). Hydrogen that evolves as a by-product during electroplating and remains in the component may cause delayed fracture at stress levels that are well below what the part can apparently support. Generally, the problems with hydrogen are more pronounced in case of high strength steels because of their microstructural susceptibility as well as their usually high hydrogen diffusion coefficient at room temperature, e.g. $2 \times 10^{-7}\ \mathrm{cm}^2 s^{-1}$ in case of 4340 steel (Devanathan *et al*, 1963). As a preventive measure to IHE after Cd-plating, a baking heat-treatment is performed to encourage outward diffusion and ultimately removal of hydrogen from the electroplated parts (Figueroa and Robinson, 2008). However, there are questions regarding the efficacy of this practice because some hydrogen atoms might be entrapped in the coating/substrate interface during outward migration (Sriraman *et al*, 2013). In addition, during inevitable delays between electroplating and baking processes in industrial practice, diffusive

hydrogen might accumulate and be entrapped at areas of high stress concentration. This may further reduce the efficiency of baking and enhance the risk of IHE. Because of the aforementioned problems, along with the strict safety requirements in the aerospace sector, there is demand in industry to develop a non-destructive evaluation (NDE) tool for distinguishing nascent IHE in Cd-plated, SAE 4340 steel components. The present study serves to address this demand in its own capacity by investigating potential NDE solutions through experiments and simulations. Research on NDE of IHE is still in its infancy as a result of difficulties in hydrogen detection and the seemingly lack of distinguishable hydrogen-induced defects. Hence, results of the present research could expand the technical knowledge for detection and prevention of nascent HE in various components of different applications.

According to the definition proposed by American Society for Non-destructive Testing (ASNT), non-destructive evaluation is "the examination of an object with technology that does not affect the object's future usefulness" (Shull, 2001). To examine an object non-destructively, the guiding principal is to find a physical phenomenon (e.g. propagation of acoustic waves in solids) that can interact with, and be affected by, the flaws within a test specimen or the variations in material properties. The information obtained from these interactions can then be interpreted to determine the quality or integrity of the object. Well-known NDE methods include liquid penetrant (PT), magnetic particle (MT), X-ray radiography (RT), ultrasound (UT) and eddy current (EC) testing. Each method is based on a different physical phenomenon and offers its own set of advantages and disadvantages. NDE methods are widely used for structural health monitoring as well as quality control of manufactured parts in a variety of fields, e.g. detection and sizing of flaws in welded structures or inspection of aircraft parts for defects such as fatigue cracks. An NDE method is selected and modified based on requirements for a specific application. In case of IHE of electroplated steel samples, the proposed NDE method shall be sensitive to effects of hydrogen content on a material property (e.g. electrical conductivity or local hardness). This immediately rules out the possibility of using methods such as PT or MT, because the former can only reveal surface-breaking cracks and the latter is usually sensitive only to well-defined flaws. Moreover, the proposed NDE method shall minimize measurement errors due to random variations in

irrelevant parameters (e.g. minor differences between coating characteristics). A simple way to achieve this is by repetition of measurements at different locations on a test piece and averaging the results. It is also beneficial for the proposed method to be applicable in a production environment and be less limited in terms of sample size and geometry. Similar to other fields of engineering, NDE evolves and improves by technological advancements, most notably by advancements in sensor development as well as data processing capabilities of computers. Following this trend, the proposed method for NDE of IHE should effectively incorporate state of the art equipment to increase the accuracy of measurements and take advantage of computer programming and simulation software to better process and analyse the measurement results.

Concentration and state of dissolved hydrogen into a material can be evaluated via measuring hydrogen outgassing rate from the surface under a controlled temperature ramp during thermal desorption analysis (TDA). TDA is a powerful tool for detection and understanding the effects of hydrogen. However, it is basically a destructive technique because the temperature ramp can affect the microstructure and properties of material (e.g. by precipitation of carbides or reconfiguration of dislocations in steel) (Nagumo, 2016). The heat required for TDA can also lead to evaporation of low-melting-point metallic coatings such as Cd. An alternative approach to TDA is the bombardment of samples containing hydrogen with high-energy ion-beams (usually Nitrogen-15) using nuclear physics tests. There are two techniques for this purpose (Lanford, 1992): first is nuclear reaction analysis (NRA) during which nuclear reactions between the bombarding ion-beam and hydrogen atoms are quantified to determine the amount of hydrogen. Second is energy recoil detection (ERD) based on counting the number of hydrogen ions recoiled out of the sample through elastic collision with the incident ion-beam. The problem with these tests is that they are very expensive and time-consuming and require laboratory-based equipment. These issues limit the application of nuclear-based methods for NDE of HE to specialized and highly sensitive cases. There are also methods for visualization of hydrogen distribution and revealing the locations of hydrogen accumulation, namely Tritium autoradiography and neutron tomography (NT) (Nagumo, 2016). These methods are

impractical for regular industrial inspections because they are also expensive and time-consuming, and they may involve radioactivity that poses a serious environmental hazard.

According to recently published results revolving around fracture mechanics tests for evaluation of HE in case of Cd-plated 4340 steel samples, most of hydrogen evolved during electroplating tends to concentrate inside the coating, at the coating/substrate interface or in the steel near the coating (Laliberté-Riverin *et al*, 2020[I]). This was indeed guessed to be the case since the start of the present study, i.e. winter 2017. Consequently, the proposed NDE technique for IHE in Cd-plated steel parts were chosen to be particularly sensitive to surface and subsurface variations in material properties due to effects of hydrogen. NDE methods based on surface acoustic waves (SAW) as well as high frequency eddy current testing (ECT) were selected because of the aforementioned reasons. Related studies in case of bare steel alloys have demonstrated that both of these techniques could be sensitive to direct or indirect effects of hydrogen on steel (Zielinski & Fiore, 1982; Ye *et al*, 2013; Koenig *et al*, 2010; Zhou *et al*, 2018).

Ultrasounds are high frequency (> 20 kHz) mechanical waves that can travel through a material by elastically vibrating constituent particles in different modes (such as longitudinal or shear). They have been employed for various industrial NDE applications since the middle of 20^{th} century. The basic technique for UT is transformation of a voltage pulse by a transducer into an ultrasonic pulse. The signal is then transmitted to a receiver and is transformed back into an electrical pulse to be observed on an oscilloscope. During UT, backscattering of signals or changes in characteristics of ultrasound (such as velocity and attenuation coefficient) after propagation in test piece can be analysed to reveal the presence of flaws, assess geometrical features, and evaluate variations in material properties. Ultrasonic NDE techniques offer numerous advantages including high sensitivity to reveal subsurface and small flaws, volumetric scanning ability, and applicability for different types of materials such as metals, ceramics and polymers (Shull, 2001). Ultrasonic measurements using bulk wave modes have been previously employed for NDE of HE with good results (Hasegawa, 1988; Kruger *et al*, 1999). However, these works have been focused on detection of microcracks in extreme cases

of hydrogen damage, the results of which cannot be generally applicable to nascent IHE in electroplated steel parts, where such defects may not be present per se.

SAW, also known as ultrasonic surface waves or Rayleigh waves, are a specific mode of ultrasound propagating on the surface of materials with a penetration depth of about one wavelength. Because of frequency-dependent penetration depth of SAW, they show dispersive behavior (e.g. change in velocity by frequency) when propagating in a material with depth-dependent gradient of properties (e.g. an electroplated test piece) (Balogun & Achenbach, 2012). Ultrasonic surface waves possess exceptional characteristics such as high sensitivity to near-surface defects or material variations, ability to follow curved paths, and travelling far distances without losing much energy (Shull, 2001). Earlier studies established the potential of SAW for non-destructive characterization of surface damage (Warren *et al*, 1996), determination of subsurface hardness profile (Gordon *et al*, 1993), and coating thickness measurement (Lakestani *et al*, 1995). However, similar to other ultrasonic guided wave modes, application of SAW in the field of NDE have been limited because of difficulties during inspection as well as complications in interpreting the measurement results. With that being said, SAW-based methods have seen renewed interest in the past decade as a result of advancements in instrumentation for generation/reception of ultrasonic vibrations as well as development and implementation of sophisticated signal processing algorithms along with efficient and stable simulation codes (see for example Wang & Rokhlin, 2001 and Doerr *et al*, 2017). Recent publications show potential applicability of SAWs for sensitive NDE applications such as monitoring the evolution of fatigue crack in titanium alloy (Connolly & Rokhlin, 2013), determination of hardness gradient in carburized steel (Singer & Kufner, 2017), and evaluation of sensitization in stainless steel (Doerr *et al*, 2017). In case of nascent IHE, although conventional ultrasonic techniques have not shown good detectability, methods based on SAW velocity and attenuation measurements have exhibited sensitivity to effects of dissolved hydrogen on microstructure and material properties (Zielinski & Fiore, 1982; Ye *et al*, 2013). Despite this fact, these studies were limited to SAW measurements during direct electrochemical hydrogen charging of uncoated stainless alloys at high current densities, the results of which might not be applicable to the present case. Furthermore, the advantages

offered by more advanced techniques for generation and detection of SAW (such as laser method) for NDE of IHE has not been explored yet. Novel signal processing procedures and computer simulations for understanding the changes in SAW behavior due to IHE are lacking. More importantly, to date, dispersive properties of SAW have not been utilized to evaluate IHE. The majority of the present research tries to examine these unexplored possibilities for the first time.

ECT is a well-known electromagnetic NDE method with numerous applications for quality control and flaw inspection, e.g. thickness measurement of metallic coatings or detection and sizing of small cracks on aircraft components. EC probes measure a material's response to an external electromagnetic field that induces eddy currents of a specific frequency range in the inspected part. Using this response, the condition of the part is evaluated for presence of defects (e.g. porosity) or variations in material properties (e.g. hardness). ECT directly interrogates electrical conductivity and magnetic permeability. Similar to SAW, the penetration depth of eddy currents decreases with increasing frequency. ECT provides a noncontact, portable and rapid non-destructive testing (NDT) solution that is particularly sensitive to surface and near-surface material property variations. However, it is limited only to conductive parts. The sensitivity of ECT to a wide range of parameters (such as probe liftoff and tilt) also makes interpretation of results increasingly complex (Shull, 2001). There are a few works published relatively recently on the use of eddy currents at frequencies lower than 100 kHz for non-destructive detection of hydrogen presence and evaluation of its effects in steel alloys (Koenig *et al*, 2010; Zhou *et al*, 2018; Bellemare *et al*, 2020 [II]). In fact, results obtained by Koenig *et al* (2010) and Zhou *et al* (2018) clearly demonstrated the exceptional sensitivity of EC probe impedance to hydrogen content in steel. However, they used custom-made coils favoring limited geometries and they did not employ high frequencies. For the first time, this study tries to employ portable, commercially available ECT test units and spot probes as well as computer simulation to assess the feasibility of a simple ECT routine suitable for detection of nascent IHE in Cd-plated high strength steel parts.

The present thesis is part of a collaborative research effort between academics from *École de technologie supérieure, Université de Montréal* and *École Polytechnique de Montréal* as well as industrialists from aerospace sector including *Safran*, *Héroux-Devtek* and *Bell Helicopter*. This comprehensive project, called DPHM-601, was defined and funded by *Consortium de Recherche et d'Innovation en Aérospatiale au Quebec* (CRIAQ). The aim was to find a material property that is sensitive to direct or secondary effects of hydrogen content and exploit this property for the development of a non-destructive technique to detect nascent IHE in electroplated, high strength steel parts. It was not intended to study the mechanisms underlying HE nor to propose methods to avoid it. Instead, the emphasis was on use of the existing literature along with the results obtained by other peers involved in DPHM-601. To develop an effective NDE technique for HE, experimental efforts were focused on samples with manufacturing conditions that were of particular interest for our industrial partners. Hence, direct hydrogen charging was excluded from the experimental approach, and attention was paid to the effects of hydrogen retained after electroplating. The present dissertation serves the objectives of DPHM-601 by investigating the potential of ultrasonic and electromagnetic techniques for NDE of HE. For this purpose, industrial partners provided the author three batches of Cd-plated, disk-shaped, quenched, and tempered SAE 4340 high strength steel test coupons with different preparation conditions. They included samples that were baked immediately (lowest HE susceptibility), baked after a long delay or not baked at all (highest HE susceptibility) after Cd-plating. Other academic contributors worked on direct hydrogen detection (nuclear and outgassing techniques) as well as on mechanical testing and failure analysis of separate samples prepared of the same material with similar manufacturing conditions but with different geometries suitable for their tests (Larochelle *et al*, 2017; Laliberté-Riverin *et al*, 2020[I]; Laliberté-Riverin *et al*, 2020[II]; Bellemare *et al*, 2020 [I]). Their experiments focused on assessing the spatial distribution of hydrogen, evaluating HE severity, and determining the critical hydrogen concentration as well as the stress intensity threshold for the onset of IHE by means of TDS, fracture mechanics tests and microscopy techniques.

As already mentioned, in the present study, a method based on ultrasonic surface waves along with eddy current testing were tried. In case of SAW, a 10-MHz broadband piezoelectric transducer and a laser vibrometer was used to generate and detect surface ultrasound vibrations, respectively. SAWs were measured on numerous spots during line scans on several samples with similar manufacturing conditions to ensure the repeatability of the results. The measured data were processed by signal processing algorithms developed in MATLAB® in order to obtain SAW velocity and attenuation coefficients for each sample. In-house algorithms based on Fast Fourier Transform (FFT) were utilized to calculate SAW phase velocity dispersion and dispersive attenuation curves. In addition, coatings were characterized by laser and optical microscopy techniques and the results were used to assess their effects on non-destructive measurements. Micro-indentation hardness profiles were obtained near the surface of samples to understand the effects of hydrogen on local mechanical properties and to indirectly confirm the presence of diffusive hydrogen. Results of these tests, along with the data published by other collaborators in DPHM-601, were used to interpret NDE results. Furthermore, experimental phase velocity dispersion curves were simulated via Disperse® in order to evaluate near-surface gradient of elastic moduli of steel and Cadmium caused by dissolved hydrogen. The original contributions from the aforementioned experiments were gathered in the form of two scientific articles. The first article concerns SAW velocity and attenuation measurements, and the second investigates changes in the dispersive behavior of SAW due to presence of hydrogen. These papers are presented in this dissertation as Chapters 2 and 3, respectively. Their titles are as follows:

1) Hamidreza Shahmiri & Martin Viens, « Non-destructive Evaluation of Electroplating-induced Hydrogen Embrittlement in Cd-coated High Strength Steel Using Ultrasonic Surface Waves ». Paper manuscript submitted to *Materials Evaluation* in April 2021.

2) Hamidreza Shahmiri & Martin Viens, « Feasibility of Surface Acoustic Waves Dispersion Measurements for Non-destructive Evaluation of Hydrogen Embrittlement in Cd-plated High Strength Steel ». Paper manuscript submitted to *Materials Evaluation* in May 2021.

Regarding the eddy current method, feasibility of employing a commercially available testing setup using a simple spot probe at 100-500 kHz working frequencies was investigated. Probe liftoff data were measured on several samples. Model-based CIVA® simulations using realistic physical properties of probe and sample were performed at 100 kHz and zero liftoff. Effects of variations in electrical conductivities of Cd and steel as well as relative permeability of steel were investigated. Results were compared to experimental data to assess hydrogen-induced variations in the aforementioned material properties. The outcomes of this investigation were included in chapter 4 in form of an article entitled as:

3) Hamidreza Shahmiri, Ehsan Mohseni & Martin Viens, « Application of Eddy Current Testing and Simulations for Non-destructive Evaluation of Hydrogen Embrittlement in Cd-plated High Strength Steel ». Paper manuscript submitted to *Journal of Nondestructive Evaluation* in May 2021.

Before presenting the research outcomes in the aforementioned manuscripts, chapter 1 provides the theoretical backgrounds of SAW and ECT methods along with a comprehensive and critical review of recent important publications related to this project. At the end of this dissertation, the conclusions will be presented.

CHAPTER 1

LITERATURE REVIEW

This chapter is dedicated to exploring basic concepts as well as reviewing publications related to the subject matter of this dissertation. The first section briefly introduces important notions, theories, and manifestations of hydrogen embrittlement followed by a review of the latest findings regarding IHE in Cd-plated, 4340 steel parts. The second section examines theoretical and technological backgrounds of surface acoustic waves. The third section discusses the basics and applications of eddy current testing and simulations followed by a review of recent literature regarding their application in NDE of HE.

1.1 Hydrogen embrittlement

1.1.1 Hydrogen states in metals

Hydrogen is adsorbed in metals and alloys in the form of molecule or ion and diffuses in the bulk after dissociating into atoms. The atomic hydrogen can either enter into preferred interstitial lattice sites of the crystal structure of a metal, or it can be trapped by defects. In solid solution, atomic hydrogen forms bonding with the host metallic ions by partial sharing of electrons. Solid solubility of hydrogen (θ) in iron depends on hydrogen gas pressure, temperature, crystal structure of metal, and alloying elements. The relationship between θ [atomic ratio] with hydrogen gas pressure p [0.1 MPa] and the temperature T [K] at equilibrium is governed by Sievert`s Law expressed as follows (Hirth, 1980):

$$\theta = 0.00185\sqrt{p}\exp(-3440/T) \tag{1.1}$$

The entry of hydrogen into metals induces an increase in local volume, expressed by molar volume of hydrogen $\bar{V}_H$ [$\mathrm{cm}^3/\mathrm{mol}$]. For α-iron, the hydrogen concentration in solid solution

C_h [atoms $-$ H. cm^{-3}] under hydrostatic stress σ_h [0.01 MPa] in elastic region at a constant hydrogen pressure is expressed as (Wriedt & Oriani, 1970):

$$C_h = C_0 \exp\left(\frac{\sigma_h \bar{V}_H}{RT}\right) \tag{1.2}$$

Where C_0 [atoms $-$ H. cm^{-3}] is the hydrogen concentration at zero stress and R [= 8.314 J. K^{-1}. mol^{-1}] is the ideal gas constant. equation (1.2) indicates that the hydrogen concentration in solid solution increases at stress concentrated areas such as root notches. Hydrogen concentration at a stress-concentrated area, e.g. ahead of a crack tip, can increase about 100 times by applying 2-5 GPa of hydrostatic tensile stress (Nagumo, 2016).

The equilibrium hydrogen concentration in a metal under standard conditions calculated from equation (1.1) is very low. In practice, however, the hydrogen present in material can be much higher due to trapping of hydrogen at various defects. Hydrogen tends to accumulate on high-energy sites within microstructure of a material. Applied stress and strain can increase hydrogen concentration by enhancement in trapping sites (Nagumo, 2016).

Hydrogen can move within a metal either by diffusion or by transportation via dislocations. The driving force for hydrogen diffusion is the concentration gradient of lattice hydrogen. The steady-state flow of hydrogen in a metal J_∞ [atoms $-$ H. $\mathrm{cm}^{-2}.s^{-1}$] is expressed by Fick`s first law of diffusion as follows:

$$J_\infty = -D_H \frac{dC}{dx} \tag{1.3}$$

Where D_H [$\mathrm{cm}^2.s^{-1}$] is the diffusion coefficient or diffusivity of hydrogen, C [atoms $-$ H. cm^{-3}] is the hydrogen concentration in metal, and x [cm] represents the position. In addition to lattice diffusion, hydrogen can be transported by dislocations. This is more important for steels at low temperatures, in which the hydrogen diffusivity is low (Nagumo, 2016).

1.1.2 Effects of hydrogen embrittlement on mechanical properties

Hydrogen embrittlement manifests in various mechanical testing of steels. In tensile tests, it appears as a premature fracture near the apparently elastic region. Degradation of tensile properties occurs mostly by weakly-trapped diffusive hydrogen, and strongly-trapped non-diffusive hydrogen is almost immune to degradation. Susceptibility of tensile specimens to hydrogen embrittlement depends on material, strain rate and test temperature. Manifestation of hydrogen embrittlement in tensile tests of mild steel has been more prominent at room temperature. At a constant test temperature, the fracture strain of mild steel tensile specimens decreases by decreasing the strain rate. (Nagumo, 2016).

Various fracture mechanics tests are employed for evaluation of the effect of hydrogen embrittlement on the toughness of material. Fracture toughness is usually expressed in terms of stress intensity factor (K). Hydrogen embrittlement can reduce the threshold stress intensity (K_{TH}) values. Internal hydrogen can also accelerate the crack growth during fatigue tests, thus reducing the number of cycles to failure substantially. Delayed fracture tests are also important for evaluating the degradation of mechanical properties of high strength steels by hydrogen. Delayed failure in steel occurs by controlled initiation and growth of a crack, both of which are controlled by interaction between H concentration and triaxial stress state. The incubation period is believed to be due to stress-induced diffusion of H to the point of crack initiation. The fracture time decreases by increase in the concentration of preserved hydrogen (Nagumo, 2016).

Effects of hydrogen on elastic behavior of materials is not well established. As stated before, the solid solubility of hydrogen in α-iron at room temperature is extremely low, and as a result, the hydrogen-induced changes in elastic moduli of iron are also small. However, measurements of shear modulus of hydrogen-charged polycrystalline α-iron in temperatures as low as 100 K has shown a decrease of about 8% in shear modulus of iron by 1 at. % hydrogen. A reduction in elastic modulus by increase in hydrogen content was also reported for a Ti - Mo alloy. On

the other hand, experiments on Tantalum, Niobium and Vanadium specimens demonstrated that their Young`s moduli increased linearly with hydrogen concentration (Nagumo, 2016).

Because of low hydrogen concentration at room temperature, the presence of various traps and different testing conditions, predicting the effects of hydrogen content on flow stress of iron and steels at various deformation stages is complicated. Effects of hydrogen on flow stress also depend on thickness and grain-size of specimens. Experimental results on various iron and steel specimens show both softening and hardening effects by solute hydrogen atoms. While softening is often associated with thin, high purity iron specimens at low temperatures, hardening by hydrogen is more frequently observed at room temperature for alloyed steel as well as thick pure iron specimens (Nagumo, 2016).

1.1.3 Microstructural analysis of hydrogen embrittlement

Understanding the effects of microstructures on hydrogen embrittlement is important for proper selection or design of materials against hydrogen degradation. Thermal and mechanical processing of materials induce various defects, and each defect interacts with hydrogen in its own way. The potential energy of hydrogen atom near defects is lower than usual lattice sites because of elastic and electronic interactions. Variations of hydrogen concentration around these defects and alterations assisted by hydrogen in their densities and structures, especially when the material is under stress, are important for understanding hydrogen embrittlement. Regarding the effects of hydrogen on dislocation mobility, widely different hypotheses have been proposed. Some studies pointed out that hydrogen increases dislocation mobility, while others emphasized impingement of dislocations by hydrogen atoms. However, dislocations are not the primary sites for hydrogen trapping, and other defects may play a more dominant role. For example, hydrogen can accumulate along grain boundaries. The role of voids or cracks on hydrogen embrittlement of deformed steels is also very important, since hydrogen in the bulk tends to concentrate in these areas in order to decrease its binding energy. Fine precipitates such as carbides and nitrides as trap sites for hydrogen are also crucial in hydrogen embrittlement of high strength steels. Grain size effects on hydrogen embrittlement are also

complex. However, it was shown that the critical stress intensity threshold for high purity 4340 steel subjected to HE improved by increase in grain size (Nagumo, 2016).

Fractographic features under hydrogen embrittlement are not uniform over the entire fracture surface. In most cases, there is a change over the crack path from Microvoid Coalescence (MVC) to Quasi-Cleavage (QC) and then to Intergranular (IG) features, which suggests a transition from ductile to brittle behavior. In other words, hydrogen suppresses the extension of plastic deformation on crack propagation and thus leads to strain localization. Hydrogen also causes strain localization through reduction of stacking fault energy. Strain localization areas, particularly intense slip bands on surfaces, can act as crack nucleation sites (Nagumo, 2016).

Internal strain and associated dislocation configurations are decisive for HE susceptibility of high-strength steels. Increase in tempering temperature of martensitic steels reduces the susceptibility to HE due to enhanced stability of substructures by decreasing the internal strain levels. This is achieved by more precipitation of excess dissolved carbon in form of carbide and recovery of dislocation structures. At the same strength levels, resistance to hydrogen-induced delayed fracture in bainite microstructure (QC dominant fracture surface) is higher than tempered martensite (IG dominant fracture surface) because of the differences in cementite formation sites (Nagumo, 2016; Bhadeshia, 2004).

1.1.4 Mechanisms proposed for hydrogen embrittlement

There is no universal agreement on mechanism of hydrogen embrittlement due to difficulties in detection of hydrogen behaviors and details of microstructural changes during hydrogen embrittlement. Various mechanisms have been proposed for HE. Since failure by HE is a mechanistic event, the proposed theories can be classified in two groups of brittle fracture models and plasticity dominated models. Brittle models examine the function of hydrogen on fracture of materials by considering crack extension through decohesion of atomic bonds or phases as a result of decreased cohesive strength by hydrogen. The plasticity-dominated

models, on the other hand, emphasize hydrogen-enhanced plastic instability at the tip of the crack, stating that hydrogen-assisted nucleation, growth, and linkage of fine-scale voids, even in macroscopically brittle specimens, leads to fracture. Each of these models assumes some parameters to fit theoretical and observed behaviors. For application of each model, the effects of hydrogen pressure and material microstructure should be considered (Nagumo, 2016). It is believed that instead of a single mechanism, a complex process involving many of the proposed mechanisms accounts for the degradation of the properties of steel by hydrogen (Hirth, 1980). In the next paragraphs, important theories for HE will be discussed.

Internal cracks named as “snowflakes”, “fisheye” or “white spots” are among the earliest known hydrogen-induced defects in steels. Internal pressure theory states that high internal pressure due to entry of molecular hydrogen causes cracking. This theory is based on Griffith`s criteria for brittle fracture. The Griffith condition for the initiation of brittle fracture from a crack of half-length $a$ [mm] in a solid of surface energy $\gamma$ [μJ/mm$^2$], Young`s modulus E [GPa] and Poisson`s ratio of ν in plane strain condition is given as:

$$\sigma_f = \sqrt{2E\gamma/\pi(1-\nu^2)a} \tag{1.4}$$

Where σ_f [MPa] is the fracture stress. For internal pressure theory, an incipient crack is a prerequisite for brittle fracture (Nagumo, 2016).

Griffith’s condition for brittle fracture does not specify the microscopic origin of the crack extension. Lattice decohesion theory states that the extension of crack proceeds by breaking atomic bonds at the crack tip, and instability occurs when the stress concentration at the tip of the crack exceeds the cohesive force between atoms. Based on that, an important mechanism of HE called hydrogen enhanced decohesion (HEDE) has been proposed. In HEDE, hydrogen reduces the cohesive strength between atoms at the crack tip and thus promotes brittle fracture (Nagumo, 2016). In excellent agreement with this theory, measured values for critical stress intensity factor in crack-opening loading mode, K_{IC} [Mpa.m$^{0.5}$] of hydrogen-charged AISI 4340 steel were shown to be a decreasing function of hydrogen at the position of maximum

tensile stress (Oriani & Josephic, 1974). HEDE is more frequently associated with high strength steels subjected to HE because of the IG features observed on fracture surfaces (Bellemare *et al*, 2020 [I]).

Hydrogen enhanced localized plasticity (HELP) states that hydrogen in solid solution increases dislocation activity and expands a plastic zone ahead of the crack tip. The role of hydrogen on stabilization of lattice defects is predicted by the defect acting agent (DEFACTANT) mechanism. Developed based on HELP, this mechanism emphasizes on reduction of activation energy of dislocation sources and also facilitation of kink pair formation by hydrogen. Another theory proposed based on interplay between HELP and HEDE mechanisms suggests that hydrogen transported by activated dislocations causes decohesion at grain boundaries or martensite lath boundaries (Nagumo, 2016).

It is proposed that adsorbed hydrogen enhances the injection of dislocations from crack tip and promotes the coalescence of the crack with voids ahead of the crack. In adsorption-induced dislocation emission (AIDE) mechanism, hydrogen at subsurface sites contributes to bond - weakening. It is also assumed that void nucleation occurs at small and large particles in sites of localized strain such as around crack tips, intersections of slip bands or dislocation-cell boundaries (Nagumo, 2016).

Hydrogen-enhance strain-induced vacancy (HESIVT) theory states that hydrogen enhances strain-induced creation of vacancies leading to premature fracture. Stabilization of excess vacancies by hydrogen through forming clusters decreases the stress carrying capacity of material. These clusters may also act as void sources (Nagumo, 2016).

1.1.5 Internal hydrogen embrittlement in case of Cadmium-plated 4340 steel

This section is dedicated to a review of two newly published articles by the peers involved in DPHM-601 that were directly related to the subject matter of this dissertation. These works

investigated fracture mechanics tests, TDS, and fractography on Cadmium-plated 4340 steel samples subjected to HE.

The main ideas behind the first paper (Bellemare *et al*, 2020 [I]) were to investigate hydrogen embrittlement in Cd-plated, notched-steel bars manufactured under various conditions (different plating current densities, different baking delays and different stripping geometries), to assess the contribution in HE of hydrogen present in different regions (steel, Cd coating, and MnS traps), and to establish a critical hydrogen concentration as an embrittlement threshold. These tasks were carried out by means of sustained-load tests (SLT), TDS, and microscopic observation of fracture surfaces as well as coating morphology. SLT notched-bar samples were made from AISI 4340 steel heat-treated to a tempered martensite microstructure The notched bars were electroplated in a Cd bath after surface preparation in different conditions: embrittled samples (ES) were plated at a current density of 10.8 $mAcm^{-2}$ for 30 minutes and non-embrittled samples (NES) were plated at 70 $mAcm^{-2}$ for 6 minutes. The fracture surface of broken specimens were examined by a scanning electron microscope (SEM). The Cd coating surface and its cross-section were also studied by SEM. After SLT, TDS tests were carried out on the notched bars. It was assumed that the hydrogen in steel was uniformly distributed.

The results and conclusions obtained by Bellemare *et al* are summarized as follows: 1) SLT: None of the NES specimens broke. Among ES specimens, two specimens broke before 200 hours with different times to failure. Other ES samples all sustained the load for 200 hours. 2) Fracture surfaces: both IG zones and mixed-mode zones were observed. The extent of IG zones were highly variable among the broken samples. 3) Cadmium coating morphology: While the coating for NES was highly porous, the coating for ES was more compact although it still showed some porosity. 4) TDS results: There was ambiguity in determination of the source of the first peak (around 300℃). The authors mentioned that this peak seems to come from the evaporation of Cd coating during TDS when hydrogen in both the Cd coating and the weak traps (dislocations and grain boundaries) leaves the samples. There was surprizing variability in total hydrogen concentrations measured for ES specimens. Most notably, one of the ES specimens, that did not show HE according to SLT results, had a higher average total hydrogen

concentration than a broken specimen. It was found that hydrogen in both Cd coating (high concentrations ranging from 200 to 1500 ppma) and MnS traps did not contribute to HE. No impact of the baking delay on the baking efficiency was found. By subtracting the hydrogen concentrations in Cd and MnS traps from total hydrogen concentration, a true critical threshold of 0.6 ppma (0.01 ppmm) was found.

The second paper is entitled "Internal hydrogen embrittlement of pre-cracked, cadmium-plated AISI 4340 high strength steel with sustained load tests and incremental step-loading tests" (Laliberté-Riverin *et al*, 2020[I]). In the introduction of this paper, the authors mentioned the costly baking process, the efficacy of which is subjected to controversy especially when a long delay between electroplating and baking is involved. They also mentioned the drawbacks of 200-hours sustained-load tests for determination of HE, most notably the complexities in interpretation of results based on a fracture mechanics approach that arise from the sample geometries. Their study was aimed at determining for the first time the K_{TH} for IHE in the as-plated conditions. For this purpose, they employed incremental step loading (ISL) tests. The embrittled samples were produced by omitting the baking process, and the embrittlement status in these samples was confirmed by SLT tests. Effect of a 100-hour delay between electroplating and baking was studied. TDS tests were also used to gain insight on the location of hydrogen as well as calculation of trap energies and concentrations.

Blanks for machining were extracted from an AISI 4340 billet of 3.5-inch diameter. Heat-treated blanks were used to machine samples for fracture mechanics tests (notched bar samples for SLT and CT samples for ISL tests). Machined parts were stress-relieved. Then, after surface preparation, the parts were electroplated with Cd at current density of 10.8 mA/cm^2 for 30 minutes, some of which were immediately-baked (IB), some baked after 100 hours delay (LB) and some were not baked (NB) to create different HE susceptibilities. Baking was done at 190 ºC for 24 hours. Samples that broke during fracture mechanics tests were later used for fractography as well as extraction of TDS specimens. Finally, microscopy techniques were used to characterize the Cd coating. The Cd coating exhibited a dense deposit with some small voids as well as features of a hexagonal close packed (HCP) crystal structure. Please note that

the manufacturing conditions of the samples (except the geometry) were similar to those used for NDE experiments in the present dissertation.

SLT results showed the HE susceptibility of the AISI 4340 steel in the NB manufacturing condition. However, the fracture loads varied among samples. This could suggest, as was the case for the previous paper (Bellemare *et al*, 2020 [I]), that there were variations in hydrogen concentration and/or base-material properties among SLT-NB samples that could affect their degree of embrittlement. In line with this hypothesis, TDS results on two SLT-NB samples showed widely different total hydrogen concentrations of 0.812 and 0.671 μmol.mol^{-1}, while for other ISL samples in LB or IB conditions, there was a small variation between 0.237-0.285 μmol.mol^{-1}. Similar to the previous paper (Bellemare *et al*, 2020 [I]), fracture surfaces of NB samples exhibited IG features of varying sizes near the crack initiation site, where no discontinuities or second-phase particles could be found.

ISL tests were performed on fatigue pre-cracked CT samples according to various loading plans and preloading conditions. The data obtained were analysed to calculate K values and the lowest value would indicate the K_{TH}. Unlike SLT, the results of ISL for samples of different manufacturing conditions were highly variable and inconclusive. More specifically, among 6 NB samples only two showed clear signs of embrittlement (occurrence of subcritical crack growth and presence of IG zone). Surprisingly, TDS results from ISL samples showed lower average total hydrogen concentration for ISL-NB than ISL-IB and ISL-LB. The authors argued that total hydrogen concentration is not a good predictor for HE. No particular trend was observed during ISL in K values compared to manufacturing conditions or load rate. No threshold for the onset of HE (K_{TH}) was determined in this paper (Laliberté-Riverin *et al*, 2020[I]). In a separate study based on HELP-mediated HEDE mechanism for HE, the authors used the size of observed IG zones on broken SLT specimens in combination with finite element analysis to obtain a K_{TH} value of 9 MPa.m$^{0.5}$ for Cd-plated, 4340 steels (Laliberté-Riverin *et al*, 2020[II]).

After analysing TDS curves for both SLT and ISL samples, the authors concluded that the concentration of hydrogen in or close to the coating (exact location not specified), referred to as $C_{H,Cd}$, is a reliable predictor for HE between baked and not baked samples. The authors proposed that hydrogen in or close to the coating in NB samples could indeed migrate during loading to areas of high stress concentrations and cause HE. The main difference between SLT and ISL samples was that for the former hydrogen had to migrate from coating up to 150 to 200 μm, while in the latter it had to migrate 6.4 mm to reach the tip of the notch. Finally, it should be mentioned that no evidence was found to distinguish between late-baked and immediately baked samples, in line with the conclusions from the previous work (Laliberté-Riverin *et al*, 2020[I]).

1.2 Ultrasonic surface waves

1.2.1 Brief introduction to ultrasound

Ultrasonic waves are high frequency acoustic waves vibrating above the audible frequency spectrum of human ears, i.e. 20 kHz. These waves induce small, periodic stresses which result in reversible deformation of a material in the elastic region. Ultrasound offers some features that make it attractive for NDE applications. It can be produced by sources that are inexpensive, sensitive, and reliable. Compared to electromagnetic waves, ultrasound travels much slower, which provides a way to display information in time, create variable delay and so on. Moreover, ultrasound easily penetrates opaque materials which makes it a very desirable tool to probe and image the interior of opaque objects. UT is widely used in industry for detecting and characterizing flaws in components, measuring dimensions of parts, and evaluating changes in material properties. It is generally conducted via analysing the amplitude and position of indications (e.g. presence of a back-scattered signal) or assessing changes in ultrasound properties with the aide of signal processing techniques. Two basic features of an ultrasonic wave are its velocity and attenuation coefficient, which depend on the physical properties of the material in which it propagates. There are two main types of an ultrasonic wave that can propagate in bulk of a material: longitudinal or pressure wave and transverse or

shear wave. For a longitudinal wave, the stress of the periodic compression and rarefaction of the particles is along the direction of propagation. In the transverse wave mode, particles move perpendicular to the direction of wave propagation through periodic shear motions. There are also other modes of ultrasound, most notably surface ultrasonic (Rayleigh) waves and Lamb waves, that are guided by physical boundaries of the structure in which they propagate. Despite their complex physics, guided wave modes are attractive for specialized NDE applications because of their unique features (e.g. minimal loss of energy during propagation and the ability to follow curved paths) (Shull, 2001; Cheeke, 2012; Bar-Cohen *et al*, 2003).

Most ultrasonic waves can be described in terms of harmonic (sinusoidal) waves. A harmonic wave has the following characteristics: period of time τ [s]; wavelength (period of space) λ [m]; linear temporal frequency (or simply frequency) $f = 1/\tau$ [s^{-1}]; angular temporal frequency $\omega = 2\pi f$ [rad/s]; angular spatial frequency (or wavenumber) $k = 2\pi/\lambda$ [rad/m]; and wave velocity $V = f\lambda = \omega/k$ [m/s]. Wave equations describe changes in displacement or pressure due to acoustic wave propagation in time and space. Most conveniently in case of a longitudinal wave mode propagating in a one dimensional (x) solid, acoustic wave equation can be derived by equating the expressions for the force obtained from Hooke's law, which describes linear elasticity, with that of Newton's second law of motion.

For a planar wave propagating in a one-dimensional, homogeneous, isotropic material, the longitudinal (L) and shear wave (S) speeds in [m/s] can be derived from wave equations as:

$$V_L = \sqrt{E/\rho} \tag{1.5}$$

$$V_S = \sqrt{\mu/\rho} \tag{1.6}$$

respectively, where ρ [kg/m^3], E [Pa] and μ [Pa] are material`s density, Young`s modulus and shear modulus. For solid materials, $V_L \approx 2V_S$. In practice, ultrasonic inspection is conducted using three-dimensional bulk waves. The difference between one-dimensional waves and bulk

waves in longitudinal mode is that the Poisson`s effect must be considered in the bulk waves. (Shull, 2001; Cheeke, 2012).

When an ultrasonic wave encounters a boundary between two media with different physical properties, it may change in one or more of the following ways: A reflection and/or transmission, a change in direction of travel (refraction), and a conversion from one type of wave to another (mode conversion). For prediction of how the direction, amplitude, and mode of a wave changes when it interacts with a boundary, the angle of incidence, the acoustic impedances of the two media, and the boundary conditions (continuity of particle velocity, acoustic pressure, and phase of the wave) shall be considered. When an ultrasonic wave is incident at right angle on an interface between two mediums, only transmission and reflection occur. At an oblique incidence, however, mode conversion and refraction must also be considered. Acoustic impedance is a measure of opposition to acoustic flow, which dictates the relationship between acoustic pressure and particle velocity (Shull, 2001; Cheeke, 2012).

During ultrasonic inspection, the intensity of a received ultrasonic beam may be considerably less than the intensity of initial transmission, due to loss of beam energy, which is quantified by attenuation coefficient. Attenuation occurs by a number of factors, including absorption, scattering, and beam spreading. The overall attenuation of an ultrasonic waves travelling a distance Δx [m] can be expressed mathematically by a logarithmic relationship as:

$$8.686\alpha\Delta x = \alpha_{dB/m}\Delta x = 20\log\left(\frac{P_0}{P}\right) \tag{1.7}$$

Where α is the attenuation coefficient in nepers per meter [Np/m], $\alpha_{dB/m}$ is the defined attenuation coefficient in decibels per meter [dB/m], P is measured acoustic pressure amplitude at a distance Δx from the initial measurement point, and P_0 is the initially measured acoustic pressure amplitude (Shull, 2001).

Piezoelectric transducers are the most common method for generation and detection of ultrasonic waves. These transducers generate ultrasonic waves by indirect piezoelectric effect,

in which certain materials undergo mechanical vibrations when subjected to an alternating voltage. Piezoelectric transducers can also detect ultrasonic waves by converting them to measurable electrical pulses (direct piezoelectric effect). Piezoelectric transducers may be normal beam or angled beam, where angled beam transducers are usually longitudinal normal transducers attached to a wedge typically made of acrylic plastic. The plastic wedge must be designed to reduce or eliminate internal reflections that could result in false echoes. Ultrasonic transducers are characterized by several factors, most importantly: a) frequency response; b) near field and far field; and c) beam divergence.

1.2.2 Ultrasonic surface waves

Ultrasonic surface waves, also known as SAW, Rayleigh waves, or simply surface waves, were first discovered by Lord Rayleigh in 1885. The unique characteristic of these waves is a combination of longitudinal and shear waves. Rayleigh waves are a simple case of guided waves, and their effective energy are confined to about one wavelength beneath the material`s surface. They are mechanical waves travelling along an interface between a semi-infinite, solid medium and air. Rayleigh waves can travel long distances and follow curved paths on the surface of an object. They have very low attenuation on solids. However, these waves leak energy into liquid couplants (Shull, 2001).

Surface waves possess unique characteristics that make them useful for some very specialized inspection problems. They are of great value in NDE applications when we must inspect the surface or near-surface region of a part. Rayleigh waves can be attenuated by lattice imperfections, roughness, grain boundaries, and all the defects that can attenuate bulk waves. Defect detection in material surface coatings, layers, or surface modifications is best carried out with Rayleigh waves. Scattering of Rayleigh waves by defects such as cracks, voids and delamination in these structures is analogous to the bulk wave situation, so that a defect echo could be detected by pulse echo studies. Leaky SAW is also suited for determination of elastic constants and density through acoustic microscopy (Cheeke, 2012). However, surface roughness can of course limit the travel capability of Rayleigh waves and generate significant

competing noise in received Rayleigh wave signals (Schmerr, 1998). Moreover, in actual inspections, the additional reflections occurring at sharper corners may also cause some difficulties (Bray & Stanley, 1997). The surface disturbance due to passage of a Rayleigh wave is confined in a layer of thickness of order one wavelength (λ_R). The displacement, while actually very small, is retrograde at the surface and progressive lower down (Cheeke, 2012). For NDE applications the detection of transverse (u_z) displacements due to SAW are preferential to that of longitudinal (u_x) displacements.

The velocity of a Rayleigh wave, V_R, is approximately given by (Cheeke, 2012):

$$\frac{V_R}{V_S} \cong \frac{0.87+1.12\nu}{1+\nu} \tag{1.8}$$

where V_S and ν are shear wave velocity and the Poisson`s ratio of the material, respectively.

1.2.3 SAW dispersion

Since the penetration depth of SAW is frequency-dependent, different depths of the surface region can be sampled by the SAW signal as the ultrasound frequency is varied. In a multi-layered structure or a structure with depth-dependent properties, the inspected material at each frequency possess a different set of elastic properties and/or density, hence the SAW velocity and attenuation will be different. This phenomenon, known as dispersion, is not unique to SAW but can be observed in other acoustic wave modes as well as electromagnetic waves (Cheeke, 2012). Known gradients of properties can be used to predict the dispersive behavior of SAW, which is classified in NDE as a forward problem (see for example Gordon *et al*, 1993). On the other hand, experimental SAW dispersion curves can be fit with analytical, semi-analytical, or numerical models in order to obtain depth-dependant variations in properties for an inhomogeneous sample, which is classified in NDE as an inverse problem (see for example Szabo, 1975). In case of surface-treated metals such as a cold-worked or electroplated structure, the measured dispersion of the surface wave arises from material effects of surface treatments (presence of coating, microstructural changes, residual stresses, etc) (Ruiz & Nagy,

2004). One of the main challenges during NDE of material using SAW dispersion measurements is the accuracy of measurements. This is because variations of SAW velocity due to material surface modifications are often very small, typically less than 1% (Safaeinili *et al*, 1997; Ruiz & Nagy, 2004).

For numerical modelling of SAW dispersion in a multi-layered media, variants of transfer matrix method (e. g. global matrix method or δ-matrix method) which are computationally efficient and stable are usually employed (Schmidt & Tango, 1986; Wang & Rokhlin, 2001; Goossens *et al*, 2007; Singer & Kufner, 2017). A description of a transfer matrix method will be reproduced based on that given by Singer & Kufner (2017) as follows: Assuming a material with *n-1* layers stacked on a semi-infinite half-space (*n-th* layer), the displacement and stresses due to propagation of SAW at the top of layer m ($m < n$) can be related to the displacements and stresses at the bottom of this layer according to

$$W_{m,m} = E_m . W_{m,m-1} \tag{1.9}$$

Where W is a row vector that represents the displacements and stresses at layer interfaces, and E is the layer matrix, the entries of which can be constructed from elastic constants or alternatively from longitudinal and shear velocity components. Using the matrix product:

$$F = E_1 . E_2 . \ldots . E_n \tag{1.10}$$

a connection between the displacements and stresses at the top of the half space and at the top of the multilayer system can be established:

$$W_{n,n} = F . W_{1,0} \tag{1.11}$$

By substituting stress-free boundary conditions into equation (1.11), a set of four equations can be obtained. This set of equations is rearranged in terms of the unknown amplitude factors of the wave solutions. From the resulting coefficient matrix, the characteristic determinant can be

calculated, the roots of which yield the SAW velocity at a given frequency. Of course, there are considerable subtilities in the formulation of entries of transfer matrix. They will be found in the previously mentioned publications. Alternatively, SAW dispersion curves can be simulated using a semi-analytical finite element (SAFE) method, the details of which can be found in literature (Marzani *et al*, 2008).

A simple analytical model for dispersion of SAW in a medium with depth-dependent properties with continuous profiles have been proposed by Balogun & Achenbach (2012). This model was for the special case where "the dependence of the elastic properties is vanishingly small such that the corresponding first derivatives are negligibly small compared to other terms.". For an isotropic solid with depth (z) dependent density $\rho(z)$ and elastic properties $\lambda(z)$ and $\mu(z)$, with depth profiles $\lambda(z) + 2\mu(z) = (\lambda_0 + 2\mu_0)f(z)$, $\mu(z) = \mu_0 g(z)$, $\rho(z) = \rho_0 h(z)$, the dispersion relation is as follows (Balogun & Achenbach, 2012):

$$\left\{\frac{\left(\frac{V_R}{V_{L0}}\right)^2}{1-\left(\frac{V_R}{V_{L0}}\right)^2}(f_1 - h_1) + 4k\left[1 - \left(\frac{V_R}{V_{L0}}\right)^2\right]^{1/2}\right\} \times \left\{\frac{\left(\frac{V_R}{V_{S0}}\right)^2}{1-\left(\frac{V_R}{V_{S0}}\right)^2}(g_1 - h_1) + 4k\left[1 - \left(\frac{V_R}{V_{S0}}\right)^2\right]^{1/2}\right\} - 4k^2\left[2 - \left(\frac{V_R}{V_{S0}}\right)^2\right]\left[2 - \left(\frac{V_R}{V_{S0}}\right)^2\right] = 0 \tag{1.12}$$

where k is the Rayleigh wave number, V_R is the Rayleigh wave velocity, V_{L0} and V_{S0} are longitudinal and shear wave velocities at surface (depth z = 0), and f_1, g_1 and h_1 are first-order derivatives of $f(z)$, $g(z)$ and $h(z)$. Equation (1.12) is only valid for a simplified high-frequency approximation, in which stresses vanish at the surface. According to Balogun & Achenbach (2012), this equation showed good compatibility with numerical results.

SAW phase-velocity dispersion curves can be measured experimentally from signals obtained during line scans with consecutive changes in distance between SAW source and detection spots. This can be achieved using either a phase spectral analysis (Singer & Kufner, 2017) or a two-dimensional FFT (Goossens *et al*, 2007). These methods will be further elaborated with

reference to their applications in section 1.2.6. It suffices to say here that for either of these methods, a relatively broad-band ultrasound pulse detected at numerous points with sufficiently small distances using an adjustable laser detection system is preferred to achieve desirable accuracy levels.

1.2.4 Methods for generation and detection of SAW

In this section, common methods in the field of NDE for generating Rayleigh waves will be reviewed. These techniques are restricted to low-frequencies ($\leq$ 30 MHz) for various reasons, most notably because at higher frequencies industrial quality surfaces would scatter and attenuate Rayleigh waves (Cheeke, 2012). The simplest and most commonly used technique for generating and detecting surface acoustic waves is wedge method. In this method, piezoelectric transducer producing longitudinal waves is placed on the surface of a wedge coupled to a solid. The angle of the wedge needs to be set to the optimum angle for generation of SAW, known as the Rayleigh angle (θ_R). According to Snell`s law, θ_R is given by:

$$\theta_R = \sin^{-1}\left(\frac{V_w}{V_R}\right) \tag{1.13}$$

where V_w and V_R are the longitudinal wave speed in the wedge material and the Rayleigh wave speed in the inspected material, respectively. The prerequisite for the wedge method to work is that the Rayleigh velocity in the specimen must be greater than the wave velocity in the wedge ($V_w < V_R$). The wedge method is the most efficient approach for generation of surface waves that will propagate unidirectionally. It is also possible to use a longitudinal transducer immersed in water, which acts as the wedge material, to generate SAW. This method eliminates the problems inherent of contact techniques. However, surface waves will rapidly leak into the immersion tank fluid and do not travel far distances (Shull, 2001).

Ultrasonic surface waves can also be generated by creating a longitudinal wave straight into a solid by simply placing a longitudinal, normal beam transducer on the specimen surface (Shull, 2001). However, a considerable portion of the initial ultrasound wave energy is leaked into the

specimen in form of longitudinal wave. It is also possible to place a longitudinal wave transducer on the edge of a rectangular specimen to generate unidirectional ultrasonic surface waves (Bar-Cohen *et al*, 2003).

Another possibility is to use a periodic comb-like exciter. A comb structure is built on a metallic plate with an array of parallel grooves. A longitudinal piezoelectric transducer is then placed on the back of this comb structure, and the whole configuration is pressed against a test sample (Bar-Cohen *et al*, 2003). In this method, twice the gap spacing should equal the Rayleigh wavelength for the Rayleigh waves to add constructively, while the bulk waves add destructively (Shull, 2001). The disadvantage of this method is that only a small portion of the initial ultrasound energy is transformed into surface wave and the rest is leaked in the form of longitudinal wave. Moreover, unlike the wedge method, the surface wave generated with this method is bidirectional (Penttinen & Luukkala, 1974; Danicki, 2000). Finally, interdigital transducers (IDT) can be used to generate and receive SAW. An IDT device consists of two interlocking comb-shaped arrays of metallic electrodes deposited on a piezoelectric substrate. The use of IDTs in the field of NDE is not considered practical (Cheeke, 2012).

EMATs have been used for generation and detection of ultrasonic surface waves. A surface wave EMAT configuration usually consists of a meander-line coil and a vertical magnetic field (Kang *et al*, 2013). EMAT method is inherently a non-contact method, which is not affected by the geometrical irregularities of the specimen surface. There are ongoing investigations to improve the performance of EMATs (Kang *et al*, 2013).

Another possibility for generation and detection of SAW is the laser method. When a laser pulse is focused on the surface of a solid material for a few nanoseconds, it can produce an elastic pulse resulting in generation of ultrasonic surface waves along with bulk waves through thermoelastic (low-energy pulse) as well as ablative interactions (high-energy pulse). Although laser-based generation of SAW can produce extremely wide-band, omnidirectional signals, there are concerns regarding the damage that the laser pulse can impose to thin coatings. Laser-based detection of ultrasonic vibrations is commonly carried out using an interferometry

method. Interferometry techniques employ the principle of optical interference to recover acoustic information from the light reflected from or scattered by a surface subject to ultrasonic vibrations (Shull, 2001). A laser vibrometer is generally a two-beam laser interferometer that measures the frequency (or phase) difference between a reference beam and a test beam. Laser-based detection of SAW for NDE applications have been investigated by several researchers (Duquennoy *et al*, 2001; Ruiz & Nagy, 2004; Longo *et al*, 2010). These works demonstrated the high accuracy of laser-based SAW measurements without typical issues inherent to contact techniques. However, they mentioned the requirement of polished and shiny surfaces as well as high sensitivity to environmental vibrations as the main disadvantages. An important example of laser vibrometers for the field of NDE is laser Doppler vibrometer (LDV) that has been used for spatial scanning of SAW (Longo *et al*, 2010). Helium-neon lasers (633 nm, red beam) are the most commonly integrated in LDVs.

1.2.5 Use of SAW for NDE

Publications related to the use of SAW for non-destructive detection of hydrogen and evaluation of its effects are very limited in number. However, as will be discussed in the following paragraphs, these works illustrate the sensitivity of both SAW attenuation and velocity to effects of dissolved hydrogen (Zielinski & Fiore, 1982; Ye *et al*, 2013).

Zielinski & Fiore (1982) studied time-dependent dislocation pinning by hydrogen atoms in face centered cubic (FCC) stainless alloys using an immersion SAW technique. The surface wave attenuation between 6 and 7 MHz was continuously measured during and after H charging. Results showed that H charging reduced attenuation coefficient in time, the extent of which was increased by charging current density. This trend was reversed during H egress. The measured attenuation during H-charging may come from changes to material surface conditions induced by the cathodic charging process in addition to the damping effect of dislocation-pinning by hydrogen atoms. For the case of H egress, however, the changes in attenuation was predominantly due to dislocation damping. An analytical model proposed by Granato-Hikata-Lucke was used to describe dislocation damping by hydrogen atoms. The

authors further confirmed the validity of their analytical model with experimental data. They concluded that "ultrasonic surface waves provide an excellent tool for the study of H ingress or egress *in situ*". Ye *et al* (2013) investigated NDE of hydrogen embrittlement in AISI 304 stainless steel specimens using SAW velocity measurements as well as bulk longitudinal ultrasound velocity measurements. The specimens were H-charged for various times at cathodic current density of 50 mA/cm^2. SAW and bulk wave measurements were performed on the length and through thickness dimensions, respectively. Evidence from XRD, SEM, and hardness tests demonstrated that martensite transformation occurs within the subsurface region of the specimens. SAW wave measurements showed that SAW velocity decreases significantly with cathodic charging time. This was ascribed primarily to elastic modulus reduction resulting from hydrogen-induced phase transformation in the subsurface region. The decrease in SAW velocity at 10 MHz was more pronounced than 5 MHz (more penetration depth). This was because the region immediately beneath surface had higher hardness than deeper regions. Unlike SAW, ultrasonic bulk longitudinal wave measurements did not show any changes in velocity with hydrogen charging time. This was because hydrogen-induced changes in microstructure were concentrated in near-surface regions, where the SAW propagates. The authors concluded that unlike bulk wave modes, SAW velocity measurements are sensitive to effects of hydrogen concentrated in surface regions of H-charged stainless-steel specimens.

Evaluation of the properties of SAW propagating on solid media has been carried out, among other things, for solving various NDT problems. The potential of SAW-based methods have been investigated for detection, characterization, and monitoring the evolution of fatigue cracks and surface damage (Warren *et al*, 1996; Herrmann *et al*, 2006; Longo *et al*, 2010; Connolly & Rokhlin, 2013), evaluation of microstructure and assessment of material deterioration phenomena (Gao *et al*, 2001; Doerr *et al*, 2017), coating thickness measurements (Lakestani *et al*, 1995), depth profiling of materials with near-surface gradient of properties (Glorieux *et al*, 2000; Goossens *et al*, 2007), evaluation of the effects of surface treatments such as changes in roughness, residual stresses and cold-work effects (de Billy *et al*, 1987; Duquennoy *et al*, 2001, Ruiz & Nagy 2004), and determination of surface hardness gradients (Gordon *et al*, 1993; Safaeinili *et al*, 1997; Singer & Kufner, 2017). Results of these

investigations demonstrate the sensitivity and reliability of SAW-based NDE methods while showing the experimental procedures and research trends in this field. In the following paragraph, a few recent examples of the applications of SAWs will be briefly introduced.

Ruiz and Nagy (2004) investigated SAW velocity dispersion on shot-peened aluminum surfaces. They used a highly-accurate method for obtaining dispersion curves (more than 0.1% accurate) based on piezoelectric-generation in 2-15 MHz spectrum and laser detection of ultrasound by slow stepwise scanning in the direction of propagation. The resulting curves indicate clearly that SAW dispersion increases with shot-peening intensity, primarily due to increase in surface roughness and partly through other material effects including compressive residual stresses and cold-work effects. Longo *et al* (2010) used a SAW-based method for sizing of surface-breaking cracks of different sizes in a steel beam (crack depths of 0.2, 0.3 and 0.4 mm) as well as a fatigue crack (depth of 1 mm) in an aircraft component. SAW were generated using a wedge method (4 MHz center frequency) and detected using an LDV with a slow scan (100 points) on a 2 cm line where the crack was positioned in the middle on the line. Sizing was carried out using signals with good SNR by fitting the parameters of the theoretical model for the low pass filtering effect of a crack on the transmitted waves. Average estimated depths for the cracks were 0.16, 0.25, 0.37, and 1.04 mm, which indicate the high sensitivity of the method for sizing cracks with depths larger than 0.4 mm. Singer and Kufner (2017) used an inversion algorithm for SAW-velocity dispersion curves in order to non-destructively determine hardness gradients in gas-carburized steel. The inversion algorithm can be summarized as follows: First, hardness profiles were estimated by a model developed based on the solution to Fick's second law of diffusion. Then, these profiles were discretized in a layered model. After that, SAW dispersion curves were calculated from the model via a modified transfer matrix method. Next, simulated dispersion curves were fitted to the experimental ones by changing model parameters. Finally, numerically obtained hardness profiles were compared with those measured by Vicker's method for verification. Experimental SAW measurements were carried out with an all-laser method. The hardness profiles estimated from the inversion algorithm exhibited excellent agreement to Vicker's tests.

1.3 Eddy current

Eddy current testing is a low-cost NDE method based on electromagnetic induction. It is used for inspection of surface and sub-surface regions in conductive materials. A simple ECT setup consists of a driver-pickup coil connected to an alternating current (AC) source. The electrical current flowing in the coil generates a primary magnetic field. When this field is coupled to a conductive material (e.g. by placing the coil near a metal part), eddy currents are induced due to Faraday's law of induction. According to Lenz's law, eddy currents are generated in such a way to create a secondary magnetic field that opposes the primary magnetic field. Changes in the net magnetic flux through the coil, for example by presence of defects, can in turn change the electrical impedance of the coil. Changes in the coil impedance can then be evaluated for non-destructive examination of the inspected material. The density of eddy currents depends on the proximity of the coil to the test piece (lift off), test frequency (ω), as well as electrical conductivity (σ) and magnetic permeability (μ) of the inspected material. The penetration depth of eddy currents (i.e. skin depth) decreases with increase in ω, σ and μ (Shull, 2001).

The eddy current sensors respond to a number of parameters, namely conductivity, magnetic permeability, liftoff, conductor thickness, and probe and sample geometry. However, this set of parameters provides a wide range of useful information about conductive materials. ECT is a mature and proven technology for inspection and maintenance of metallic parts and structures in chemical, power, automotive and aerospace industries. It is used widely for accurate thickness measurements (tube wall-thickness, sheets thickness, thin-film thickness, etc.), material identification, detection of inclusions and discontinuities, microstructural evaluation after heat-treatments, determination of the depth of case hardening, and so on (Shull, 2001). In the next paragraph, recent works on NDE of HE using ECT by Koenig *et al* (2010), Zhou *et al* (2018), and Bellemare *et al* (2020, [II]) will be reviewed. This review is presented here to demonstrate the feasibility of using ECT for detection of hydrogen and its effects in high strength steels, while identifying the challenges and limitations faced during the experiments.

Koenig *et al* (2010) used low-frequency impedance measurements based on ECT to detect and monitor hydrogen content in pipeline steel. They measured the impedance of encircling coils wrapped around X80 cylindrical steel specimens at f = 100 Hz. Results indicate that coil impedance increases with increasing hydrogen content with good sensitivity. It was argued that dissolved hydrogen increases the resistivity of steel. Zhou *et al* (2018) applied ECT for characterization of HE in 2.25Cr-1Mo-0.25V steel alloy. To induce different degrees of embrittlement, samples were hydrogen charged at a high current density for various periods. ECT was performed at 10 kHz frequency using two spot probes, one on the measured sample and one on the reference sample. For each sample, measurements were compared in H-charged and not-charged conditions. According to the results, ECT signal amplitude increased with H content until it reached a saturation point. The authors concluded that ECT could be applied in NDE of HE in the studied steel. Bellemare *et al* (2020, [II]) investigated ECT for NDE of HE in Chromium-plated, notched-bar samples using encircling coils at operating frequencies of 10 Hz to 100 kHz. Samples were electroplated at a high current density for a few hours, then were progressively baked at a wide range of temperatures and times to produce various hydrogen concentrations. Hydrogen concentrations in coated and stripped samples were evaluated by TDS. Results showed that ECT impedance measurements were not sensitive to hydrogen content.

CHAPTER 2

Non-Destructive Evaluation of Electroplating-induced Hydrogen Embrittlement in Cd-coated High Strength Steel Using Ultrasonic Surface Waves

Hamidreza Shahmiri[a] & Martin Viens[a]

[a] Department of Mechanical Engineering, École de technologie supérieure (ÉTS),
1100 Notre-Dame Street West, Montréal (Québec), H3C 1K3, Canada

Paper manuscript submitted to *Materials Evaluation*, April 2021

Abstract

Development of a nondestructive evaluation (NDE) method to detect nascent hydrogen embrittlement (HE) in electroplated high strength steel parts is becoming important for aerospace industry. This research investigates the feasibility of surface acoustic waves (SAWs) measurements to distinguish between cadmium (Cd) plated SAE 4340 steel samples with low and high HE susceptibilities. SAWs were generated with a 10 MHz piezoelectric transducer and detected by line scans via a laser Doppler vibrometer (LDV) setup. Using signal processing algorithms in MATLAB®, SAW velocities as well as attenuation coefficients were estimated. Depth profiles of steel hardness near coatings were also evaluated using Vickers microindentation tests. Average steel hardness in not-baked samples was slightly increased. Cd coatings were characterized by laser and optical microscopy methods. Small variations found in thickness and surface roughness of the Cd-coatings among the samples did not significantly affect the NDE results. On average, samples in not-baked condition (high HE risk) exhibited lower SAWs attenuation coefficients compared to immediately-baked and late-baked conditions (low HE risk). However, it was not possible to distinguish between the manufacturing conditions of individual samples due to overlaps in attenuation measurement results. SAW velocities as estimated by cross-correlation method were found not sensitive to manufacturing conditions.

2.1 Introduction

Hydrogen embrittlement (HE) is a serious problem for structural materials, particularly for high strength steels, which may lead to sudden failure of industrial components (Sriraman *et al*, 2013). It manifests in high strength steels by reduction in time to fracture during delayed fracture tests (Johnson *et al*, 1958) as well as decrease in ductility during tensile tests (Takai & Watanuki, 2003). Various processes such as melting and solidification, electroplating, acid pickling and welding as well as environmental degradation could lead to introduction of hydrogen into steel. Very low concentrations of hydrogen in steel (< 1 ppm) suffice to induce embrittlement (Zamanzadeh *et al*, 1982). Despite extensive research, HE mechanisms are not completely understood and agreed upon (Barrera *et al*, 2018). Lattice decohesion theory implies that hydrogen atoms reduce the cohesive strength of metallic atoms at crack tips and promote brittle fracture (Oriani & Josephic, 1974). Hydrogen-enhanced strain-induced vacancy theory (HESIVT) states that hydrogen encourages the creation of lattice defects during plastic straining, which leads to premature fracture (Nagumo, 2004).

High strength steel components are used for manufacturing landing gears of aircraft (Wang & Chang, 2018). For protection against corrosion, a sacrificial coating such as Cadmium (Cd) is applied to these components via electroplating (Sriraman *et al*, 2013). Hydrogen can evolve during electroplating, penetrate into the material and cause embrittlement (Figueroa & Robinson, 2008). In order to encourage the egress of hydrogen, a baking heat-treatment is performed on Cd-plated steel parts, during which the material is heated at a temperature usually not higher than 200℃ for up to 24 h (Sriraman *et al*, 2013). However, the hydrogen may not totally diffuse out by baking and hence the risk of embrittlement may not be eliminated (Zamanzadeh *et al*, 1982).

There is a demand in aerospace industry for development of a reliable non-destructive evaluation (NDE) method to assess HE in Cd-plated high strength steel parts. This can help manufacturers to distinguish damaged parts and repair or discard them before service to prevent possible losses. Numerous studies reported that hydrogen evolved during Cd-plating

of steel parts tends to concentrate at the surface regions inside the coating, at the coating/steel interface and in the steel near the coating (Zamanzadeh *et al*, 1982; Sriraman *et al*, 2013; Wang & Chang, 2018; Laliberté-Riverin *et al*, 2020[I]]. Consequently, the proposed NDE method for this application shall be particularly sensitive to near-surface variations in material properties. Several experimental works demonstrated the feasibility of exploiting ultrasonic surface waves for NDE of materials degradation near surface (Zielinski & Fiore, 1982; Warren *et al*, 1996; Connolly *et al*, 2013; ; Ye *et al*, 2013; Zeitvogel *et al*, 2014; Doerr *et al*, 2017).

Ultrasonic surface waves, also known as surface acoustic waves (SAWs) or Rayleigh waves, are high-frequency (f > 20 kHz) mechanical waves that propagate on surface, while their amplitude decays exponentially with depth. Researchers successfully utilized SAWs for non-destructive assessment of surface damage (Warren *et al*, 1996), fatigue (Connolly *et al*, 2013), stress corrosion cracking (Zeitvogel *et al*, 2014) and sensitization (Doerr *et al*, 2017). To the best of our knowledge, there were no reports on application of ultrasonic surface waves for NDE of HE in high strength steels. However, a few researchers investigated variations in characteristics of SAWs due to electrolytic hydrogen charging in stainless alloys. A. Zielinski and N. F. Fiore (1982) found that SAW attenuation coefficient decreased during electrolytic hydrogen charging of FCC stainless alloys and increased during subsequent hydrogen egress. They attributed the increase in SAW attenuation to unpinning of dislocations as hydrogen diffuses out. They concluded that SAW-based methods were applicable to in situ evaluation of hydrogen ingress or egress. C. Ye *et al* (2013) observed significant decrease in SAW velocity with extension in hydrogen charging time of AISI 304 stainless steel specimens. They ascribed this behavior to hydrogen-induced hardening of material at subsurface regions caused by a martensitic transformation. The authors also demonstrated that SAWs were more sensitive to local degradation of material than bulk ultrasonic wave modes.

For the first time, this research investigates the feasibility of a non-destructive testing method based on SAW measurements to distinguish between Cd-coated, SAE 4340 high strength steel samples with low and high HE susceptibilities. A piezoelectric transducer and a laser setup were employed to generate and detect SAW, respectively. After performing line scans on the

samples, delays between signals detected at successive spots were obtained by cross-correlation in order to measure SAW velocities. Attenuation coefficients were also estimated through evaluating the decrease by propagation distance in SAW signal amplitudes. The results of measurements were compared for samples that were either not baked, baked after a long delay, or baked immediately, along with a bare steel sample. To enhance statistical significance of measured data, multiple samples for each manufacturing condition were tested. To assess possible changes in SAWs caused by variations in Cd coating quality between samples, roughness and thickness of Cd layers were characterised using laser and optical microscopy techniques, respectively. Moreover, as change in hardness may indicate the presence of hydrogen in steel (Oriani & Josephic, 1980), depth profiles of steel hardness near the surface were measured with Vickers microindentation tests. Results of the present study could potentially be useful in identifying advantages as well as limitations of SAW-based NDE methods for detection of nascent HE towards development of improved methods in future.

2.2 Manufacturing of the samples

Base material was an 89 mm diameter billet of hot-rolled, normalised, and tempered SAE 4340 high strength steel conforming to AMS6415 (2016) specifications. Flat disks were machined from the steel billet to a 0.8 µm surface finish, austenitized in a vacuum furnace at 830 ℃ for 1 h, quenched in oil and tempered for 4 h twice at 230 ℃ then 245 ℃. According to tensile tests by our industrial partners on 4 specimens, ultimate tensile strength (UTS) of 1826-1875 MPa and Young`s modulus (E) of 200.6-207.5 GPa was achieved after the heat-treatment. Before Cd-plating, the heat-treated disks were stress relieved at 190 ℃ for 8 h, steam-degreased, anodically cleaned in an alkaline solution, and surface-deoxidized by immersion for 10 s in a 6 $mol.L^{-1}$ hydrochloric acid solution.

The prepared steel disks were grouped in three batches and each batch was Cd-plated separately. All disks within each batch were Cd-plated simultaneously in the same bath. In this paper only batch 2 and batch 3 will be discussed, because electroplated Cd coatings for batch 1 were porous and non-uniform due to the high current density employed. Batch 2 and batch 3

samples were Cd-plated at a current density of 108 $A.m^{-2}$ for 30 min in a bath containing 25 $g.L^{-1}$ CdO, 125 $g.L^{-1}$ NaCN and 20 $g.L^{-1}$ NaOH with a *pH* of 12. On both sides of the disks, 50 mm -wide stripes were exposed for Cd deposition and other regions were masked. Figure 2.1 shows the geometry and dimensions of the Cd-plated steel disks.

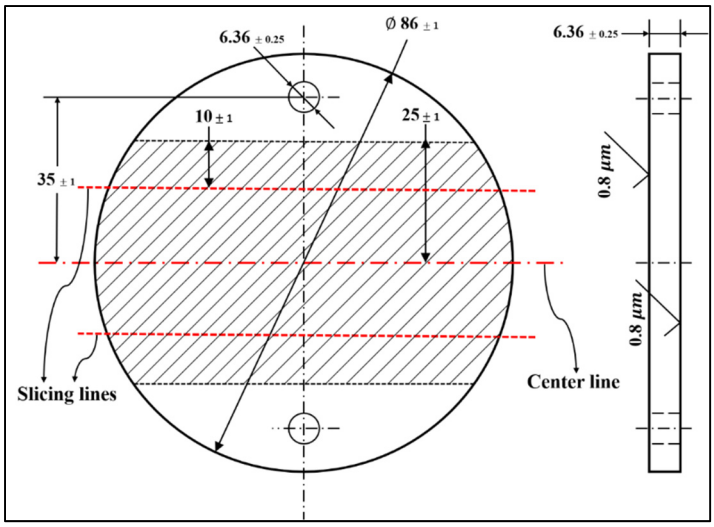

Figure 2.1 Drawing of a Cd-plated, SAE 4340 steel disk. The shaded area represents Cd-coating. Unless otherwise indicated, all dimensions are in mm

Cd-plated steel disks from Batch 2 were treated according to two different conditions: some were not-baked (**H** condition) and some were baked immediately after electroplating (**B** condition). For batch 3, in addition to **H** and **B** conditions, some disks were baked 100 h after electroplating (**L** condition). Moreover, some Cd-plated disks from batch 3 (denoted by the prefix *I*) were stripped from Cd in ammonium nitrate solution, cleaned, Cd-plated again with identical parameters and then treated according to previously described conditions. For all **B** and **L** condition samples, baking was done at 190 ℃ for 23 h. Both Cd-coated sides of the disks (denoted by A and B) were used for non-destructive measurements (except for the two first disks from batch 2). Each tested side was regarded as a separate sample. Samples were named as *B<Batch number>.<Condition>.<Disk number>.<Side tested>*. One heat-treated steel

disk was not Cd-plated (denoted by SAE 4340) to be tested for comparison. Table 2.1 summarises the manufacturing conditions of the samples.

Table 2.1 Manufacturing conditions of the test samples

Sample(s) name(s)	**Condition**	**Cd-plated**	**Baked**	N^*
SAE 4340	Bare steel disk	No	No	1
(B2.H.1.A); (B2.H.2.A); (B2.H.2.B); (B2.H.3.A); (B2.H.3.B); (B3.H.1.A); (B3.H.1.B); (B3.H.2.A); (B3.H.2.B); (B3.H.3.A); (B3.H.3.B); (B3.IH.1.A); (B3.IH.1.B); (B3.IH.2.A); (B3.IH.2.B)	H	Yes	No	15
(B2.B.1.A); (B2.B.2.A); (B2.B.2.B); (B2.B.3.A); (B2.B.3.B); (B3.B.1.A); (B3.B.1.B); (B3.B.2.A); (B3.B.2.B); (B3.B.3.A); (B3.B.3.B); (B3.IB.1.A); (B3.IB.1.B); (B3.IB.2.A); (B3.IB.2.B)	B	Yes	Yes, immediately after electroplating	15
(B3.L.1.A); (B3.L.1.B); (B3.L.2.A); (B3.L.2.B); (B3.L.3.A); (B3.L.3.B); (B3.IL.1.A); (B3.IL.1.B); (B3.IL.2.A); (B3.IL.2.B); (B3.IL.3.A); (B3.IL.3.B)	L	Yes	Yes, 100 h after electroplating	12

*Quantity of samples

2.3 Sample characterization

2.3.1 Surface roughness measurements

Surface roughness can affect SAW characteristics primarily through scattering of the signals. An experimental work by M. de Billy, G. Quentin and E. Baron (1987) involved SAW attenuation measurements on duraluminum and titanium samples with roughened surfaces. It was found that SAW attenuation increased with both surface roughness (root mean squared, 8.5-90 μm) and frequency (2-10 MHz) because of enhanced scattering effects. On another note, A. Ruiz and P. B. Nagy (2004) performed laser-based SAW velocity dispersion measurements on shot-peened aluminum specimens. They demonstrated a reduction in SAW velocity on shot-peened compared to the smooth sample, the extent of which increased with both peening intensity (Almen 6 to Almen 10) and ultrasonic frequency (2-15 MHz). They stated that the reduction in velocity was partly due to surface roughness induced scattering. In the present study, surface roughness measurements were carried out to assess their impact on SAW properties during NDE of the samples.

In order to evaluate roughness, 11 **H**, 9 **B** and 4 **L** condition samples (arbitrarily selected) as well as the SAE 4340 bare steel sample were tested using a laser (confocal) microscope. Linear and surface roughness parameters were measured on the Cd-coated regions coincident with center lines of the samples on length and had area of approximately 16 mm and 1.4 × 0.5 mm^2, respectively. The roughness parameters were calculated according to the following equations:

$$R_a = \frac{1}{n}\sum_{i=1}^{n}|Z(X_i) - Z_0| \tag{2.1}$$

$$S_a = \frac{1}{n}\frac{1}{m}\sum_{i=1}^{n}\sum_{j=1}^{m}\left|Z(X_i, Y_j) - Z_0\right| \tag{2.2}$$

where R_a and S_a are linear and surface roughness, Z and Z_0 are the local and average surface height differences with respect to the lowest measured height, and n and m are the number of

measurements on X and Y dimensions. The measured roughness data are presented in figure 2.2. Although average linear roughness of Cd-coatings on batch 3 samples ($R_a = 0.53$ µm) was slightly lower than that of batch 2 samples ($R_a = 0.77$ µm), it does not seem to be related to baking conditions.

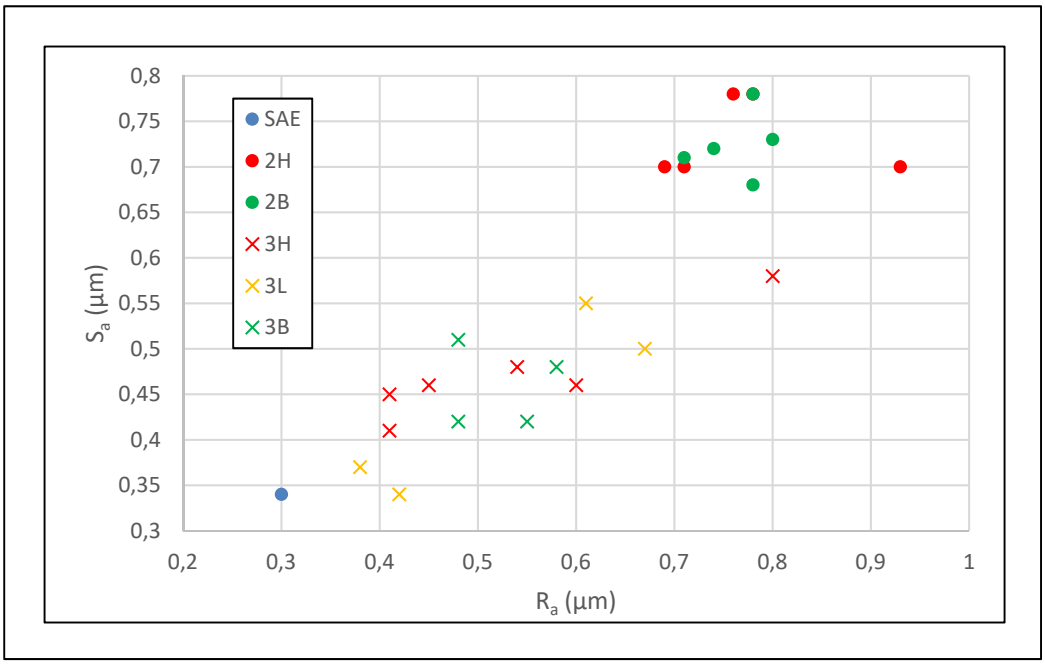

Figure 2.2 Measurement results of linear (R_a) and surface (S_a) roughness parameters (One 2H sample is overlapped by a 2B sample at 0.78,0.78 coordinates)

2.3.2 Coating thickness measurements

Characteristics of SAW propagating on a bi-layered metallic structure can vary with coating thickness depending on the test frequency as well as the microstructure and properties of both the coating and the substrate. F. Lakestani, J. F. Coste and R. Denis (1995) measured SAW velocity dispersion curves in the frequency range of 1-7 MHz on AISI 316L stainless steel specimens coated with NiCoCrAlY of 190, 250, 305 and 325 µm thicknesses. Their results clearly demonstrated the sensitivity of SAW velocity to the aforementioned differences

between coating thicknesses. Thus, coating thickness measurements were performed in this study to evaluate their effects on SAW properties.

To measure Cd-coating thickness (t_{Cd}), metallography specimens were prepared. The same samples used for roughness measurements were sectioned coincident with the slicing lines (see figure 2.1) using an abrasive cutter. This was done at low translational speeds with high amounts of lubrication to prevent overheating. The middle segments of the sliced samples were preserved and rectangular pieces (20 mm along the slicing line × 6.36 mm × 5 mm) were extracted from the remaining segments. Extracted pieces were hot-mounted using conductive powder at curing temperature of 180 ℃ for 4 min, then manually ground with abrasive papers and polished using a cloth containing diamond suspension to a perfectly smooth finish.

Optical microscopy images (500× magnification) were taken from each metallography specimen at 15 equally spaced locations all over the coating/steel interface. On each image, 6 measurements were made manually at randomly selected locations using a simple ruler tool provided by an image processing software (ImageJ (Abramoff *et al*, 2004)). Finally, the mean and standard deviation values of all thickness measurements were reported. Optical microscopy (1000× magnification) was also employed to assess the uniformity of the Cd-coatings, as can be seen in Figure 2.3. The measured thickness data are presented in figure 2.4. The average Cd-coating thickness for **H**, **B** and **L** manufacturing conditions was 10.2, 10.6 and 12.7 μm, respectively. Measured coating thickness does not seem to be related to baking conditions.

M. Zamanzadeh *et al* (1982) showed that Cd coatings at $t_{Cd} \geq 1\ \mu m$ could act as a barrier against hydrogen absorption at room temperature, while K. R. Sriraman *et al* (2013) demonstrated that electroplating-induced microcracks in Zn-Ni coatings acted as hydrogen escape pathways. Since the coating characterization results showed that Cd layers on measured samples were thick and uniform, it can be expected that not-baked samples retained the hydrogen evolved during electroplating. Laliberté-Riverin *et al* (2020)[I] performed thermal desorption spectroscopy (TDS) tests on Cd-plated, AISI 4340 steel samples prepared for

sustained load tests (SLT) and incremental step loading tests (ISL). These samples were manufactured of the same heat-treated steel lot with similar electroplating/baking conditions as the present work. SLT samples which were not baked (**H** condition) had higher total hydrogen concentrations ($C_{H,tot}$) than those that were baked immediately (**B** condition) or after 100 h (**L** condition), although this was not the case for ISL samples. Moreover, during SLT, only the not-baked samples failed. Based on these facts, it is safe to assume that **H** condition samples had higher hydrogen contents and therefore higher risks of HE than **B** or **L** conditions.

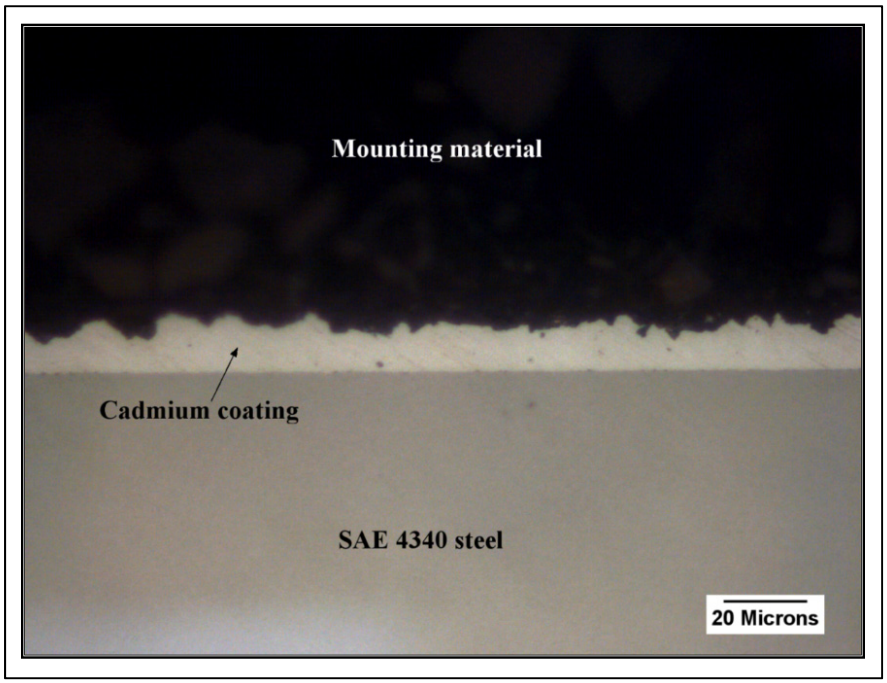

Figure 2.3 Optical microscopy image (1000× magnification, digitally enhanced contrast) from the polished cross section of a Cd-plated, SAE 4340 steel sample

2.3.3 Microindentation hardness tests

In the previous section, it was argued that **H** condition samples contained more hydrogen than other manufacturing conditions. R. A. Oriani and P. H. Josephic (1980) showed that hydrogen atoms in dissolved (diffusive) state invariably harden 1045 steel by making cross slip of

dislocations more difficult. Moreover, it is the diffusive hydrogen which can lead to HE of steel during subsequent loading (Takai & Watanuki, 2003; Sriraman *et al*, 2013). Hardness measurement can therefore be seen as an indirect method to assess risks of HE in steel samples. Depth profiles of steel hardness near Cd-coatings were measured on the polished metallography specimens using Vickers microindentation method. All tests were performed according to ASTM E384-17 standard (2017) with 100 gf load and 12 s dwell time. Hardness values were measured at 14 different depths of steel ranging from 40 to 600 µm below the Cd coating interface. For each depth, 3 hardness values were measured at locations separated by a distance larger than 6 times the diameter of indentations.

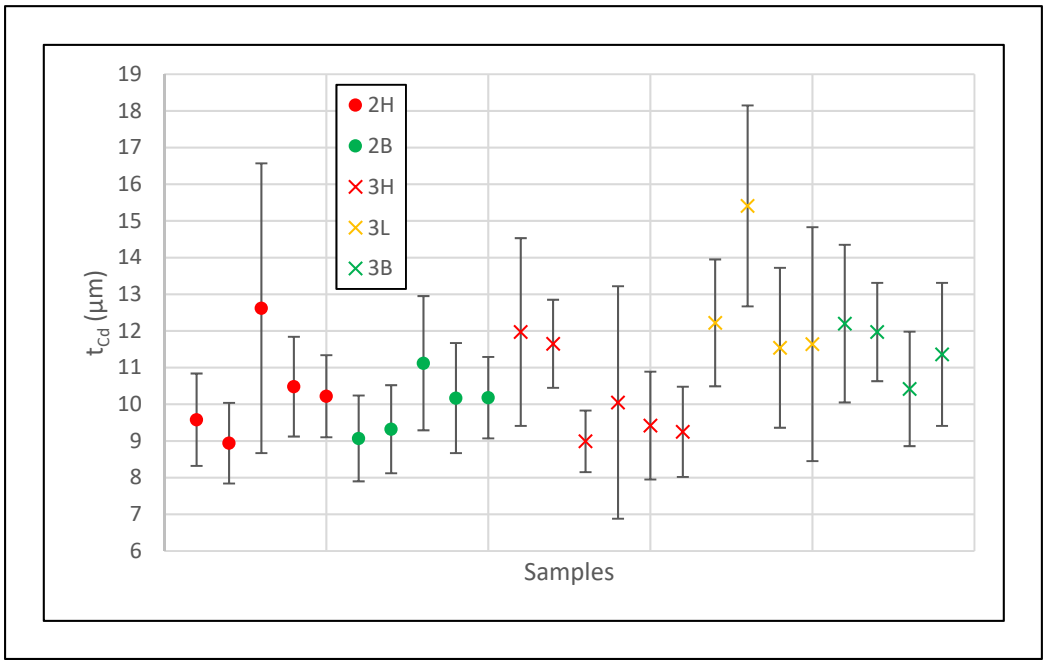

Figure 2.4 Cd coating thickness data. Error bars represent standard deviation of measurements

Measured depth profiles of steel hardness near the Cd-coatings for samples of different manufacturing conditions are shown in figure 2.5. Average steel hardness values for different manufacturing conditions calculated based on the data of figure 2.5 are presented in Table 2.2.

On average, while the baked samples **(B** and **L** conditions) as well as the bare SAE 4340 steel had similar hardness values, not-baked samples (**H** condition) were hardened by 0.8−2.1%.

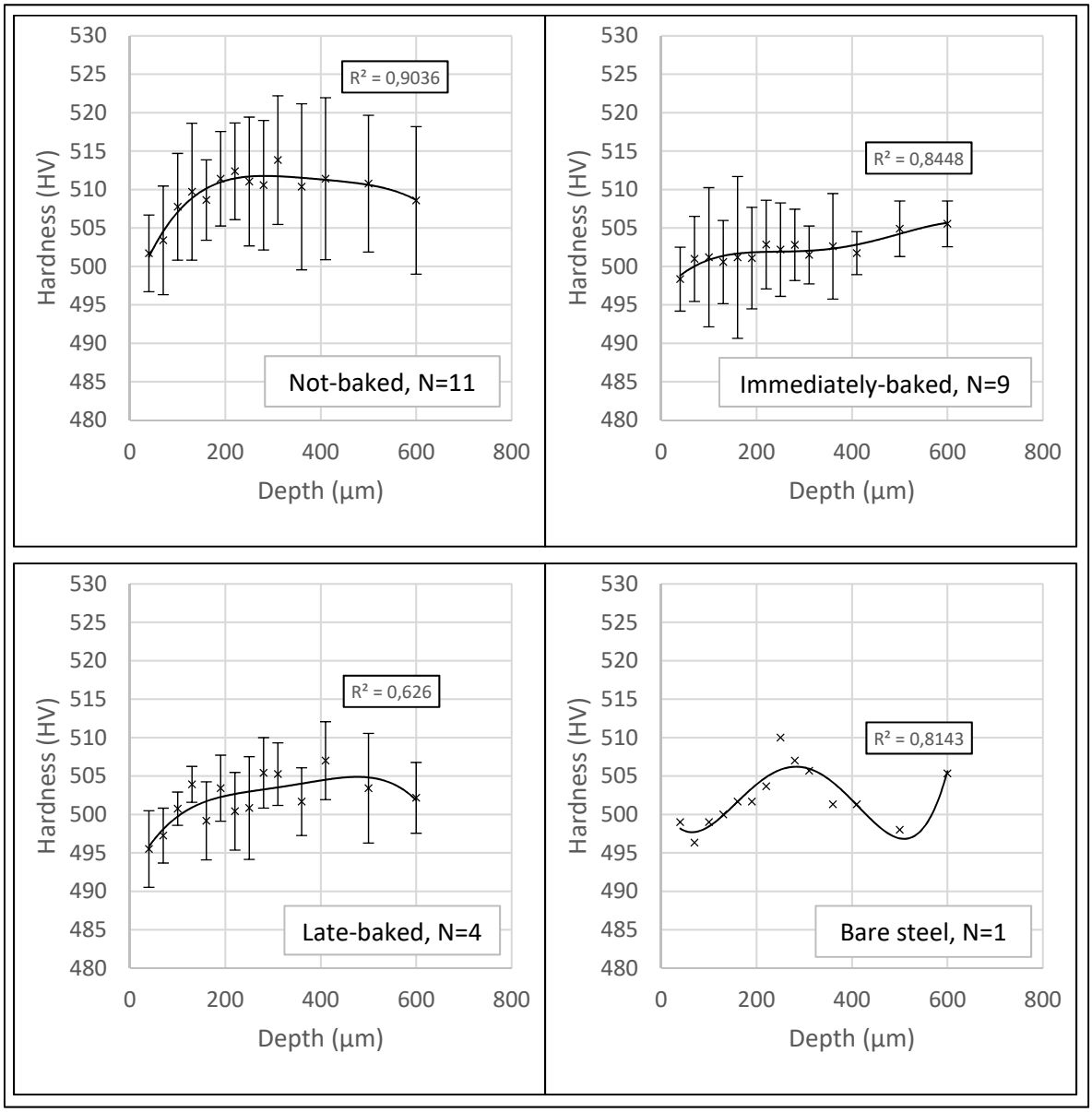

Figure 2.5 Depth profiles of the steel hardness for different manufacturing conditions. The curves were fitted to the data using a 4-th degree polynomial model. N indicates number of test samples. Error bars show standard deviations

Table 2.2 Average steel hardness data for different manufacturing conditions of the samples. N indicates number of test samples × number of indentation depths

Manufacturing condition	**Average hardness** (standard deviation), HV	**N**
H	509.4 (8.3)	154
B	502.1 (5.9)	126
L	501.9 (5.3)	56
SAE 4340	502.1 (5.8)	14

Based on previous discussion, hardness data seems to indicate that, for **H** condition samples, hydrogen atoms are dissolved within steel. On the other hand, the fact that **B** and **L** condition samples had equal average hardness with the bare SAE 4340 steel may suggest that the mobile hydrogen diffused out from steel during the baking process. This assumption is consistent with experimental results by E. M. K. Hillier and M. J. Robinson (2004), who reported full recovery of the mechanical properties of Cd-plated, AISI 4340 steel samples after baking at 200 ℃ for 24 h.

2.4 Non-destructive measurements using ultrasonic surface waves

2.4.1 Experimental setup

Figure 2.6 shows a schematic diagram of the setup used for non-destructive measurements via SAWs. The surface ultrasound source was a 10 MHz piezoelectric transducer of 6.35 mm diameter coupled to a plastic wedge specially designed to create SAWs on steel. A commercial ultrasound test unit was employed to excite the transducer using 400 V, 9.6 MHz square electrical pulses at a repetition frequency of 350 Hz. Vertical surface displacements due to propagation of SAWs were detected by a HeNe laser sensor head connected to a vibrometer controller. The SAWs signals were acquired at a rate of 5 GHz via a HD oscilloscope trigger synchronized to the pulser. The samples were placed on a computer-controlled XY translation

table driven by a high precision stepping motor. Ultrasonic vibrations were transferred to the samples by applying standard liquid couplant on the surface then putting pressure on the wedge by attaching it to the sample using a miniature C-clamp. The wedge was fixed on one end of the samples in a way that the direction of its tip was along the samples' center line (see figure 2.1). The laser unit was also fixed vertically above the table at the proper distance recommended by the laser's manufacturer in a way that a 50 μm diameter laser spot was focused perpendicular to sample`s surface. The distance between the tip of the wedge and the laser focal spot could be changed by moving the samples using the translation table. For all measurements, SAW signals were acquired at 150 equally spaced spots on a 15 mm line coincident with the center line. The distance between the first SAW detection spot and the wedge tip was set to 30-40 mm in order to avoid unwanted near-field effects of the piezoelectric transducer. All the measurements were performed at room temperature. It should be mentioned that SAW signals on the same sample exhibited different noise levels from spot to spot. To address this issue, the signals were averaged between 150 to 1000 times depending on the perceived level of noise.

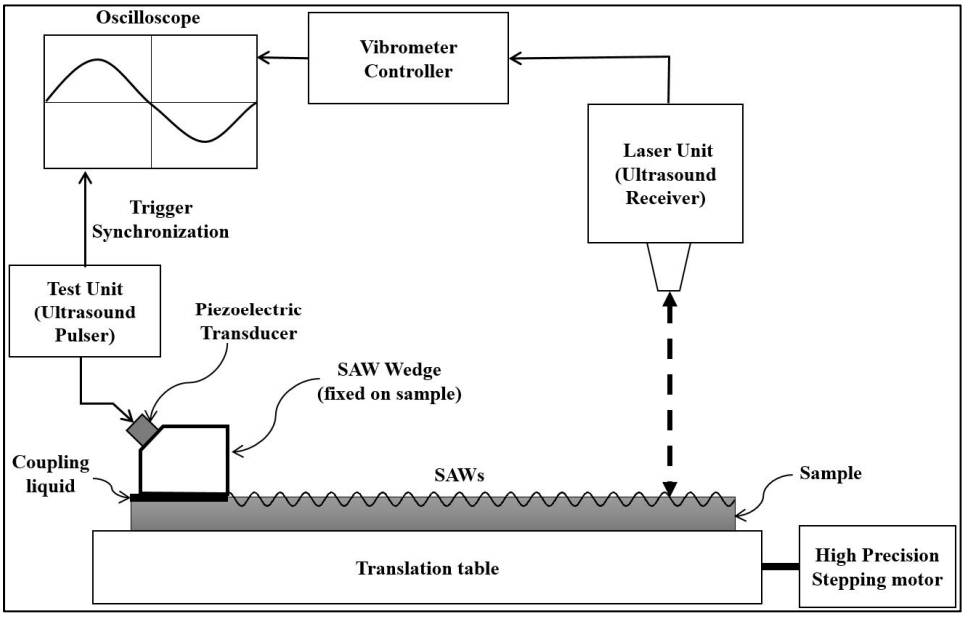

Figure 2.6 Schematic diagram of the SAWs measurements setup

2.4.2 Signal processing

Figure 2.7 shows a SAW waveform of high signal-to-noise ratio (SNR) detected with the described setup. For the purpose of this work, SNR was considered as the ratio of the maximum absolute value of the main peak amplitude divided by the standard deviation of all recorded amplitudes. For each sample, SAW velocity (V_r) was calculated using the first half sections of recorded signals (0-32 µs, which only contains the main peak, see figure 2.7) by implementing a MATLAB® code according to the following steps: First, SNR values were determined, and noisy signals were rejected (SNR < 6). Then, time delays between each two successive signals were calculated using a cross-correlation function pre-defined in MATLAB® (finddelay). For rejected signals, the delays were interpolated. After that, cumulative delays between the signals were plotted versus the cumulative distances between the detection spots. Finally, a linear fitting was performed on the obtained distance-time graph. The slope of the regression line yielded V_r.

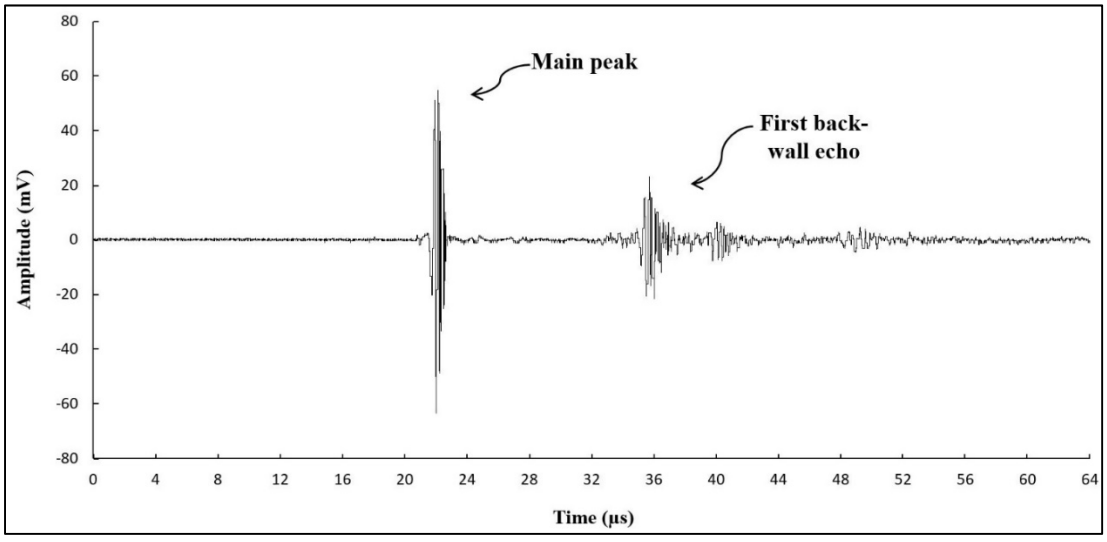

Figure 2.7 SAW waveform with high SNR detected on a Cd-coated, SAE 4340 high strength steel sample

To calculate SAWs attenuation coefficient (α), the following algorithm was developed in MATLAB®: First, weak signals were excluded (SNR < 9). Then, a low pass filter with a threshold of 20 MHz was used to remove high-frequency noise. After that, a Hilbert transform was used to compute the signal envelopes. Then, the maximum amplitudes for the main signal (A) and the first backwall echo (FBW) were obtained from the data. The amplitude decay for two consecutive signals was calculated using equation (2.3):

$$\alpha = \frac{10\log((A_1/FBW_1)/(A_2/FBW_2))}{dp} \tag{2.3}$$

Where dp was the difference between the index of two consecutive signals. For the rejected signals, the amplitude decays were interpolated. In the next step, Δx was calculated using $\Delta x = V_r \times \Delta t$ where a cross-correlation was applied to obtain Δt (in s). Finally, cumulative amplitude decays were plotted versus cumulative distances and the slope of the fitted regression line yielded the attenuation coefficient α. Additional explanation for the use of equation (2.3) to evaluate attenuation coefficient is provided in appendix A.

2.4.3 Results and discussion

Figures 2.8 (a) & (b) show the measured SAWs velocities and attenuation values, respectively. The obtained V_r and α values did not correlate with either roughness or thickness values. Hence, the small variations found between the Cd-coating thickness and roughness did not significantly affect the non-destructive evaluation results. It should be emphasized that most of SAW energy propagated through the steel near the coating. The effective penetration depth of SAW is about one wavelength (Cheeke, 2012). Based the measured velocities and considering Velocity = Wavelength × Frequency, a penetration depth of ~ 300 μm at 10 MHz can be estimated for the SAW.

The ranges of V_r and α values obtained for samples of different manufacturing conditions exhibited overlaps. It was therefore not possible to determine the manufacturing condition of individual samples based on single non-destructive measurements of either SAWs velocity or

attenuation coefficient. The linear regression models for velocity estimations of all samples yielded a near perfect fit (R-squared over 0.99). In case of attenuation measurements, however, R-squared values were significantly smaller and highly dispersed among samples (R-squared between 0.05 to 0.89, on average 0.46). More surprisingly, attenuation coefficients of negative values were estimated for a number of samples regardless of manufacturing condition. These problems were caused by sources of experimental error that could potentially affect the amplitude of SAW signals received by the laser system during line scans. These include 1) different surface conditions among samples, 2) possible misalignment of the plastic wedge when mounted on the samples, and 3) unwanted changes in the ultrasonic coupling between the plastic wedge and the sample during the scan as a result of running or evaporation of the water-based liquid couplant used for measurements. Since these errors were random in nature, their effect could be reduced by averaging NDE results for each manufacturing condition.

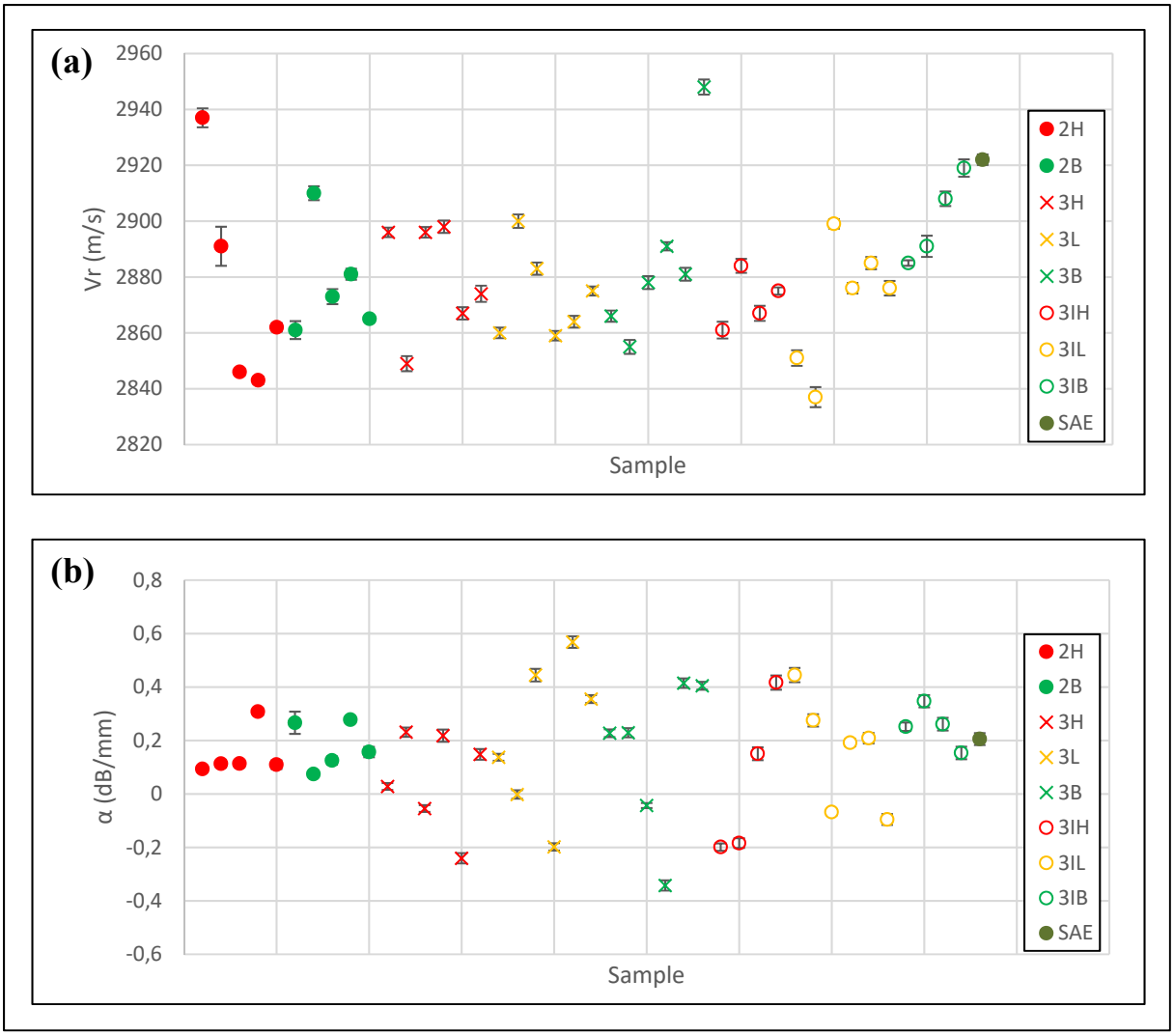

Figure 2.8 Results of (a) velocity and (b) attenuation measurements of SAW. Error bars show standard errors of estimated slopes of the linear regression lines

Table 2.3 compares average SAWs velocities and attenuation coefficients for different manufacturing conditions. The differences observed between average velocities for different manufacturing conditions did not seem significant. Taking into account the high accuracy of velocity measurements using the present setup, it can be inferred that SAW velocity was not sensitive to hydrogen content. Differences in SAWs velocities of individual samples most likely reflected variations in base steel chemical composition and microstructure (hence density and elastic properties) at different locations of the steel billet where the disks were

extracted. It should be added that states of residual stresses were similar for all samples because the steel disks were stress-relieved before Cd-plating. On another note, Y. Hasegawa (1988) reported a 7% reduction in speed of ultrasonic shear waves on hydrogen-attacked regions of carbon steel, caused by hydrogen-induced cracks along the grain boundaries. However, hydrogen attack is much more severe than electroplating-induced HE in terms of hydrogen pressure. Hence the results of SAW velocity measurements may indicate that the microstructure of samples were not damaged by hydrogen involved during the electroplating process.

Table 2.3 Average SAWs velocity and attenuation coefficients for different manufacturing conditions

Manufacturing condition	**Average V_r** (standard deviation), m/s	**Average α** (standard deviation), dB/mm	**Sample size**
H	2876 (24)	0.083 (0.181)	15
B	2887 (24)	0.187 (0.183)	15
L	2872 (18)	0.188 (0.232)	12

Not-baked samples (**H** condition) exhibited a lower averaged SAWs attenuation coefficient than the baked ones (**B** and **L** conditions). Decrease in attenuation of ultrasound in steel by dissolved hydrogen was reported in literature (Zielinski & Fiore, 1982), attributed to dislocation pinning by hydrogen atoms. It is therefore a possibility that higher concentration of hydrogen dissolved in Cd coating as well as the steel near the coating (as evidenced by Laliberté-Riverin *et al* (2020)[I]) caused the decrease in average SAWs attenuation in not-baked samples. Another possible explanation could be microstructural changes in Cd layer induced by thermal effects during baking. Further experiments were required to confirm either of these hypotheses, the extent of which was out of scope of the present research. It should be noted that ultrasonic attenuation shall be significantly increased by an increase in the amount of scatterers when hydrogen-induced damage is present (Hasegawa, 1988; Kruger *et al*, 1999). Since this was not the case, **H** condition samples were not damaged right after hydrogen

evolution during electroplating. In other words, the failure of not-baked samples in sustained load tests by S. Laliberté-Riverin *et al* (2020)[I] may suggest that the deterioration of steel by dissolved hydrogen only occurs when stress and deformation is applied.

2.5 Conclusions

The conclusions derived from this work could be summarized as follows:

1) Cd-coatings were uniform and of low porosity. Small variations among surface roughness (0.3-0.8 μm) as well as coating thickness (9-15 μm) of samples did not significantly affect NDE results.
2) A slight enhancement in average steel hardness (from 502 to 509 HV) was observed in samples that were not baked after Cd-plating (**H** condition) compared to those that were baked immediately (**B** condition) or baked after 100 h (**L** condition).
3) A decrease in average SAWs attenuation coefficient for **H** condition was measured compared to that of **B** and **L** conditions (from 0.19 to 0.08 dB/mm) although error bars were too large to distinguish between individual samples.
4) Estimated SAWs velocities (2837-2948 m/s) did not seem sensitive enough to manufacturing conditions.

SAW attenuation measurements seemed to exhibit a potential for distinguishing between Cd-plated, high-strength steel samples in baked (low HE susceptibility) and not-baked (high HE susceptibility) manufacturing condition. However, because estimated attenuation coefficients were exceedingly small, experimental errors largely affected the measurements. Based on this, more can be done in the future to improve the proposed SAWs measurement setup. To increase the accuracy of attenuation measurements, it is recommended to design a holder to precisely fix the piezoelectric transducer orientation and exert a constant and optimal force to couple it to the sample. During line scan by the laser setup, at any given distance from the ultrasound source, lateral scanning can be used to detect signals with highest amplitudes. It is also recommended to excite the input transducer with high energy tone bursts to secure a high SNR.

Appendix A:

Ultrasonic attenuation coefficient is usually evaluated by the following equation:

$$\alpha = \frac{20\log(A_1/A_2)}{\Delta x} \tag{2.4}$$

Where A_1 and A_2 are the amplitudes of the main echoes before and after propagation for a distance of Δx. In order to reliably estimate α using equation (2.4) during a line scan, the signal amplitudes shall not be significantly affected by variations in the ultrasonic coupling between the receiver and the test piece at different locations. This was not the case in the present study due to variation of the efficiency of the laser system coupling from point to point, probably as a result of surface roughness as well as local differences in the reflectivity of Cd coating surfaces. In order to circumvent this problem, the amplitudes of all collected signals were normalized by the amplitudes of their respective FBW envelopes. In other words,

$$\begin{aligned}
\alpha &= \frac{20\log(A_1/A_2)}{\Delta x} \\
&= \frac{20\log(FBW_2/FBW_1)}{\Delta x} \\
&= \frac{1}{2}\times\frac{20}{\Delta x}[\log(A_1/A_2) + \log(FBW_2/FBW_1)] \\
&= \frac{10\log\left(\frac{A_1}{A_2\left[\frac{FBW_1}{FBW_2}\right]}\right)}{\Delta x}
\end{aligned} \tag{2.5}$$

which is equivalent to equation (2.3).

CHAPTER 3

Feasibility of Surface Acoustic Waves Dispersion Measurements for Non-Destructive Evaluation of Hydrogen Embrittlement in Cd-plated High Strength Steel

Hamidreza Shahmiri[a] & Martin Viens[a]

[a] Department of Mechanical Engineering, École de technologie supérieure (ÉTS),
1100 Notre-Dame Street West, Montréal (Québec), H3C 1K3, Canada

Paper manuscript submitted to *Materials Evaluation*, May 2021

Abstract

It is desirable to develop a non-destructive evaluation (NDE) method to assess the susceptibility to hydrogen embrittlement (HE) in electroplated high strength steel components. To this end, dispersive behavior of surface acoustic waves (SAW) in cadmium (Cd)-coated, SAE 4340 steel was evaluated. SAW were generated by a 10 MHz piezoelectric transducer and detected during line scans via a laser Doppler vibrometer (LDV) setup. Samples were manufactured by the following conditions: not baked after electroplating with high HE susceptibility, immediately- and late- baked with low HE susceptibility, and a bare steel disk. Velocity dispersion curves were obtained by a 2D FFT algorithm. The majority of curves overlapped in a band of velocities regardless of manufacturing conditions. According to computer simulation results, this was due to small variations in base steel elastic properties while the actual differences in Cd-coating characteristics had little impact. Dispersive attenuation curves were obtained by comparing the frequency spectra of the signals. Estimated attenuation coefficients were very small and the measured data were strongly affected by experimental uncertainties. In conclusion, SAW dispersion measurements were not feasible for NDE of nascent HE due to their high sensitivity to variability in material parameters that could cover the effects of hydrogen.

3.1 Introduction

In aerospace industry, certain components made of high strength steel are electroplated with sacrificial coatings such as Cadmium (Cd) to enhance their corrosion resistance (Sriraman *et al*, 2013). During this process, hydrogen evolves and penetrates the steel (Sriraman *et al*, 2013; Laliberté-Riverin *et al* (2020)[I]). Electrodeposited Cd layer effectively prevents the egress of hydrogen at room temperature (Zamanzadeh *et al*, 1982). The diffusive hydrogen retained in the microstructure may later induce a loss of ductility in steel leading to premature fracture when the component is stressed. This material deterioration phenomenon is known as hydrogen embrittlement (HE) (Takai & Watanuki, 2003; Barrera *et al*, 2018). Even a low hydrogen concentration is sufficient to cause HE (Zamanzadeh *et al*, 1982), the mechanisms for which are still under dispute (Barrera *et al*, 2018). In industrial practice, steel parts are baked almost immediately after Cd-plating to encourage hydrogen egress (Laliberté-Riverin *et al* (2020)[I]). However, there are uncertainties regarding the full elimination of the risk of HE after baking as well as the role of a delay between electroplating and baking (Zamanzadeh *et al*, 1982; Laliberté-Riverin *et al* (2020)[I]). It is therefore beneficial to detect nascent HE in Cd-plated high strength steel components by a non-destructive evaluation (NDE) method before exposure to operating conditions. Most of hydrogen evolved during Cd-plating tends to be found inside the coating, at coating/steel interface or in the steel near the coating (Sriraman *et al*, 2013; Wang & Chang, 2018; Laliberté-Riverin *et al* (2020)[I]). Thus, variations in material properties caused by hydrogen presence in the microstructure would most likely be concentrated in the surface regions. Accordingly, employing an NDE method based on surface acoustic waves (SAW), which are particularly sensitive to such variations, could be a viable option.

SAW are a simple case of ultrasonic guided waves where the longitudinal and shear motions are coupled together and travel at a common velocity (Cheeke, 2012). The displacement amplitude of SAW decays rapidly with depth (Cheeke, 2012). It is largest in the direction perpendicular to the surface (Cheeke, 2012). SAW velocity (V_r) on a homogeneous, isotropic semi-infinite solid can be estimated using the shear wave velocity (V_t) and the Poisson's ratio (ν) according to equation (3.1) (Cheeke, 2012):

$$V_r \cong V_t \times \frac{0.87+1.12\nu}{1+\nu} \tag{3.1}$$

V_t can in turn be determined as:

$$V_t = \sqrt{\frac{E}{2(1+\nu)\rho}} \tag{3.2}$$

where E and ρ are the Young's modulus and the density of the solid, respectively. These equations indicate that changes in V_r could reflect variations in the elastic properties and density of material. Because of the exponential decay in SAW energy with depth, the particles movements are practically confined in a layer of thickness of one wavelength (λ_r) (Cheeke, 2012). Since the wavelength is inversely proportional to the frequency (f) by the velocity ($V_r = f\lambda_r$), different depths of the surface region can be sampled by SAW as the frequency is varied. If there is a gradient of properties below the surface, the velocity can change at different frequencies as a result of the dispersion of SAW. A simple analytical model for dispersion of SAW in a medium with depth-dependent properties have been proposed by Balogun and Achenbach (2012). Like velocity dispersion, dispersive attenuation curves can be obtained to evaluate changes in attenuation coefficients of SAW at various penetration depths (Zhang & Achenbach, 1990). Ruiz & Nagy (2004) measured SAW dispersion curves with high accuracy by means of a wedge method for generation and a laser method for detection of SAW along with sophisticated signal processing procedures. The phenomenon of SAW dispersion has been employed for NDE applications such as thickness measurement of metallic coatings (Lakestani *et al*, 1995) and determination of surface hardness gradient in steel samples (Gordon *et al*, 1993).

The potential of SAW-based methods for NDE of HE is not well investigated. The few related works found in literature measured variations in attenuation (Zielinski & Fiore, 1982) and velocity (Ye *et al*, 2013) of SAW due to effects of hydrogen on microstructure. However, these experiments did not consider the dispersion of SAW. Moreover, they were performed during

direct cathodic hydrogen charging on stainless alloys, the results of which might not be applicable to the case of high strength steels where the effects of hydrogen shall be detected after electroplating. The present research tries to evaluate hydrogen-related changes in SAW velocity dispersion and dispersive attenuation curves in Cd-plated, SAE 4340 high strength steel samples manufactured according to different baking conditions. A non-destructive measurement method based on piezoelectric generation and laser detection of surface ultrasonic vibrations was applied. SAW phase velocity dispersion curves were obtained by developing a 2D FFT algorithm in MATLAB®. Simulations were performed using Disperse® to understand the effects of variations in Cd coating characteristics and steel properties on velocity dispersion curves. Hypothetical hydrogen-induced gradients of properties were added in the model to simulate the lower and upper limit dispersion curves of not-baked samples. This was done by introducing a modified steel layer below Cd coating. Effects of hydrogen on attenuation of SAW were also investigated by examining dispersive attenuation curves. Finally, feasibility of the proposed method for NDE of HE was discussed.

3.2 Methodology

3.2.1 Material and samples

Flat disks were machined from SAE 4340 high strength steel billets that were heat-treated to a tempered martensite microstructure. These disks were Cd-plated in three batches but batch 1 samples were neglected due to high porosity in the Cd-coating. Batch 2 and batch 3 disks (taken from the same billet) were 89 mm in diameter, 6.36 mm in thickness and 0.8 μm in surface finish. The steel used to manufacture these disks had a Young's modulus of 200.6-207.5 GPa and ultimate tensile strength (UTS) of 1826-1875 MPa. These samples were Cd-plated on a 50 mm wide stripe on the middle of the disks at a current density of 108 A/m^2 for 30 min. Batch 2 samples (6 disks) were either not baked (**H** condition) or baked immediately after electroplating at 190 ℃ for 23 h (**B** condition). For batch 3 (16 disks), in addition to **H** and **B** manufacturing conditions, some disks were baked after 100 h delay (**L** condition). Moreover, a number of samples from batch 3 were stripped from Cd then re-electroplated and

treated according to the aforementioned manufacturing conditions, denoted as **IH**, **IB** and **IL**. Both sides of Cd-plated samples were used for SAW measurements. Samples were named as *B<Batch number>.<Manufacturing condition>.<Disk number>.<Side tested>*. One bare SAE 4340 steel disk sample of 76.2 mm in diameter (taken from the 1st batch) heat-treated with similar procedures was tested for comparison purposes. A color code was used during presentation of results as follows: red for **H** condition, green for **B** condition, yellow for **L** condition and blue for bare SAE 4340 steel.

3.2.2 SAW measurements

SAW were generated by a wide band 10 MHz piezoelectric ultrasound transducer of 6.35 mm in diameter mounted on a SAW wedge for steel. A commercial test unit was used to excite the transducer with 400 V, 9.6 MHz square electrical pulses at a repetition frequency of 350 Hz. Vertical displacements due to passage of SAW were received via a HeNe laser sensor head producing a 50 μm diameter laser spot, a vibrometer controller and a HD oscilloscope trigger synchronized to the pulser. The transducer was fixed on one end of the test sample in a way that its tip was directed along the disk diameter which crossed the center of the Cd-plated stripe (the center line). The relative distance between SAW source and receiver was changed by moving the sample using a precision XY translation table.

SAW were detected at 150 equally spaced spots on a 15 mm line on the center of samples in a time span of 0-64 μs at a sampling rate of 5 GHz (exceptionally, 0-32 μs for B2-B-1-A at a sampling rate of 10 GHz). All measured SAW waveforms contained a main peak arriving earlier and a backwall echo arriving later. At each detection spot, signals were arbitrarily averaged for 150-1000 times (depending on the perceived level of noise). Line scans started 30-40 mm away from the tip of the wedge in order to avoid near field effects. Signal to noise ratio (SNR) was calculated as the maximum absolute value of the main peak amplitude divided by the Standard Deviation (SD) of all recorded amplitudes. SNR values varied significantly by detection spot due to changes in laser coupling. These variations could be caused by surface conditions (roughness, waviness, reflectivity) as well as table vibrations. Waveforms received

on the coated samples had smaller amplitudes and lower SNR levels than those on the bare steel because the Cd coating surface was less reflective than that of steel. A slight spreading of SAW signals was observed on coated samples which was due to dispersion of SAW as a result of the presence of the coating. Figure 3.1 shows the main SAW peaks on a Cd-coated steel sample.

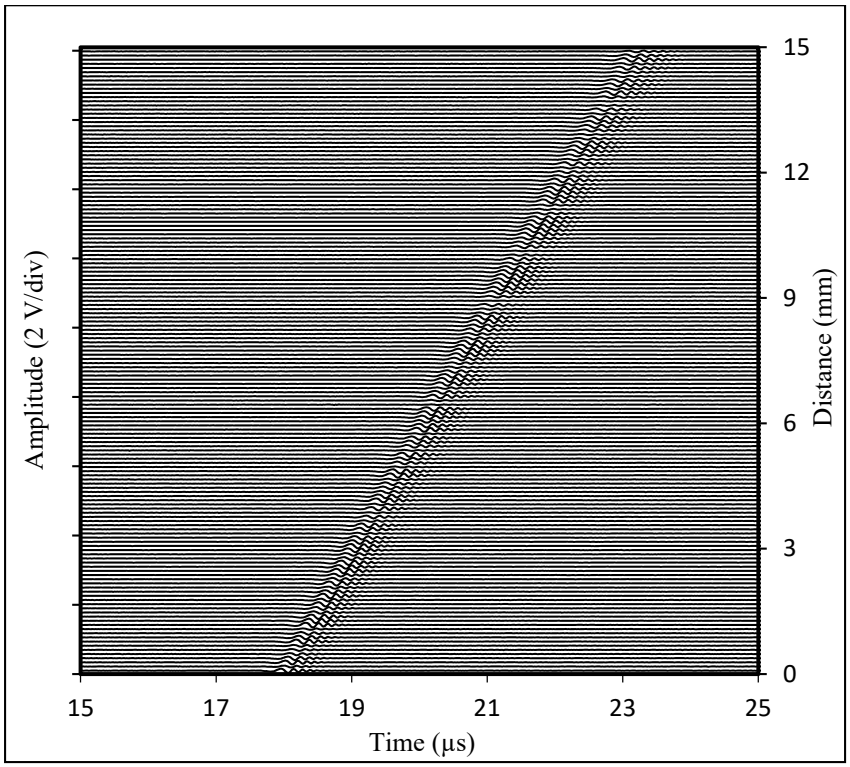

Figure 3.1 SAW main peaks in time and space domains as measured on a Cd-coated steel sample (B3-H-1-A)

3.2.3 Signal processing

3.2.3.1 Velocity dispersion

An algorithm was implemented in MATLAB® to calculate SAW velocity dispersion curves. Firstly, signals were split in half so that they only contained the main peaks. Then all the signals

were unbiased with respect to the time axis. For each individual sample, an array containing amplitudes of the raw SAW signals was constructed where the rows and columns corresponded to space and time, respectively. The arrays were zero padded in space domain to a size of 1100. A two-dimensional FFT was then applied in order to obtain angular frequency (ω) and wavenumber (k) spectra, an example of which is shown in figure 3.2. A frequency resolution of 31.25 kHz (38.46 kHz in case of the bare steel) and wavenumber resolution of $\approx 9.1\ \mathrm{m}^{-1}$ was achieved. Using $\omega - k$ plots, the wavenumbers at which the FFT amplitudes were maximal (k_{max}) were found for every frequency. Finally, phase velocities of SAW (V_r) were calculated using $V_r = \omega/k_{max}$. Moving averages of the V_r values were plotted in the 5-10 MHz frequency range. Each data point covered 10 adjacent velocities.

3.2.3.2 Dispersive attenuation

The frequency dependence of SAW attenuation coefficients was evaluated by a code developed in MATLAB®. First, signals with SNR < 9 were rejected. The remaining signals were denoised via the wavelet denoise function (wdenoise) by the False Discovery Rate (FDR) method (Abramovich *et al*, 2006). The performance of denoise algorithm is demonstrated in figure 3.3. Denoised signals were split in two halves, one containing the main peak and the other the first backwall echo. A Hilbert transform was applied to compute first backwall echo envelopes. Then, the maximum amplitudes of these envelopes denoted by *FBW* were estimated. After that, FFT was used to obtain the frequency spectra of the main peaks denoted by *A(f)* in 5-10 MHz range. As an example, figure 3.4 illustrates the spectra of two main peaks detected further away on the same sample. Subsequently, the frequency dependent amplitude decay for two consecutive signals was computed using:

$$\alpha(f) = \frac{10\log[(A_1(f)/FBW_1)/(A_2(f)/FBW_2)]}{dp} \tag{3.3}$$

where dp was the difference between the index of the two signals. For the rejected signals, the amplitude decays were interpolated. Normalisation of A by FBW in equation (3.3) was carried out in order to compensate the variations in laser coupling at different detection spots (except

for B2-B-1-A for which the signals only contained the main peaks). In the next step, the difference in travelled distances between two consecutive signals (Δx in mm) was computed. For every frequency, the averaged attenuation coefficients were finally computed by finding the slope of cumulative amplitude decays plotted versus cumulative distances.

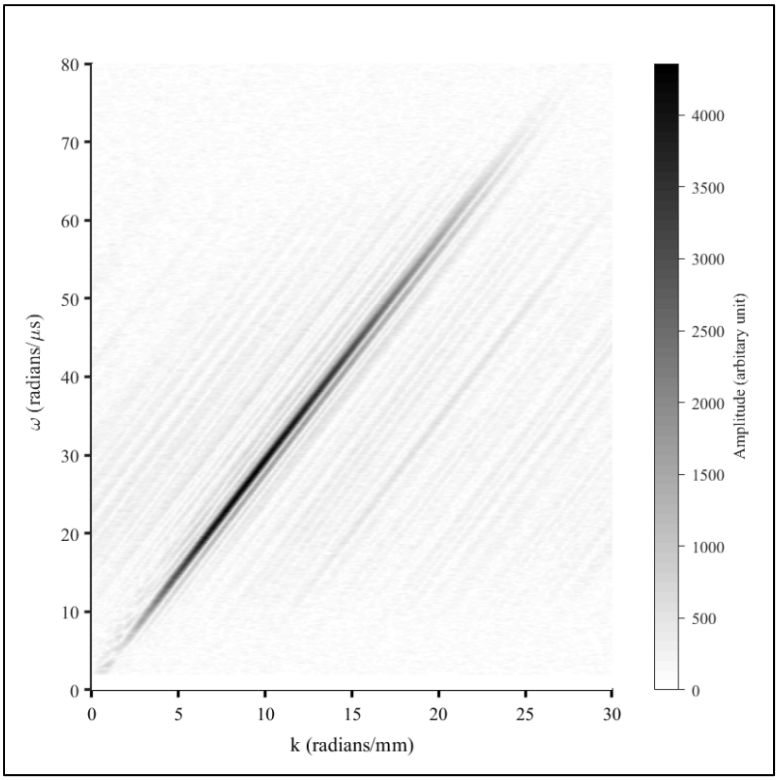

Figure 3.2 Angular frequency versus wavenumber plot obtained by 2D FFT on SAW (sample: B3-H-1-A)

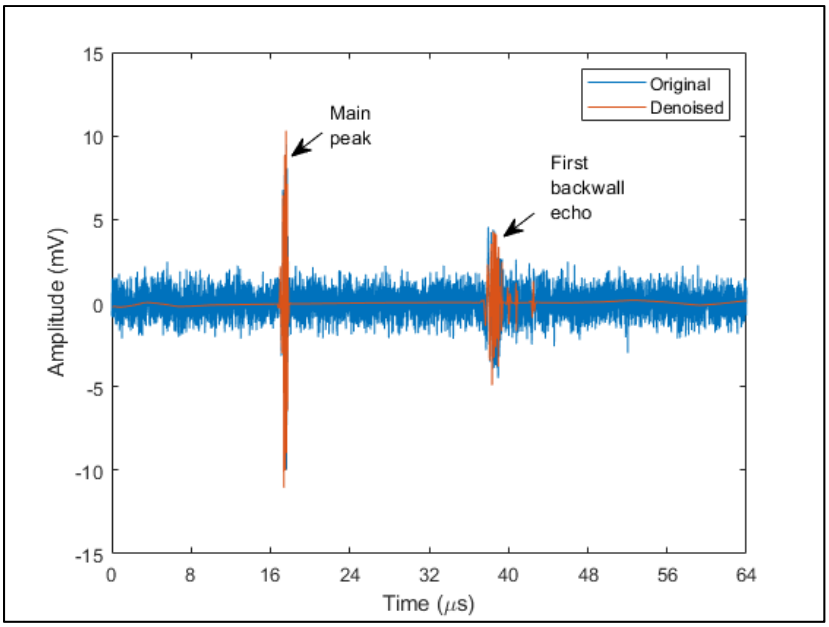

Figure 3.3 A raw SAW signal and its denoised version showing the main peak and the backwall echo (sample: B2-H-1-A)

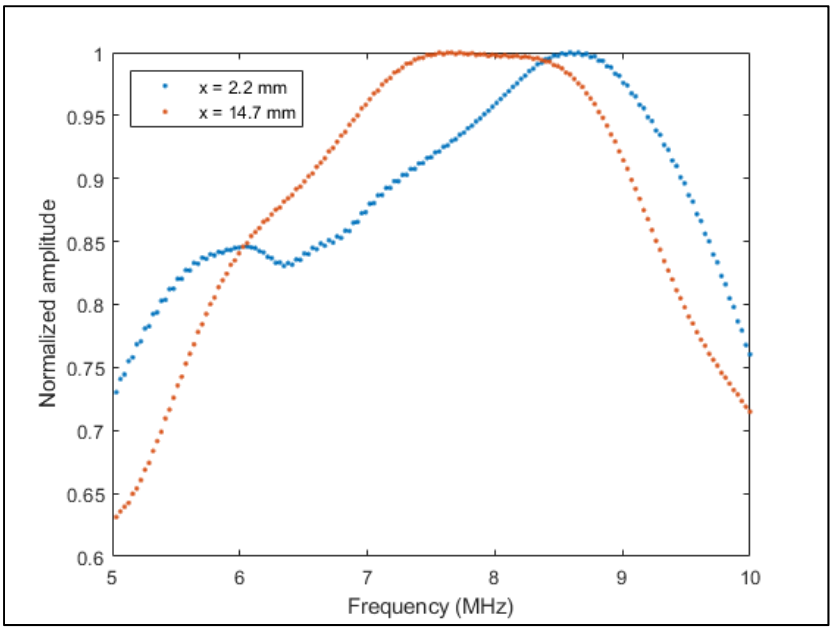

Figure 3.4 Frequency spectra of the main peaks from two denoised SAW signals on B2-H-1-A sample. The distance of detected signal from the source was indicated by *x*

3.2.4 Velocity dispersion simulations

SAW velocity dispersion curves for Cd-coated samples were simulated in Disperse® through global matrix method (Pavlakovic *et al*, 1997) using a 2D model comprising of a Cd layer of known thickness t_{Cd} on a steel half space. To simulate the velocity dispersion, either the elastic properties and density of Cd ($E_{Cd}, \nu_{Cd}, \rho_{Cd}$) and steel ($E_{St}, \nu_{St}, \rho_{St}$), or the velocities of longitudinal and shear ultrasound waves in Cd ($V_{l,Cd}, V_{s,Cd}$) and steel ($V_{l,St}, V_{s,St}$) were required. Effects of Cd thickness on velocity dispersion of SAW were investigated through changing t_{Cd} values. To examine the impact of variations in Cd microstructure and properties, dispersion curves were simulated for two sets of Cd velocities: one representing a normal case and the other as an extremely altered case. Moreover, to assess the effect of steel properties on SAW velocity dispersion curves, simulations were carried using two sets of longitudinal and shear ultrasound velocities in steel, one for a normal microstructure and the other for a slightly altered one. Table 3.1 shows the values of the parameters used for each of the aforementioned simulations.

Table 3.1 Cd and steel properties used for SAW velocity dispersion simulations

Studied parameter	**Material properties**								
	$\boldsymbol{\rho_{St}}$ $[\boldsymbol{g.cm^{-3}}]$	$\boldsymbol{\rho_{Cd}}$ $[\boldsymbol{g.cm^{-3}}]$	$\boldsymbol{\nu_{St}}$	$\boldsymbol{\nu_{Cd}}$	$\boldsymbol{t_{Cd}}$ $[\boldsymbol{\mu m}]$	$\boldsymbol{V_{l,Cd}}$ $[\boldsymbol{ms^{-1}}]$	$\boldsymbol{V_{s,Cd}}$ $[\boldsymbol{ms^{-1}}]$	$\boldsymbol{V_{l,St}}$ $[\boldsymbol{ms^{-1}}]$	$\boldsymbol{V_{s,St}}$ $[\boldsymbol{ms^{-1}}]$
Cd coating thickness	7.84*	8.64*	0.3*	0.3*	4, 8, 12, 15	2528*	1491*	5894**	3224**
Cd velocities	7.84	8.64	0.3	0.3	9.3***	2528, 1017	1491, 600	5894	3224
Steel velocities	7.84	8.64	0.3	0.3	9.3	1696	1000	5894, 5850	3224, 3200

* Publicly available data
** Conventional bulk UT velocity measurements on the bare steel sample
*** Optical microscopy measurements

Gradient of steel properties below the Cd coating in **H** condition samples were estimated following these steps: 1) E_{st} was determined by fitting the simulated velocity dispersion curve to the experimental curve for the bare SAE 4340 steel sample. 2) Using the E_{st} values in the experimentally measured range (200.6-207.5 GPa) and by varying E_{Cd}, the simulation results were fitted to that of a **B** condition sample which was assumed hydrogen-free. 3) A modified layer of steel (MLS) of variable thickness and Young's modulus (t_{MLS}, E_{MLS}) was added below the Cd coating in the model to represent the hydrogen-induced gradient of properties. The E_{St} and E_{Cd} values that were determined, respectively, in Steps 1 and 2 were assumed for the Cd coating and the steel half space below the MLS. By varying t_{MLS} and E_{MLS}, simulated curves were fit to experimental data for two **H** condition samples, which exhibited the upper and lower limit velocity dispersion curves.

3.3 Results and discussion

3.3.1 Velocity dispersion

3.3.1.1 Measured data

Figure 3.5 shows averaged velocity dispersion data for different manufacturing conditions. Using the estimated velocities, SAW penetration depths in Cd-coated samples were calculated as ~ 0.6 to 0.3 mm between 5 to 10 MHz. For every individual Cd-coated sample, V_r decreased almost linearly by frequency (1.6% from 5 to 10 MHz). This dispersive behavior was predominantly due to the ultrasound velocity being lower in Cd than in steel. With increase in the frequency, the penetration depth of SAW decreased and V_r was more affected by the presence of the Cd layer. In case of the bare steel sample, a smaller dispersion (0.5% from 5 to 10 MHz) was observed, which could be attributed to imperfect surface conditions.

For every manufacturing condition, the majority of SAW velocity dispersion curves overlapped in a certain band of velocities. Hence, the manufacturing conditions of individual samples could not be distinguished. However, a few not-baked samples showed higher or lower

velocities than the described dispersion band. No clear distinction could be made between regular and re-electroplated samples.

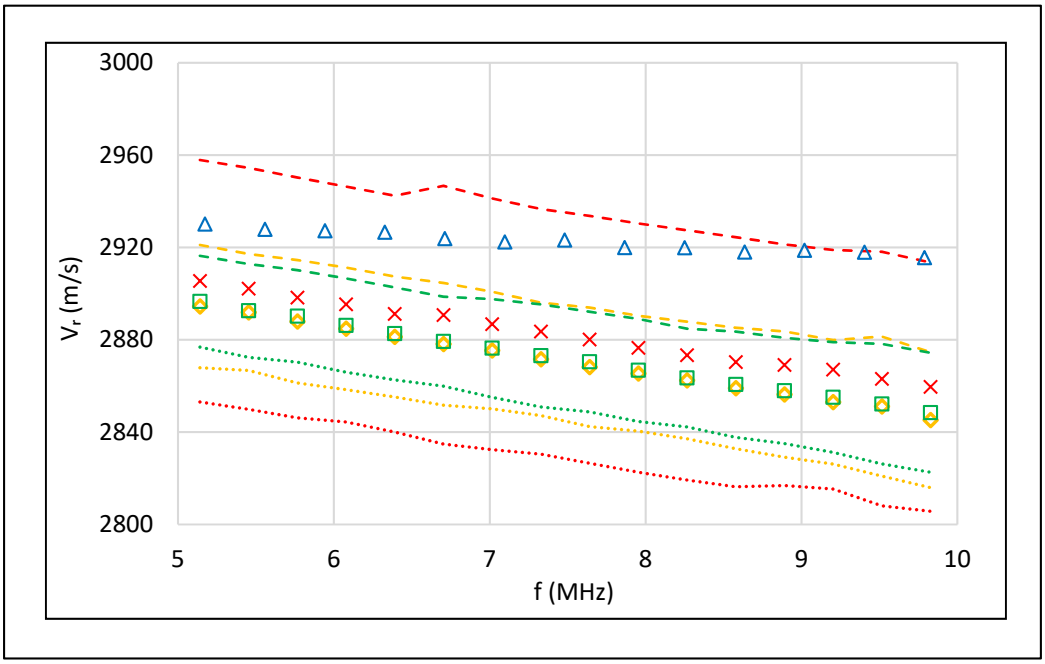

Figure 3.5 Experimental SAW velocity dispersion data for different manufacturing conditions: **H** (red, 15 samples), **B** (green, 15 samples), **L** (yellow, 12 samples), bare steel (blue, 1 sample). Data markers show mean velocities ($\bar{V}_r$). Dashed and dotted curves show, respectively, $\bar{V}_r + 2SD$ and $\bar{V}_r - 2SD$

3.3.1.2 Effects of Cd coating characteristics

Coating thickness variations can affect SAW velocity dispersion curves (Lakestani *et al*, 1995). In figure 3.6 (a) the simulated dispersion curves for different Cd thicknesses were compared to experimental curves of B2-H-1-A and B3-B-2-B samples. According to optical microscopy observations, the difference between coating thickness on these samples was 2.4 µm. However, a coating thickness difference of 8 µm was required to simulate the observed differences in V_r at low frequencies. Additionally, by increase in t_{Cd} the slope of the simulated velocity dispersion curves increased but this was not the case for the experimental curves. Therefore,

variations in Cd coating thicknesses alone could not explain the differences between the experimental velocity dispersion curves.

Variations in propagation velocities of longitudinal and shear ultrasonic waves in Cd can reflect changes in its microstructure and properties. In figure 3.6 (b), the simulated SAW velocity dispersion curves for two different sets of Cd velocities were compared to experimental curves for B2-H-1-A and B3-B-2-B samples. Results indicated that a drastic decrease in Cd longitudinal and shear velocities (60%) only causes a small downward vertical shift in dispersion curves (16 m/s at 5 MHz). On the other hand, optical and laser microscopy evidence suggested that the quality of Cd coatings (uniformity, thickness, and roughness) were relatively similar for the tested samples. Thus, differences in microstructure and properties of Cd coatings did not primarily cause the observed variations in experimental velocity dispersion curves.

3.3.1.3 Impact of steel properties

Figure 3.6 (c) shows the simulated SAW velocity dispersion curves for two sets of steel ultrasound velocities along with the experimental dispersion curves for B2-H-1-A and B3-B-2-B samples. The results showed that a decrease of only 0.75% in steel ultrasound velocities shifts the simulated dispersion curve downward by more than 20 m/s. This means that variations in steel properties, unlike Cd, have a strong impact on the SAW dispersion curves. Consequently, the observed differences between the experimental velocity dispersion curves shall be explained by the variations in steel properties.

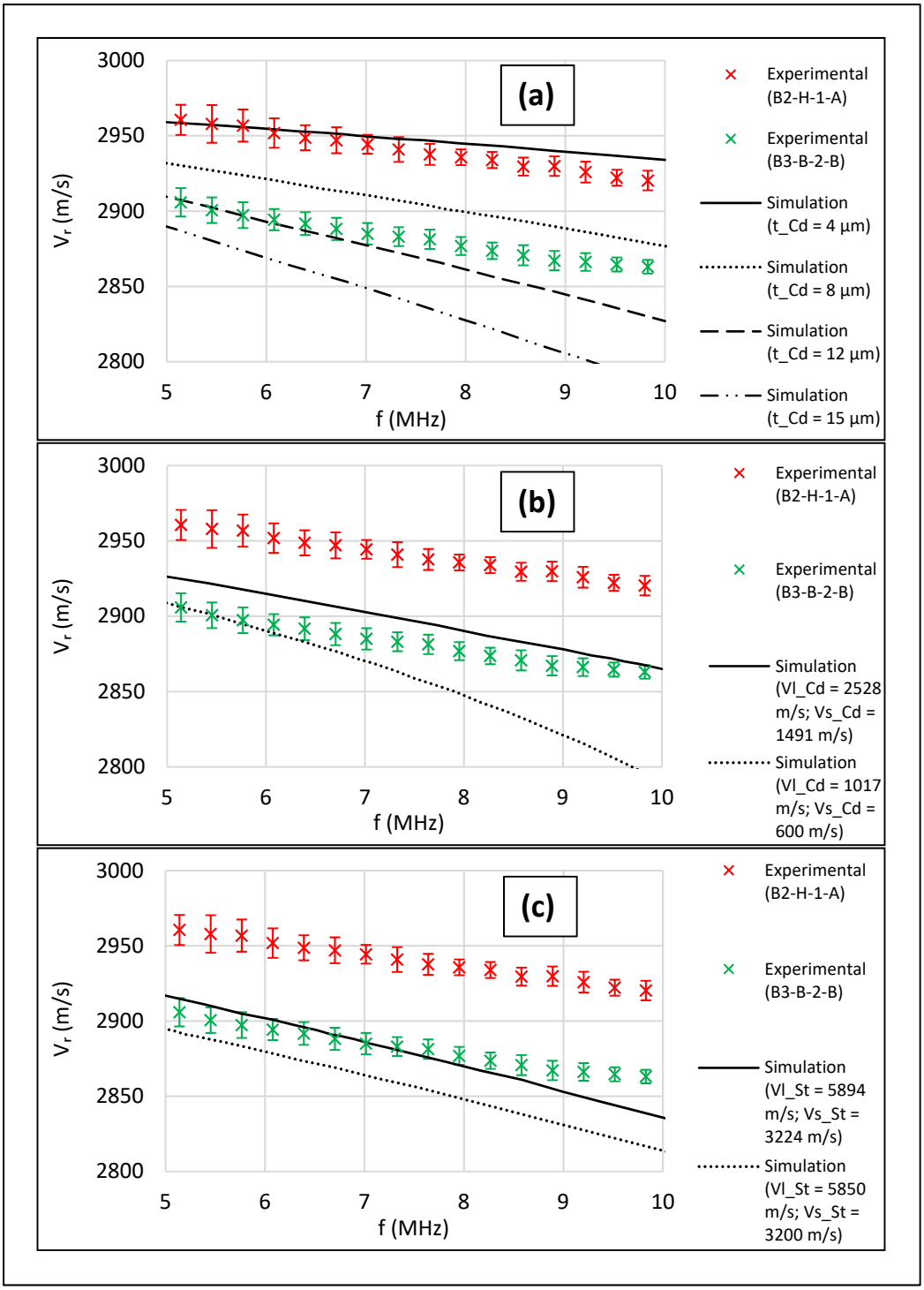

Figure 3.6 SAW velocity dispersion curves simulated by changing (a) Cd layer thicknesses, (b) Cd velocities and (c) steel velocities. Experimental data for one **H** and one **B** condition sample were included for comparison. Error bars show $\pm 2SD$ limits for the measured data

3.3.1.4 Estimation of hydrogen-induced gradient of steel properties below the coating

Figure 3.7 (a) shows the experimental SAW velocity dispersion curve for the bare steel sample and the simulated curve. Using these curves, the steel Young's modulus was estimated as $E_{st} = 202.4$ GPa that was within the measured range in tensile tests ($E_{st} = 200.6 - 207.5$ GPa). Simulations predicted no dispersion for bare steel because the effects of surface roughness were not considered in simulations. Figure 3.7 (b) shows experimental and simulated SAW velocity dispersion curve for B3-B-2-B sample, for which no hydrogen-induced gradient of properties was assumed. The lower simulated curve used $E_{St} = 202.4$ GPa as determined in figure 3.7 (a) and $E_{Cd} = 64$ GPa based on publicly available data for pure Cd. For the fitted simulation, however, both E_{St} and E_{Cd} were changed. E_{St} was changed to 205.9 GPa in order to fit the 5 MHz frequency intercept. This value was still in the measured range for E_{St} by tensile tests. E_{Cd} was increased to 100.3 GPa in order to fit the slope. Such drastic enhancement of Young's modulus in Cd coating (37.6%) could indicate a difference between the chemical composition of the coating (probably a partially-oxidized Cd alloy) compared to pure bulk Cd.

Figure 3.7 (c) shows simulated SAW velocity dispersion curves fitted to the experimental curves for B2-H-1-A and B3-H-1-B samples representing higher and lower limits of dispersion curves for **H** condition. This was done by adding a modified steel layer (MLS) with different elastic constant below the coating. It can be observed that for the lower velocity limit, a 100 µm modified layer with $E_{MLS} = 198$ GPa was required to fit the simulation to experiment. The estimated Young's modulus for this sample was close to the lower limit of tensile tests results. For the higher velocity limit, a 600 µm MLS with $E_{MLS} = 213$ GPa was added below coating; a Young's modulus considerably higher than the range measured in tensile tests.

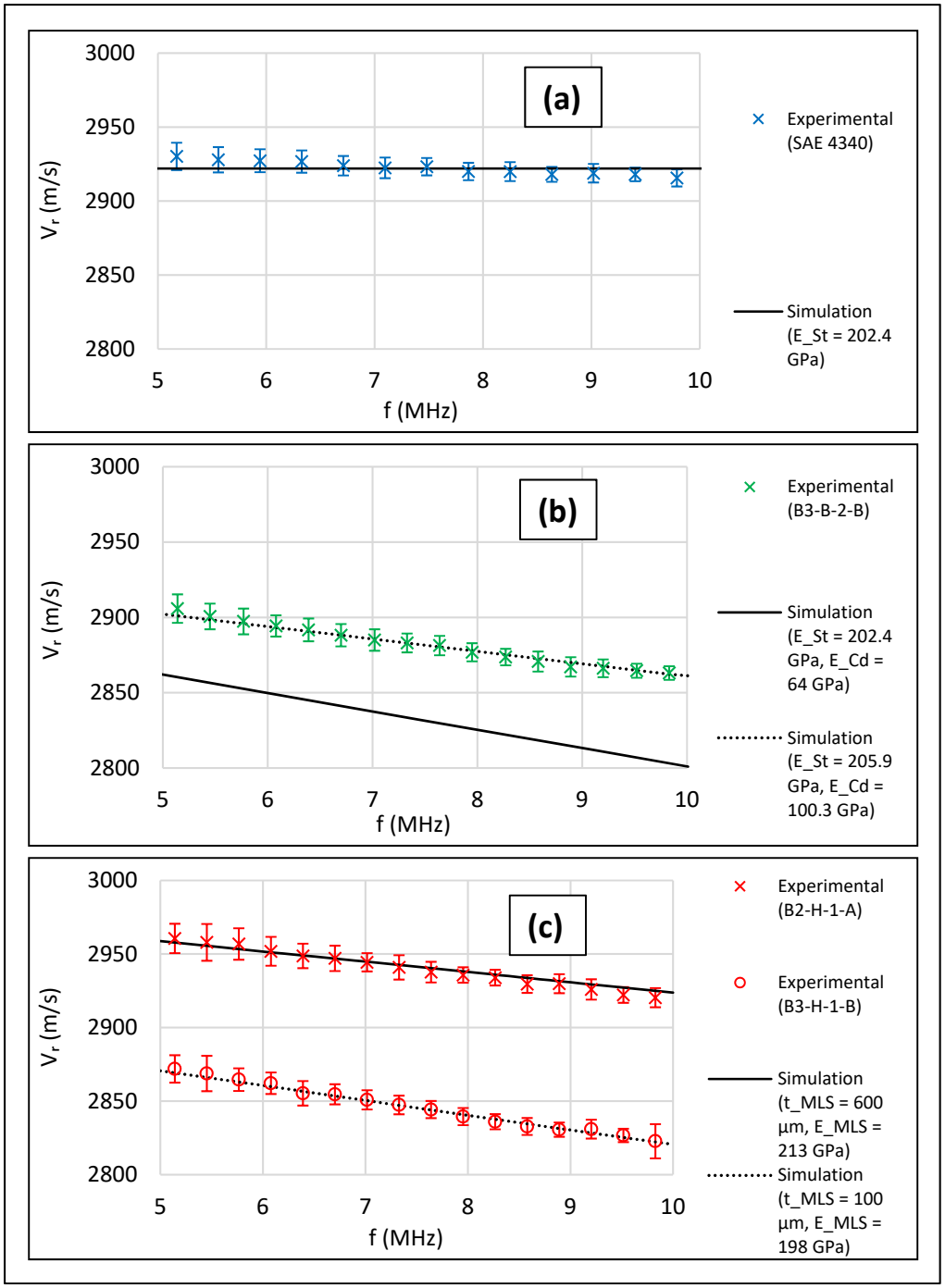

Figure 3.7 Simulated vs. experimental SAW velocity dispersion curves for (a) the bare steel sample, (b) a **B** condition sample, and (c) two **H** condition samples representing lower and upper limits of measured dispersion curves. Error bars show $\pm 2SD$ limits for the experimental data

Evidence derived from the simulations strongly suggests that there were variations in steel elastic properties among samples regardless of their baking conditions. These variations were most likely due to local inhomogenities in the microstructure and chemical composition of the base steel billet, from which the steel disks were extracted. For a few **H** condition samples, however, there was an apparent enhancement in steel Young's modulus, which might be ascribed to higher concentration of hydrogen dissolved in steel near coating. It is unclear why theses samples showed a different trend than the majority of **H** condition samples. However, considerable variations in hydrogen concentration among not-baked samples may have played a role. This argument is based on evidence from thermal desorption spectroscopy (TDS) tests on Cd-plated, 4340 steel samples produced with electroplating/baking conditions similar to the present research (Laliberté-Riverin *et al* (2020)[I]). TDS results showed different hydrogen concentrations in samples manufactured with the same conditions.

3.3.2 Dispersive attenuation

Figure 3.8 shows averaged dispersive attenuation data for different manufacturing conditions. At any given frequency, the estimated attenuation coefficients for individual samples varied in a wide range including negative values regardless of manufacturing conditions. This was due to experimental errors that interfered with attenuation measurements. For example, differences in surface conditions among samples, as well as table vibrations, could affect laser coupling. Also, possible misalignment of the direction of the wedge with the scan line could disrupt the measurements as a result of the beam divergence due to ultrasonic diffraction. More importantly, the estimated attenuation coefficient for SAW was very small, which could exacerbate the problems associated with experimental uncertainties.

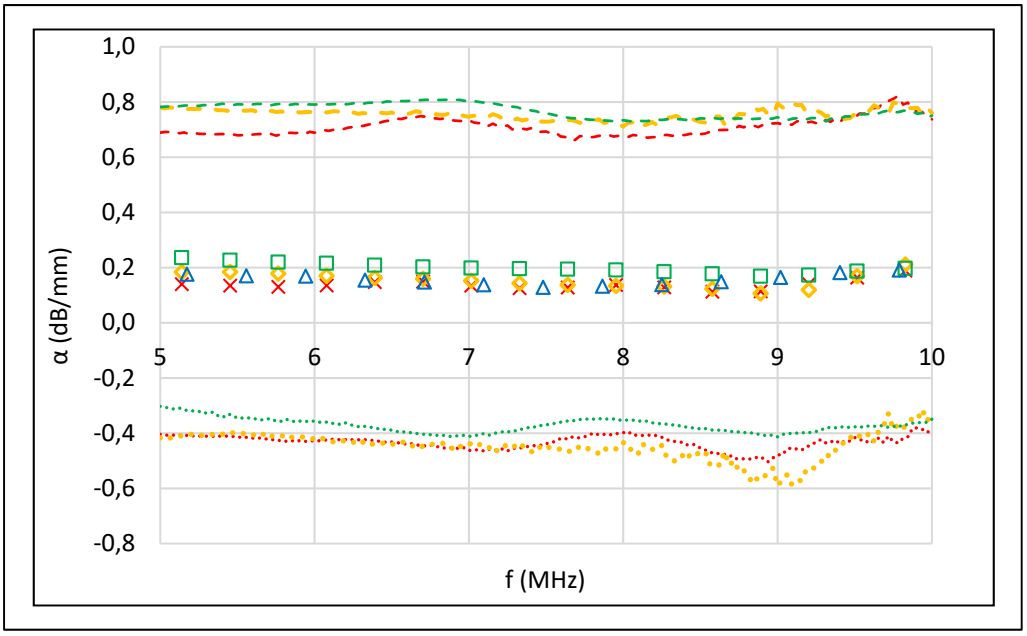

Figure 3.8 Experimental SAW dispersive attenuation data for different manufacturing conditions: **H** (red, 15 samples), **B** (green, 15 samples), **L** (yellow, 12 samples), bare steel (blue, 1 sample). Data markers show mean attenuation coefficients ($\bar{\alpha}$). Dashed and dotted lines show, respectively, $\bar{\alpha} + 2SD$ and $\bar{\alpha} - 2SD$

The error bars for estimated attenuation coefficients were too large to allow drawing a solid conclusion. However, it seemed that on average, not-baked samples had lower attenuation coefficients than immediately-baked samples especially at lower frequency end. This may be explained by reduced dislocation damping caused by dislocation pinning effects of dissolved hydrogen in steel microstructure, as suggested by A. Zielinski and N. F. Fiore (1982).

3.4 Conclusions

The conclusions derived from this work can be briefly stated as follows:

1) The majority of SAW velocity dispersion curves for samples in both not-baked and baked conditions overlapped in a certain range of velocities caused by small differences

in base steel properties. Actual differences among Cd coatings' characteristics did not have a significant impact on velocity dispersion curves.

2) Estimated SAW attenuation coefficients were very small. Experimental uncertainties strongly affected SAW attenuation measurements.
3) SAW dispersion measurements using the described setup were not deemed feasible for distinguishing Cd-coated high strength steels in not-baked (high HE risk) and baked (low HE risk) conditions.

CHAPTER 4

Application of Eddy Current Testing and Simulations for Non-Destructive Evaluation of Hydrogen Embrittlement in Cd-plated High Strength Steel

Hamidreza Shahmiri[a], Ehsan Mohseni[b] & Martin Viens[a]

[a] Department of Mechanical Engineering, École de technologie supérieure (ÉTS), 1100 Notre-Dame Street West, Montréal (Québec), H3C 1K3, Canada

[b] Center for Ultrasonic Engineering (CUE), Department of Electronic & Electrical Engineering, University of Strathclyde, 204 George Street, Glasgow G1 1XQ, UK

Paper manuscript submitted to *Journal of Nondestructive Evaluation*, May 2021

Abstract

Feasibility of eddy current testing and simulations for non-destructive evaluation (NDE) of nascent hydrogen embrittlement (HE) in cadmium (Cd)-plated, SAE 4340 steel samples was studied. Samples were either baked immediately after electroplating (low HE susceptibility, 8 samples) or not baked (high HE susceptibility, 8 samples). Probe liftoff data (0-400 µm) were measured at different testing frequencies (100-500 kHz). Model-based, semi-analytical eddy current simulations in CIVA® were used to evaluate the effects of changes in electrical and magnetic properties of steel and Cd on probe impedance. At 100 kHz for every liftoff, a decrease of ~ 3 to 4% in magnitude of averaged probe impedance relative to air was measured on not-baked samples compared to baked ones. However, not every individual sample could be distinguished due to overlap in measured data. Based on simulation results, the measured difference in averaged impedance was attributed to decrease in electrical conductivity of both the Cd coating and steel near coating due to effects of hydrogen. It was concluded that eddy

current testing method has potential for distinguishing between samples in baked and not-baked conditions although more work is needed to enhance the precision of measurements.

4.1 Introduction

The unexpected failures due to hydrogen embrittlement (HE) could cause undesirable service interruptions and hence result in considerable economical costs (Louthan, 2008). HE is a well-known problem in different industrial sectors where the components are exposed to hydrogen during some manufacturing processes such as acid pickling, etching, annealing, and electroplating (Evers *et al*, 2013). The presence of hydrogen in high strength steels, such as martensitic SAE 4340, is particularly detrimental due to the elevated susceptibility of microstructure to HE as well as the exceedingly high hydrogen diffusion coefficient in such materials (Li *et al*, 2018). The high strength SAE 4340 martensitic steel is widely used as the material for the aeronautical landing gear components subjected to high cyclic and shock loads, owing to its superior mechanical properties (Voorwald *et al*, 2007; Puchi-Cabrera *et al*, 2007). To increase the resistance of these steel components to corrosion and stress corrosion cracking, the common practice is to use chromium or cadmium plating as the protective sacrificial oxidizing layer (Conde *et al*, 2011). Beside the environmental concerns and health hazards around the toxic nature of chromium and cadmium (Aguero *et al*, 2012), the electroplating process also results in introduction of hydrogen into the steel components leading to the occurrence of HE.

Although parameters of the electroplating process such as plating time and current are carefully controlled, and the samples are baked at low temperatures for certain durations to encourage the egress of the dissolved hydrogen, there is no guarantee that the manufactured components do not experience delayed failures unless a testing method is devised and deployed to ensure that high hydrogen concentration has dropped after baking. Hydrogen concentration can be measured destructively via a few expensive laboratory-based ion beam nuclear outgassing tests, which only provide information from a few micrometers within the plated layer and the substrate after very lengthy test durations (L'Ecuyer *et al*, 1976; Lanford, 1992; Schiettekatte

et al, 2004). Moreover, thermal desorption spectroscopy (TDS), as another outgassing method, can be used to measure the hydrogen content of a material as it is subjected to a constant heat [11]. However, in a factory setting, in-situ non-destructive testing (NDT) methods can serve as a more economical and faster solution to detection of hydrogen. At the same time, it is known that the hydrogen concentrations leading to HE can be only of a ppm mass fraction (Zamanzadeh *et al*, 1982) and this might fall at the limit of many NDT methods, if not beyond them. Even though HE is well-studied by scholars (Barrera *et al*, 2018), application of NDT method for detection of hydrogen and prevention of HE has been barely researched. Among these few, the attenuation and velocity of ultrasound elastic waves is shown to be an indicator of hydrogen concentration in stainless steel, zirconium, and titanium alloys (Gomez *et al*, 2006; Lider *et al*, 2013; Ye *et al*, 2013; Bae *et al*, 2014) with Rayleigh waves being superior in sensitivity of detection. However, addition of a cadmium-plating (Cd-plating) layer can make such measurements challenging especially when Rayleigh waves are employed. Eddy current testing (ECT) has also been considered before for detection of hydrogen in ferritic alloy steel (Zhou *et al*, 2018), where signal amplitudes were shown to be correlated to HE index, which was in turn related to hydrogen-induced loss of ductility. The high hydrogen charging current densities as well as long charging times used in these experiments may not be applicable to the case of Cd-plated high strength steel where hydrogen charging conditions are usually significantly milder. Nevertheless, the results by Zhou *et al* (2018) indirectly indicate that hydrogen could alter electrical conductivity and/or magnetic permeability. Moreover, it is shown that dissolved hydrogen in steel could affect hardness (Oriani & Josephic, 1980). The variations in these parameters, in turn, would contribute to the EC probe's impedance changes (Oriani & Josephic, 1980; Zergoug *et al*, 2004; Szlagowska-Spychalska *et al*, 2013; Zhou *et al*, 2018). Therefore, EC impedance variations can be used to describe the HE phenomenon. In some previous studies, EC encircling coils have been successfully used to detect the hydrogen presence in welded and plated steel samples (Koenig *et al*, 2010; Bellemare *et al*, 2020 [II]). However, the coil geometries considered in these experiments favoured cylindrical components – which is not always the case in the industry and depending on the component, custom designs may be required to achieve the desired depth of penetration and coverage. Apart from the design point of view, the setup by Bellemare *et al* (2020 [II]) proved to be

insensitive to low hydrogen concentrations. Zhou *et al* (2018) also used surface spot coils to monitor the hydrogen-induced loss of plasticity in low carbon high alloy steels.

4.2 Methodology

4.2.1 Material and samples

Base material was a SAE 4340 high strength steel billet of 89 mm diameter with chemical composition conforming to AMS6415 (2016) specifications. The billet was heat-treated to a tempered martensite microstructure with Young's modulus of 200.6-207.5 GPa and ultimate tensile strength (UTS) of 1826-1875 MPa. Flat disks of 6.36 mm thickness were machined from the billet. These disks were electroplated with Cd in two batches at a current density of 108 A/m^2 for 30 min. Cd was deposited on a 50 mm wide stripe on both sides of each disk. After Cd-plating, the disks were either baked immediately at 190 ℃ for 23 h (**B** condition) or were not baked (**H** condition). Higher hydrogen concentration in not-baked condition within both Cd coating and steel near coating was reported by Laliberté-Riverin *et al* (2020)[I] during TDS on sustained load tests (SLT) samples produced with similar material as the present study. Not-baked SLT samples failed due to HE while baked samples did not fail. Therefore, **H** and **B** conditions could represent higher and lower HE susceptibilities, respectively. For each manufacturing condition, 8 samples were tested by ECT at room temperature (4 samples from each batch). Before non-destructive measurements, the plated disks were cut on the Cd-plated area to stripes of $77 \times 30 \times 6.36$ mm dimensions. A conventional metallography abrasive cutter was used at low cutting speeds with large amounts of lubrication.

4.2.2 Non-destructive tests

A ¼ inch, bridge-type, absolute probe with ferrite core and shielding (100-500 kHz bandwidth) along with a commercial eddy current test unit (Nortec N600C from Olympus IMS) were used for non-destructive tests at 100, 200, 300, 400 and 500 kHz frequencies (f). To obtain liftoff data on Cd-coated samples, plastic shims of 100, 200, 300 and 400 μm thicknesses were used.

During measurements, the probe was held by a rotatable holder attached to a post. The angle of the holder was set so that the probe tilt with respect to sample surface was minimal. Using the holder also helped reduce the noise associated with probe wobble. For all measurements, the probe was nulled in the air. Before testing the main samples, liftoff curves on a standard ferrite sample were recorded at the aforementioned frequencies. At each frequency, the unit display was rotated so that the ferrite traces were vertical to ensure that the vertical and horizontal axes on the unit display represented changes in probe's reactance X and resistance R, respectively. Figure 4.1 (a) demonstrates liftoff curves at 100 kHz for different materials when the ferrite trace was vertical. For testing main samples, the air point was shifted to the top left corner of the test unit screen and the horizontal and vertical gains (HGain and VGain, respectively) were selected optimally for each f. This was done to exploit all the area provided by the unit display. A screen shot image was captured from the unit display after each measurement. Captured images were processed via a MATLAB® code to quantify probe impedance change relative to air in the arbitrary unit [a.u.] as shown in figure 4.1 (b).

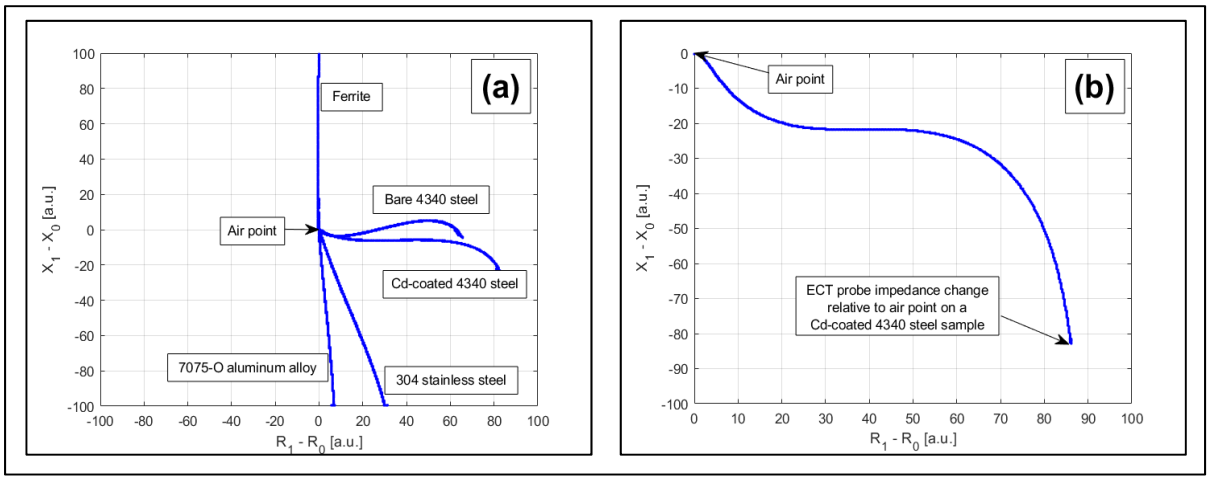

Figure 4.1 (a) ECT probe liftoff curves at 100 kHz for different materials (HGain=55 dB, VGain=55 dB). The probe was nulled in the air and the display was rotated so that the ferrite trace was vertical. (b) liftoff curve of a Cd-coated steel sample after the air point was moved to the top left corner of the screen and the gains were changed (HGain=57 dB, VGain=66 dB)

4.2.3 Simulations

Eddy current simulations were carried out in CIVA® 2016. Figure 4.2 demonstrates 3D images of the ECT probe acquired using a microfocus X-ray CT scan unit. Information derived from CT images were used to construct a realistic model of the ECT probe. Figure 4.3 shows the probe model along with the Cd-plated steel sample. Model parameters are presented in Table 4.1.

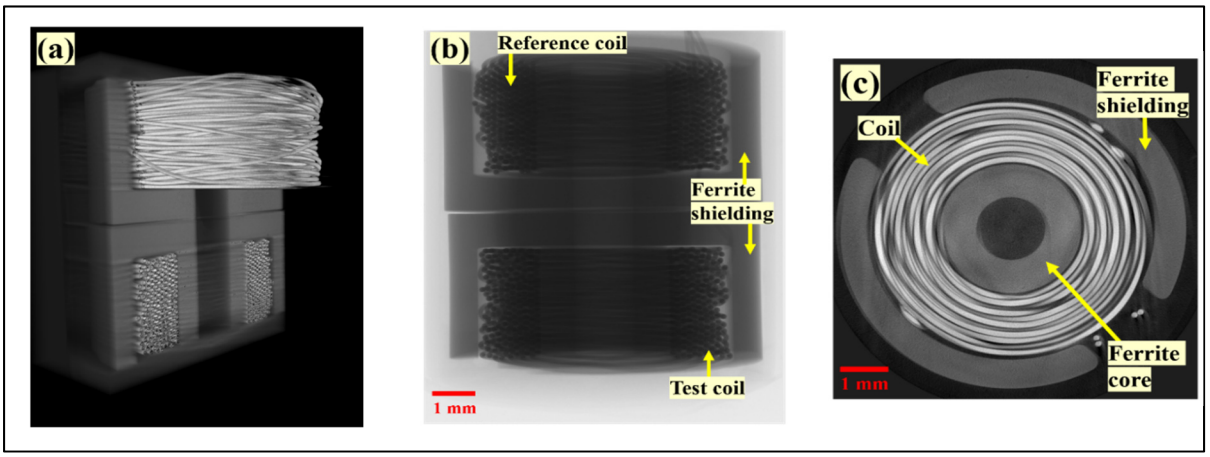

Figure 4.2 Cross sectional CT scan images from the ECT probe; (a) 3D view with lower coil and core sectioned in half, (b) front view and (c) top view

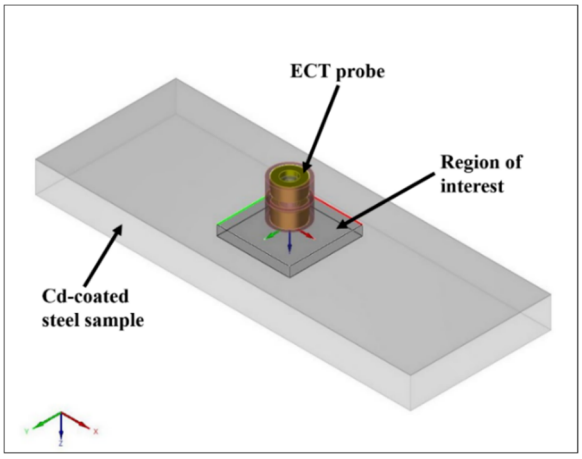

Figure 4.3 Model of the sample and the ECT probe in CIVA®

Table 4.1: ECT model parameters in CIVA®

Sample geometry				Region of interest		Coil*					
Length [mm]	Width [mm]	Steel thickness [mm]	Cd coating thickness [μm]	Size in x, y, z [mm]	Sampling steps in x, y, z [mm]	ID [mm]	OD [mm]	Height [mm]	Number of turns	f [kHz]	Liftoff [mm]
77.5	29	6.36	10	15, 15, 2	0.1, 0.1, 0.005	3	5.6	2.7	170	100	0

*Both the reference coil and test coil were modelled with same parameters.

In case of an ECT probe with ferrite core and shielding similar to the present study, CIVA uses a semi-analytical approach based on finite integration technique to compute the eddy current field (Schuhmann & Weiland, 2001). During simulations, the electrical conductivities of Cd and steel (σ_{Cd} & σ_{St}) as well as relative permeability of steel ($\mu_{r,St}$) were changed with respect to the values in literature (mentioned in Table 4.2) to study their effects on probe impedance at 100 kHz and 0 liftoff. Relative permeability of Cd ($\mu_{r,Cd}$), which is a non-magnetic material (Rumble, 2020), was assumed unchanged. In order that simulated impedances in ohm could be compared to experimental impedances in arbitrary unit, these steps were followed: To simulate ΔZ_B, material properties were set to values in literature. Following this assumption, proportionality constants between simulated and experimental resistance and reactance were obtained. Then, after changing material properties with respect to literature, the resistance and reactance obtained in simulations were converted to their equivalent in arbitrary units by dividing them by their respective proportionality constants. Finally, both experimental and simulation results were presented in form of $(\frac{\Delta R-\Delta R_B}{|\Delta R_B|}, \frac{\Delta X-\Delta X_B}{|\Delta X_B|})$ so they may be compared in the same plot.

Table 4.2: Electrical and magnetic properties of Cd and steel

Material	σ $[MS/m]$	μ_r	Reference
Cadmium	13.8	1	(Rumble, 2020)
SAE 4340 steel	1.7	15.4	(Szlagowska-Spychalska *et al*, 2013)*

*The assumed conductivity and permeability for steel were estimated within the limits of measured values on AMS 6414 (4340) steel in hardened and not hardened conditions in the mentioned reference.

4.3 Results and discussion

Figure 4.4 shows the eddy current probe liftoff data at different frequencies. Averaged impedance values measured for **B** and **H** conditions overlapped at every liftoff when frequency was between 200-500 kHz. However, for every liftoff at 100 kHz, an average decrease of ~ 3-4% in magnitude of probe impedance relative to air was observed on **H** compared to **B** condition. Yet, partial overlap between error bars at 100 kHz means it was not possible to distinguish between individual **H** and **B** sample. Coating thickness, surface roughness, and steel hardness data for **B** and **H** condition samples were presented in Table. 4.3. No correlation was found between these material characteristics and measured impedances at 100 kHz for individual samples. This could indicate that variations in these parameters did not have a significant impact on NDE results at this frequency.

Table 4.3 Cd coating characteristics as well as steel hardness values measured for **B** and **H** conditions. The numbers in parentheses show two times the standard deviation (SD) of the measured data

Manufacturing condition	t_{Cd} $[\mu m]$	R_a $[\mu m]$	**Hardness** $[HV]$
B	10.8 (2)	0.68 (0.2)	500 (3.4)
H	9.9 (1.6)	0.62 (0.4)	508 (9.6)

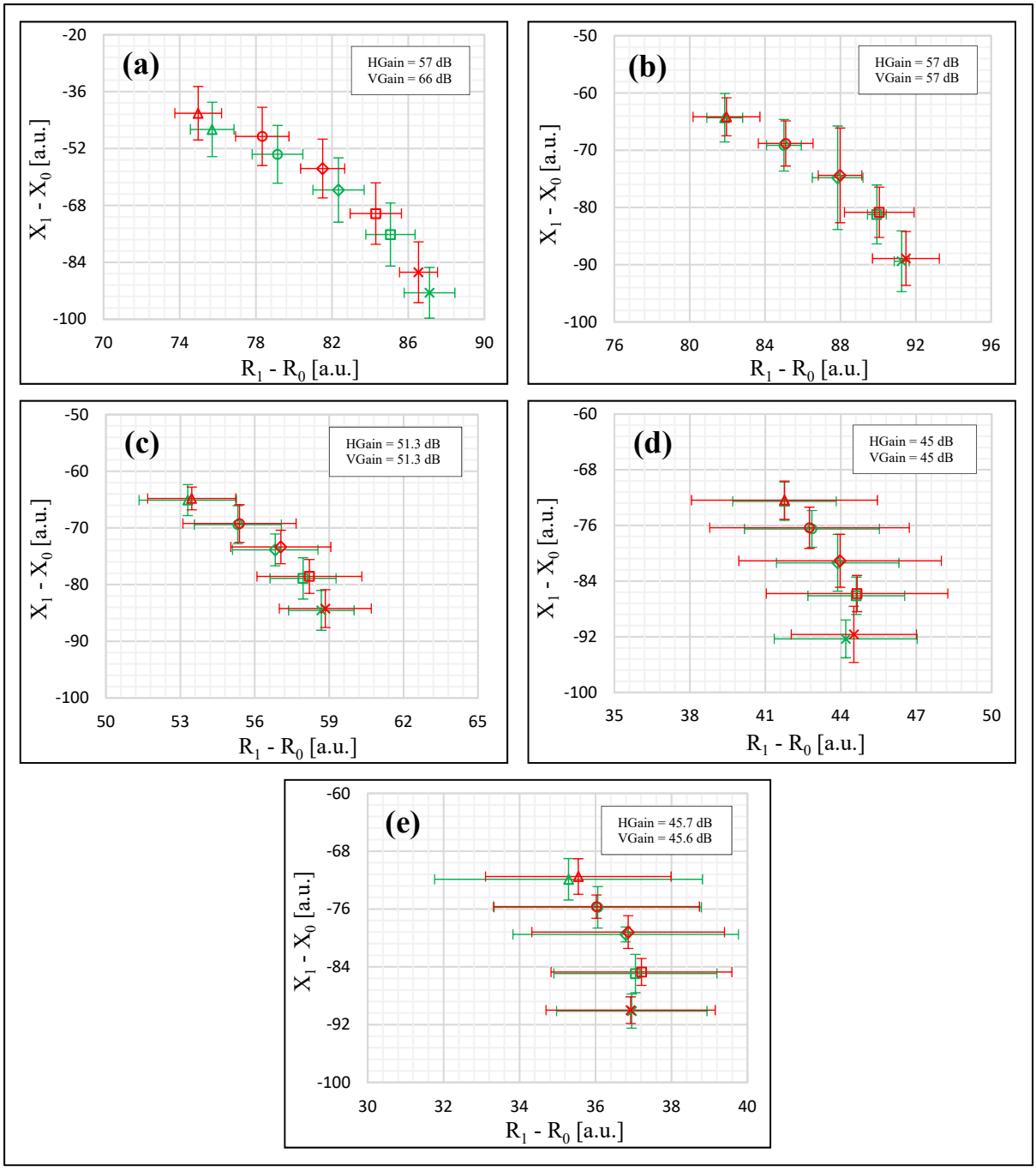

Figure 4.4 Eddy current probe liftoff data (×: 0 μm; □: 100 μm; ◊: 200 μm; ○: 300 μm; △: 400 μm) measured on Cd-coated steel samples in **H** (red, 8 samples) and **B** (green, 8 samples) manufacturing conditions at (a) 100 kHz, (b) 200 kHz, (c) 300 kHz, (d) 400 kHz & (e) 500 kHz. Error bars show $\pm 2SD$

Figures 4.5 (a), (b) & (c) show how decrease in electrical conductivities of Cd and steel as well as increase in magnetic permeability of steel affect simulated impedances at 100 kHz and zero liftoff. These figures show that changes in either of the aforementioned properties alone are not sufficient to explain experimental results. However, to fit simulation to experimental data, the most plausible scenario could be reduction in electrical conductivity of both Cd and steel near coating in **H** condition compared to **B** condition. In case of Cd, it is unclear whether this reduction was due to presence of hydrogen, or as a result different microstructure in baked and not-baked condition, or a combination of both effects. Since Cd has a low melting point, it is probable that thermal effects during baking changed its microstructure. Unlike Cd, thermal effects of baking on steel electromagnetic properties shall be minimal. The slight hardening of steel in **H** condition (Table 4.3) may indirectly indicate the presence of hydrogen near coating. Also, as Koenig *et al* (2010) suggested (referring to iron) dissolved hydrogen atoms create local strain zones, which can act as a source of current scattering. Considering these arguments, it is not improbable that reduction in electrical conductivity of steel could be an indication of dissolved hydrogen, which can lead to HE.

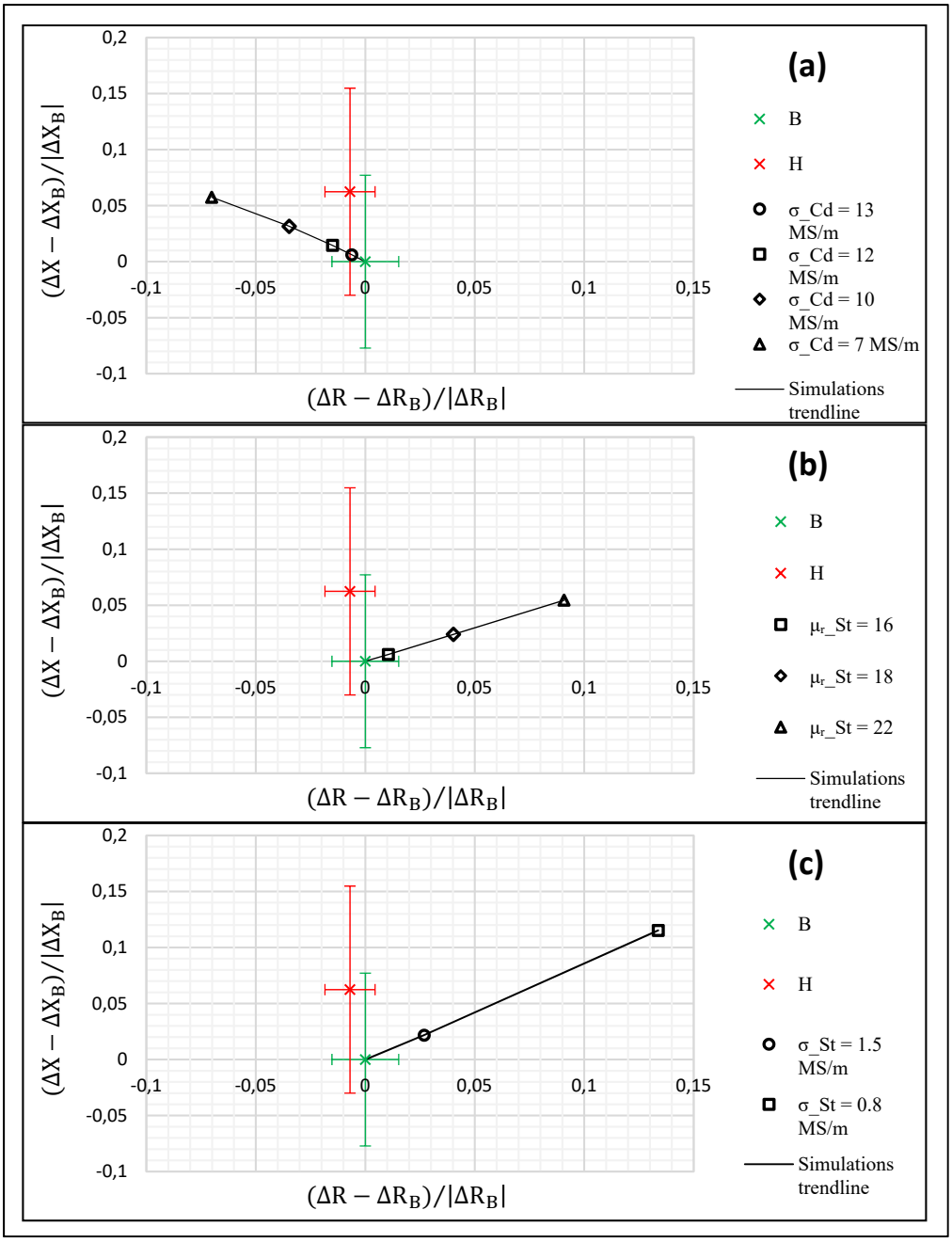

Figure 4.5 Effects of decrease in (a) Cd conductivity and (b) steel relative permeability as well as increase in (c) steel conductivity on simulated eddy current probe impedances. Simulation results were compared to surface impedances measured on **B** and **H** conditions at 100 kHz. Error bars show $\pm 2SD$

4.4 Conclusions

A commercial eddy current testing setup was used for obtaining liftoff data in 100-500 kHz frequency range on several Cd-plated high strength steel samples in baked (**B**, low HE susceptibility) and not-baked (**H**, high HE susceptibility) conditions. Effects of changes in conductivity and permeability of Cd and steel were assessed via simulations in CIVA®. The conclusions derived from this work could be summarized as follows:

1. At 100 kHz for every liftoff, a decrease of ~ 3 to 4% was observed in magnitude of averaged probe impedance relative to air on not-baked samples compared to baked ones.
2. Simulations suggested the measured decrease in eddy current signal amplitude was most likely due to lower electrical conductivity in both the Cd coating and steel near the coating in not-baked condition compared to baked condition.

It can be argued that eddy current testing has a potential to be utilized for distinguishing between baked and not baked manufacturing conditions that represent lower and higher hydrogen embrittlement susceptibility in Cd-plated steel components. However, more research should be conducted in order to enhance sensitivity and accuracy of measurements.

CONCLUSION

In this thesis, feasibility of NDE methods based on SAW and ECT to distinguish between Cd-plated high strength steel samples of low and high HE susceptibilities was studied. Samples were manufactured in not-baked (**H** condition, high hydrogen content) and immediately- or late-baked (**B** and **L** conditions, low hydrogen content) conditions. For SAW measurements, a piezoelectric transducer (10 MHz center frequency) for generation and a LDV for detection of ultrasound during line scans were used. In case of ECT, a commercial test unit along with an absolute, bridge-type, surface probe (100-500 kHz) was employed. The contributions from these studies were presented in three paper manuscripts (chapters 2 to 4).

In chapter 2, SAW velocity and attenuation measurement results were presented. For individual samples of different manufacturing conditions, both velocity and attenuation data showed overlap. Small variations found in coating thickness and roughness among samples did not seem to have a direct relationship with the NDE results. On average, **H** condition samples exhibited lower attenuation compared to **B** or **L** conditions, which was related to a slight increase in average steel hardness near coating. Estimated SAW velocities were deemed not sensitive to manufacturing conditions. Chapter 3 discussed SAW dispersion measurements and simulation results (5-10 MHz range). Velocity dispersion measurements showed considerable overlap among samples regardless of manufacturing conditions. Simulations suggested that the overlap was due to variations in base steel elastic properties among samples, while variations in coating characteristics had little impact. In case of dispersive attenuation curves, there were again large overlaps among the measured data for individual samples of different manufacturing conditions. On average, at lower frequency end, **H** condition was associated with smaller attenuation coefficients than **B** and **L** conditions. Chapter 4 discussed results of ECT liftoff measurements. At 100 kHz for every liftoff, a decrease of ~ 3 to 4% in magnitude of averaged probe impedance relative to air was observed for **H** condition. However, data for individual **H** and **B** samples showed overlap. Based on simulation results, change in impedance was attributed to decrease in electrical conductivities of both the Cd coating and the steel near the coating.

The goals of the DPHM-601 project were initially set as follows: 1) find a material property affected by hydrogen; 2) Evaluate this property by an NDE method; and 3) Relate measured changes in this property to hydrogen content. In practice, it was not possible to distinguish between the manufacturing conditions of individual samples based on either SAW or ECT measurements. It was demonstrated that material property variations had a strong impact on non-destructive measurements. Experimental uncertainties also largely interfered with the results. On average, however, SAW attenuation coefficients as well as electromagnetic properties were different in Cd-plated steel samples in baked and not baked conditions (low and high hydrogen content, respectively). These trends could be in fact due to differences in hydrogen content, although more evidence are needed to prove this hypothesis. It was not possible to directly measure hydrogen content because of logistical limitations, and the fact that such task would have made further tests on the samples impossible (damage to the thin coating). Considering these arguments, though the initial goals of the project were not fully met, the potential routes to achieve these goals via SAW and EC measurements, as well as the limitations of each method, were identified. For example, enhancement of the accuracy of ECT impedance measurements, along with devising a method to compensate for material property variations, could potentially provide a solution. Thus, the present dissertation could contribute to the future endeavors to develop a reliable NDE method for detection of hydrogen in electroplated steel parts. The experimental results (particularly the measured steel hardening in not-baked samples) may also be useful towards a better understanding of HE.

To improve the measurements accuracy and reliability, and to reduce the effects of variability in base material properties, the following recommendations may prove useful in future work:

- Modify SAW setup:
    - Design of a precision holder for the transducer
    - Use a high energy tone burst to drive transducer in order to increase SNR
    - Perform a lateral scanning at each detection distance to find the signal with highest amplitude

- Magnetize steel during ECT to isolate hydrogen-induced changes in conductivity from that of magnetic permeability
- Investigate coating microstructure and chemical composition changes due to baking by electron microscopy equipped with energy dispersive spectroscopy (SEM-EDS) in order to evaluate the effects on SAW and ECT measurements
- Perform ECT measurements on samples with different coating thicknesses to evaluate effects of coating thickness variations
- Perform shear and longitudinal ultrasound velocity measurements on each sample, then use the data to compensate for the effects of variability in elastic modulus and density during SAW measurements

BIBLIOGRAPHY

Abramoff, M. D., Magalhaes, P. J., & Ram, S. J. (2004) Image Processing with ImageJ, *Biophotonics international, 11*(7), 36-42, https://imagej.nih.gov/ij/docs/pdfs/Image_Processing_with_ImageJ.pdf

Abramovich, F., Benjamini, Y., Donoho, D. L., & Johnstone, I. M. (2006) Adapting to Unknown Sparsity by Controlling the False Discovery Rate. *Annals of Statistics*, *34*(2), 584-653. doi: 10.1214/009053606000000074

Aerospace Material Specification AMS6415U. (2016) Steel, Bars, Forgings, and Tubing 0.80Cr - 1.8Ni - 0.25Mo (0.38 - 0.43C) (SAE 4340). *SAE International*, doi: 10.4271/AMS6415U

Agüero, A., del Hoyo, J. C., Garcia de Blas, J., Garcia, M., Gutierrez, M., Madueno, L., & Ulargui, S. (2012) Aluminum Slurry Coatings to Replace Cadmium for Aeronautic Applications", Surface & Coatings Technology, *Surface & Coatings Technology, 213,* 229-238, doi: j.surfcoat.2012.10.052

Bae, D., Lee, J., Lee, S., Son, I., Baek, U., Nahm, S., & Lee, J. (2014) Evaluation on Hydrogen Embrittlement of Material using Nondestructive Test, *International Journal of Precision Engineering and Manufacturing*, *15*(6), 989-993, doi: 10.1007/s12541-014-0426-6

Balogun, O., & Achenbach, J. D. (2012). Surface waves on a half space with depth-dependent properties, *Journal of Acoustical Society of America, 132*(3), 1336-1345. doi: 10.1121/1.4739438

Bar-Cohen, Y., Mal, A. K., & ASM Committee on Ultrasonic Inspection. (2003). Ultrasonic Inspection. *ASM Handbook – Volume 17: Nondestructive Evaluation and Quality Control, ASM International,* 231-278. ISBN: 978-1-62708-152-8

Barrera, O., Bombac, D., Chen, Y., Daff, T. D., Galindo-Nava, E., Gong, P., Haley, D., Horton, R., Katzarov, I., Kermode, J. R., Liverani, C., Stopher, M., & Sweeney, F. (2018). Understanding and mitigating hydrogen embrittlement of steels: a review of experimental, modelling and design progress from atomistic to continuum. *Journal of Materials Science, 53*, 6251-6290. doi: 10.1007/s10853-017-1978-5

Bellemare, J., Laliberté-Riverin, S., Ménard, D., Brochu, M., & Sirois, F. (2020) [I]. Subtleties behind hydrogen embrittlement of cadmium-plated 4340 steel revealed by thermal desorption spectroscopy and sustained-load tests. *Metallurgical and Materials Transactions A, 51*, 3054–3065. doi: 10.1007/s11661-020-05741-0

Bellemare, J., Menard, D., & Sirois, F. (2020) [II]. Detection of hydrogen embrittlement in plated high-strength steels with eddy currents: Is the sensitivity sufficient? *Journal of Nondestructive Evaluation, 39*, article no.46, doi:10.1007/s10921-020-00691-4

Bhadeshia, H. K. D. H (2004). Tempered martensite. https://www.phase-trans.msm.cam.ac.uk/2004/Tempered.Martensite/tempered.martensite.html

Bray, D. E., & Stanley, R. K. (1997). Nondestructive evaluation – a tool in design, manufacturing, and service, *CRC Press*, ISBN: 978-0-8493-2655-4

Cheeke, J. D. N. (2012). Fundamentals and applications of ultrasonic waves. *CRC Press: 2nd edition*. ISBN: 978-1439854945

Conde, A., Arenas, M. A., & de Damborenea, J. J. (2011) Electrodeposition of Zn-Ni Coatings as Cd Replacement for Corrosion Protection of High Strength Steel, *Corrosion Science, 53*, 1489-1497, 10.1016/j.corsci.2011.01.021

Connolly, G. D., & Rokhlin, S. I. (2013). Fatigue crack monitoring in engine-grade titanium alloy by dynamic subtraction of surface acoustic wave modulation. *NDT&E International, 55*, 47-56. doi: 10.1016/j.ndteint.2013.01.009

Danicki, E. J. (2000). Efficiency of comb transducers. *2000 IEEE Ultrasonics Symposium.* doi: 10.1109/ULTSYM.2000.921513

Devanathan, M. A. V., Stachurski, Z., & Beck, W. (1963). A technique for the evaluation of hydrogen embrittlement characteristics of electroplating baths. *Journal of The Electrochemical Society, 110*(8), 886-890. doi: 10.1149/1.2425894

Doerr, C., Kim, J. Y., Singh, P., Wall, J. J., & Jacobs, L. J. (2017). Evaluation of sensitization in stainless steel 304 and 304L using nonlinear Rayleigh waves. *NDT&E International, 88,* 17-23. doi: 10.1016/j.ndteint.2017.02.007

Duquennoy, M., Ouaftouh, M., Qian, M. L., Jenot, F., & Ourak, M. (2001). Ultrasonic characterization of residual stresses in steel rods using a laser line source and piezoelectric transducers. *NDT&E International, 34*, 355-362. doi: 10.1016/S0963-8695(00)00075-X

E384 - 17. (2017) Standard Test Method for Microindentation Hardness of Materials. *ASTM International*, doi: 10.1520/E0384-17

Evers, S., Senöz, C., & Rohwerder, M. (2013) Hydrogen Detection in Metals: A Review and Introduction of a Kelvin Probe Approach. *Science and Technology of Advanced Materials, 14*, article no. 014201, doi: 10.1088/1468-6996/14/1/014201

Figueroa, D., & Robinson, M. J. (2008). The effects of sacrificial coatings on hydrogen embrittlement and re-embrittlement of ultra high strength steels. *Corrosion Science, 50*, 1066-1079. doi: 10.1016/j.corsci.2007.11.023

Findlay, S. J., & Harrison, N. D. (2002). Why aircraft fail. *Materials Today, 5*(11), 18-25. doi: 10.1016/S1369-7021(02)01138-0

Gao, W., Gloreiux, C., Kruger, S. E., Van de Rostyne, C., Gusev, V., Lauriks, W., & Theon, J. (2001). Investigation of the microstructure of cast iron by laser ultrasonic surface wave spectroscopy. *Materials Science and Engineering: A, 313*(1-2), 170-179, doi: 10.1016/S0921-5093(01)01143-1

Glorieux, C., Gao, W., Kruger, S. E., Van de Rostyne, C., Gusev, V., Lauriks, W., & Theon, J. (2000). Surface acoustic wave depth profiling of elastically inhomogeneous materials. *Journal of Applied Physics, 88*(7), 4394-4400, doi: 10.1063/1.1290457

Gomez, M. P., Domizzi, G., Lopez Pumarega, M. I., & Ruzzante, J. E. (2006) Characterization of Hydrogen Concentration in Zircaloy-4 using Ultrasonic Techniques, *Journal of Nuclear Materials, 353*, 167-176, doi: j.jnucmat.2006.01.024

Goossens, J., Leclaire, P., Xu, Xiaodong., Gloreiux, C., Martinez, L., Sola, A., Siligardi, C., Cannillo, V., Van der Donck, T., & Celis, J. (2007). Surface acoustic wave depth profiling of a functionally graded material. *Journal of Applied Physics, 102*(5), article no. 053508, doi: 10.1063/1.2774002

Gordon, G., Tittmann, B., & Singh, S. (1993). Surface acoustic wave determination of hardness: forward problem. *Review of progress in quantitative nondestructive evaluation. Springer, Boston, Ma.* doi: 10.1007/978-1-4615-2848-7_210

Hasegawa, Y. (1988), Failures from hydrogen attack and their methods of detection. *Welding International, 2*(6), 514-521. doi: 10.1080/09507118809447511

Herrmann, J., Kim, J. Y., Jacobs, L. J., Qu, J., Littles, J. W., & Savage, M. F. (2006). Assessment of material damage in a nickel-base superalloy using nonlinear Rayleigh surface waves. *Journal of Applied Physics, 99*, article no. 124913-1, doi: 10.1063/1.2204807

Hillier, E. M. K., & Robinson, M. J. (2004) Hydrogen Embrittlement of High Strength Steel Electroplated with Zinc-Cobalt Alloys. *Corrosion Science, 46*, 715-727, doi: 10.1016/S0010-938X(03)00180-X

Hirth, J. P. (1980). Effects of hydrogen on the properties of iron and steel. *Metallurgical Transactions A*, *11*, 861-890. doi: 10.1007/BF02654700

Johnson, H. H., Morlet, J. G., & Troiano, A. R. (1958). Hydrogen, crack initiation, and delayed failure in steel. *Transactions of the Metallurgical Society of AIME, 212*, 528-536, https://www.osti.gov/biblio/4288898 (doi not available)

Johnson, W. H. (1875). On some remarkable changes produced in iron and steel by the action of hydrogen and acids. *Proceeding of the Royal Society of London, 23*, 168-179. doi: 10.1098/rspl.1874.0024

Kang, L., Dixon, S., Wang, K., & Dai, J. (2013). Enhancement of signal amplitude of surface wave EMATs based on 3-D simulation analysis and orthogonal test method. *NDT&E International, 59*, 11-17. doi: 10.1016/j.ndteint.2013.05.003

Koenig, K., Lasseigne, A. N., Cisler, J. W., Mishra, B., King, R. H., & Olson, D. L. (2010). Non-contact, nondestructive hydrogen and microstructural assessment of steel welds. *International Journal of Pressure Vessels and Piping, 87*, 605-610. doi: 10.1016/j.ijpvp.2010.08.002

Kovalev, A. I., Wainstein, D. L., Mishina, V. P., & Zabilsky, V. V. (2002). Effect of residual stress on hydrogen embrittlement and stress corrosion cracking, *ASM International: Handbook of Residual Stress and Deformation of Steel,* 70-86. doi: 10.1361/hrsd2002p070

Kruger, S. E., Rebello, J. M. A., & de Camargo, P. C. (1999), *NDT&E International, 32*, 275-281. doi: 10.1016/S0963-8695(98)00052-8

L'Ecuyer, J., Brassard, C., Cardinal, C., Chabbal, J., Deschenes, L., & Labrie, J. P. (1976) An Accurate and Sensitive Method for the Determination of the Depth Distribution of Light Elements in Heavy Materials, *Journal of Applied Physics, 47,* 381-382, doi: 10.1063/1.322288

Lakestani, F., Coste, J. F., & Denis, R. (1995). Application of ultrasonic Rayleigh waves to thickness measurement of metallic coatings. *NDT&E International, 28*(3). 171-178. doi: 10.1016/0963-8695(95)00010-U

Laliberté-Riverin, S., Bellemare, J., Sirois, F., & Brochu, M. (2020)[I]. Internal hydrogen embrittlement of pre-cracked, cadmium-plated AISI 4340 high strength steel with sustained load tests and incremental step loading tests. *Engineering Fracture Mechanics, 223*, article number 106773. doi: 10.1016/j.engfracmech.2019.106773

Laliberté-Riverin, S., Bellemare, J., Sirois, F., & Brochu, M. (2020)[II]. Determination of hydrogen embrittlement stress intensity threshold by fractography. *Materialia, 12*, article number 100759. doi: 10.1016/j.mtla.2020.100759

Lanford, W. A. (1992). Analysis for hydrogen by nuclear reaction and energy recoil detection. *Nuclear Instruments and Methods in Physics Research B, 66*, 65-82. doi: 10.1016/0168-583X(92)96142-L

Larochelle, J. S., Désilets-Benoit, A., Borduas, G., Laliberté-Riverin, S., Rooda, S., & Brochu, M. (2017). Hydrogen loss during N-15 nuclear reaction analysis of high strength steel. *Nuclear Instruments and Methods in Physics Research B, 409*, 343-346. doi: 10.1016/j.nimb.2017.03.063

Li, X., Zhang, J., Fu, Q., Song, X., Shen, S., & Li, Q. (2018) A Comparative Study of Hydrogen Embrittlement of 20SiMn2CrNiMo, PSB1080 and PH13-8Mo High Strength Steels, *Materials Science & Engineering A, 724*, 518-528, 10.1016/j.msea.2018.03.076

Lider, A. M., Larionov, V. V., Garanin, G. V., & Krening, M. Kh. (2013) Ultrasonic testing for hydrogen for titanium-based materials and articles, *Technical Physics, 58*, 1395-1396, doi: 10.1134/S1063784213090181

Longo, R., Vanlanduit, S., Vanherzeele, J., & Guillaume, P. (2010). A method for crack sizing using Laser Doppler Vibrometer measurements of Surface Acoustic Waves. *Ultrasonics, 50*. 76-80. doi: j.ultras.2009.08.001

Louthan Jr, M. R. (2008) Hydrogen Embrittlement of Metals: A Primer for the Failure Analyst. *Journal of Failure Analysis and Prevention, 8*, 289-307, doi: 10.1007/s11668-008-9133-x

Marzani, A., Viola, E., Bartoli, I., Lanza di Scalea, & F., Rizzo, P. (2008) A semi-analytical finite element formulation for modelling stress wave propagation in axisymmetric damped waveguides. *Journal of Sound and Vibration, 318*, 488-505, doi: j.jsv.2008.04.028

Nagumo, M. (2004) Hydrogen Related Failure of Steels – a New Aspect. *Materials Science and Technology, 20*(8), 940-950, doi: 10.2320/jinstmet1952.62.3_267

Nagumo, M. (2016). Fundamentals of hydrogen embrittlement. *Springer Science+Business Media Singapore.* doi: 10.1007/978-981-10-0161-1

Oriani, R. A., & Josephic, P. H. (1974). Equilibrium aspects of hydrogen-induced cracking of steels. *Acta Metallurgica, 22*(9), 1065-1074. doi: 10.1016/0001-6160(74)90061-3

Oriani, R. A., & Josephic, P. H. (1980) Effects of Hydrogen on the Plastic Properties of Medium-Carbon Steels. *Metallurgical Transactions A, 11A*, 1809-1820, doi: 10.1007/BF02655096

Pavlakovic B., Lowe M., Alleyne D., Cawley P. (1997) Disperse: A General Purpose Program for Creating Dispersion Curves. *Review of Progress in Quantitative Nondestructive Evaluation, vol 16.* Springer, Boston, MA. https://doi.org/10.1007/978-1-4615-5947-4_24

Penttinen, A., & Luukkala, M. (1974). Surface wave generation by comb transducers. *Ultrasonics, 12*(6), 257-259. doi: 10.1016/0041-624X(74)90133-4

Puchi-Cabrera, E. S., Staia, M. H., Quinto, D. T., Viallalobos-Gutierrez, C., & Ochoa-Perez, E. (2007). Fatigue properties of a SAE 4340 steel coated with TiCN by PAPVD. *International Journal of Fatigue, 29*, 695-704. doi: 10.1016/j.ijfatigue.2006.07.004

Ruiz, A., & Nagy, P. B. (2004). Laser-ultrasonic surface wave dispersion measurements on surface-treated metals. *Ultrasonics, 42*, 665-669. doi: 10.1016/j.ultras.2004.01.045

Rumble, J. R. (2020) CRC Handbook of Chemistry and Physics 101st edition, *CRC Press, Section 12: Properties of solids*, ISBN: 9780367417246

Safaeinili, A., McKie, A. D. W., & Addison, R. C. (1997) Case Depth Measurement Using Surface Acoustic Wave Velocity Dispersion. *Review of Progress in Quantitative Nondestructive Evaluation, 16,* 1625-1632. doi: 10.1007/978-1-4615-5947-4_212

Schiettekatte, F., Chicoine, M., Forster, J. S., Geiger, J. S., Gujarathi, S., Kolarova, R., Paradis, A., Rooda, S., & Wei, P. (2004) ERD, 15N External Beam for NRRA in Air, HIRBS: Ion Beam Analysis Developments on The HVEC EN-1 Tandem", *Nuclear Instruments & Methods in Physics Research Section B: Beam Interactions with Materials & Atoms, 219-220*, 430-434, doi: 10.1016/j.nimb.2004.01.096

Schuhmann, R., & Weiland, T. (2001) Conservation of Discrete Energy and Related Laws in the Finite Integration Technique, *Progress in Electromagnetics Research, 32,* 301-316, doi: 10.2528/PIER00080112

Shull, P. J. (2001). Nondestructive evaluation: Theory, techniques and applications. *Boca Raton: CRC Press*. doi: 10.1201/9780203911068

Singer, F., & Kufner, M. (2017). Model based laser-ultrasound determination of hardness gradients of gas-carburized steel. *NDT&E International, 88*, 24-32, doi: 10.1016/j.ndteint.2017.02.006

Sriraman, K. R., Brahimi, S., Szpunar, J. A., & Yue, S. (2013). Hydrogen embrittlement of Zn-, Zn-Ni, and Cd-coated high strength steel. *Journal of Applied Electrochemistry, 43*, 441-451. doi: 10.1007/s10800-013-0529-2

Szabo, T. L. (1975). Residual stress measurements from surface wave velocity dispersion. *Proceedings of the ARPA/AFML Review of Quantitative NDE, 29*. https://lib.dr.iastate.edu/cnde_yellowjackets_1975/29 (doi not available)

Szlagowska-Spychalska, J. M., Spychalski, M. M., & Kurzydlowski, K. J. (2013), A Novel Approach for Measuring of Thickness of Induction Hardened Layers Based on the Eddy Current Method and the Finite Element Modeling, *NDT&E International, 54,* 56-62, 10.1016/j.ndteint.2012.12.001

Takai, K., & Watanuki, R. (2003). Hydrogen in trapping states innocuous to environmental degradation of high-strength steels. *ISIJ International, 43*(4), 520-526. doi: 10.2355/isijinternational.43.520

Voorwald, H. J. C., Padilha, R., Costa, M. Y. P., Pigatin, W. L., & Cioffi, M. O. H. (2007), Fatigue Properties of a SAE 4340 Steel Coated with TiCN by PAPVD, *International Journal of Fatigue, 29*, 471-480, 10.1016/j.ijfatigue.2006.05.003

Wang, L., & Rokhlin, S. I. (2001). Stable reformulation of transfer matrix method for wave propagation in layered anisotropic media. *Ultrasonics, 39*(6), 413-424. doi: 10.1016/S0041-624X(01)00082-8

Wang, M., Akiyama, E., & Tsuzaki, K. (2006). Determination of the critical hydrogen concentration for delayed fracture of high strength steel by constant load test and numerical calculation. *Corrosion Science, 48*, 2189-2202. doi: 10.1016/j.corsci.2005.07.010

Wang, P. N., & Chang, S. H. (2018). Effect of the mechanical properties and corrosion behaviors of nickel-cadmium duplex electroplated AISI 4340 steel by using various solid solution treatments. *Materials Transactions, 59*(3), 406-411. doi: 10.2320/matertrans.M2017282

Warren, P. D., Pecorari, C., Kolosov, O. V., Roberts, S. G., & Briggs, G. A. D. (1996). Characterization of surface damage via surface acoustic waves. *Nanotechnology, 7*, 295-301. doi: 10.1088/0957-4484/7/3/020

Wriedt, H. A., & Oriani, R. A. (1970). Effect of tensile and compressive elastic stress on equilibrium hydrogen solubility in a solid. *Acta Metallurgica, 18*(7), 753-760. doi: 10.1016/0001-6160(70)90039-8

Ye, C., Kan, W., Li, Y., & Pan, H. (2013). Experimental study of hydrogen embrittlement on AISI 304 stainless steels and Rayleigh wave characterization. *Engineering Failure Analysis, 34*, 228-234. doi: 10.1016/j.engfailanal.2013.07.021

Zamanzadeh, M., Allam, A., Kato, C., Ateya, B., & Pickering, H. W. (1982). Hydrogen absorption during electrodeposition and hydrogen charging of Sn and Cd coatings on iron. *Journal of the Electrochemical Society, 129*(2), 284-289. doi: 10.1149/1.2123813

Zeitvogel, D. T., Matlack, K. H., Kim, J. Y., Jacobs, L. J., Singh, P. M., & Qu, J. (2014) Characterization of Stress Corrosion Cracking in Carbon Steel Using Nonlinear Rayleigh Surface Waves. *NDT&E International, 62*, 144-152, doi: 10.1016/j.ndteint.2013.12.005

Zergoug, M., Lebaili, S., Boudjellal, H., & Benchaala, A. (2004), Relation Between Mechanical Microhardness and Impedance Variations in Eddy Current Testing, *NDT&E International, 37,* 65-72, doi: 10.1016/j.ndteint.2003.09.002

Zhang, C., & Achenbach, J. D. (1990) Dispersion and Attenuation of Surface Waves Due to Distributed Surface-breaking Cracks. *Journal of Acoustical Society of America, 88*(4), 1986-1992, doi: 10.1121/1.400223

Zhou, H., Xu, C., Wang, Q., Pan, H., & Chen, J. (2018). Characterization of hydrogen embrittlement in 2.25Cr-1Mo-0.25V steel by eddy current method. *Research in Nondestructive Evaluation, 29*(4), 212-220. doi: 10.1080/09349847.2017.1335921

Zielinski, A., & Fiore, N. F. (1982). Surface ultrasonic studies of time-dependent dislocation pinning by H atoms in f.c.c. stainless alloys. *Acta Metallurgica, 3*, 743-748. doi: 10.1016/0001-6160(82)90124-9